

A four-component mixture theory applied to cartilaginous tissues : numerical modelling and experiments

Citation for published version (APA):

Frijns, A. J. H. (2000). *A four-component mixture theory applied to cartilaginous tissues : numerical modelling and experiments*. [Phd Thesis 1 (Research TU/e / Graduation TU/e), Mathematics and Computer Science]. Technische Universiteit Eindhoven. <https://doi.org/10.6100/IR537990>

DOI:

[10.6100/IR537990](https://doi.org/10.6100/IR537990)

Document status and date:

Published: 01/01/2000

Document Version:

Publisher's PDF, also known as Version of Record (includes final page, issue and volume numbers)

Please check the document version of this publication:

- A submitted manuscript is the version of the article upon submission and before peer-review. There can be important differences between the submitted version and the official published version of record. People interested in the research are advised to contact the author for the final version of the publication, or visit the DOI to the publisher's website.
- The final author version and the galley proof are versions of the publication after peer review.
- The final published version features the final layout of the paper including the volume, issue and page numbers.

[Link to publication](#)

General rights

Copyright and moral rights for the publications made accessible in the public portal are retained by the authors and/or other copyright owners and it is a condition of accessing publications that users recognise and abide by the legal requirements associated with these rights.

- Users may download and print one copy of any publication from the public portal for the purpose of private study or research.
- You may not further distribute the material or use it for any profit-making activity or commercial gain
- You may freely distribute the URL identifying the publication in the public portal.

If the publication is distributed under the terms of Article 25fa of the Dutch Copyright Act, indicated by the "Taverne" license above, please follow below link for the End User Agreement:

www.tue.nl/taverne

Take down policy

If you believe that this document breaches copyright please contact us at:

openaccess@tue.nl

providing details and we will investigate your claim.

A Four-Component Mixture Theory Applied to Cartilaginous Tissues

Numerical Modelling and Experiments

CIP-DATA LIBRARY TECHNISCHE UNIVERSITEIT EINDHOVEN

Frijns, Arnoldus J.H.

A four-component mixture theory applied to cartilaginous tissues :
numerical modelling and experiments / by Arnoldus J.H. Frijns.

Eindhoven : Eindhoven University of Technology, 2000.

Proefschrift. - ISBN 90-386-0811-X

NUGI 811

Subject headings : porous media ; numerical methods / cartilage

2000 Mathematics Subject Classification : 65M60, 76T30, 92C10

Printed by Universiteitsdrukkerij Technische Universiteit Eindhoven

A Four-Component Mixture Theory Applied to Cartilaginous Tissues

Numerical Modelling and Experiments

PROEFSCHRIFT

ter verkrijging van de graad van doctor aan de
Technische Universiteit Eindhoven, op gezag van de
Rector Magnificus, prof.dr. M. Rem, voor een
commissie aangewezen door het College voor
Promoties in het openbaar te verdedigen op
dinsdag 12 december 2000 om 16.00 uur

door

Arnoldus Joannes Hubertus Frijs

geboren te Cadier en Keer

Dit proefschrift is goedgekeurd door de promotoren:

prof.dr. R.M.M. Mattheij

en

prof.dr.ir. T. Arts

Copromotor:

dr. E.F. Kaasschieter

Contents

1	Introduction	11
1.1	Anatomy of the Intervertebral Disc	12
1.2	Models of Cartilaginous Tissues	14
1.3	Objectives	19
1.4	Outline of the Thesis	20
2	Modelling of Cartilaginous Tissues	21
2.1	Four-Component Mixture Theory	22
2.1.1	Balance equations	22
2.1.2	Constitutive equations	23
2.1.3	Total set of equations	28
2.2	Reduction to a Two-Component Mixture Theory	28
3	Two-Component Mixture Theory	31
3.1	Physical Model	31
3.2	Variational Formulation	33
3.2.1	Displacement-pressure formulation	34
3.2.2	Displacement-pressure-velocity formulation	35
3.3	Finite Element Models	40
3.3.1	Displacement-pressure finite element model	40
3.3.2	Mixed finite element model	41
3.3.3	Mixed-hybrid finite element model	45
3.4	Examples	48
3.4.1	One-dimensional example	48
3.4.2	Two-dimensional example	55
3.4.3	Discussion and conclusions	58
4	Four-Component Mixture Theory	61
4.1	Physical Model	61
4.2	Variational Formulation	64
4.3	Mixed Finite Element Model	66

4.4	Electrochemical Potentials	69
5	Experiments on Intervertebral Discs	73
5.1	Introduction	73
5.2	Intervertebral Disc Tissue	74
5.3	Material and Methods	75
5.3.1	Sample preparation	75
5.3.2	Experimental set-up	75
5.3.3	Experimental protocol	76
5.3.4	Data analysis	77
5.4	Results	79
5.5	Discussion	82
5.6	Conclusions	83
6	Experiments on Hydrogel	85
6.1	Introduction	85
6.2	Material and Methods	87
6.2.1	Sample preparation	87
6.2.2	Experimental set-up	87
6.2.3	Experimental protocol	88
6.2.4	Data analysis	89
6.3	Results	92
6.4	Discussion	92
6.5	Conclusions	96
7	Conclusions and Recommendations	97
7.1	Conclusions	97
7.1.1	Numerical aspects	97
7.1.2	Experimental aspects	98
7.2	Recommendations	98
7.2.1	Numerical aspects	98
7.2.2	Experimental aspects	99
	Bibliography	101
	Index	107
	Summary	109
	Samenvatting	111
	Acknowledgements	115
	Curriculum Vitae	117

Nomenclature

Notations

a	scalar
\mathbf{a}	column
\mathbf{a}	vector
A	scalar
\mathbf{A}	matrix
\mathbf{A}	tensor
$\frac{\partial}{\partial t}$	time derivative

Symbols

c^β	concentration of ion β per unit fluid volume	$[\text{mol m}^{-3}]$
$\mathbf{B}^{\beta\gamma}$	friction tensor between components β and γ	$[\text{N s m}^{-4}]$
$\mathbf{d}(\mathbf{v}^f)$	rate of strain tensor	$[\text{s}^{-1}]$
\mathbf{D}^β	diffusion tensor of ion β	$[\text{m}^2 \text{s}^{-1}]$
e	edge (2D) or face (3D) of subdomain ω	
f^β	activity coefficient of component β	$[-]$
\mathbf{f}^α	body force of phase α	$[\text{N m}^{-3}]$
F	Faraday's constant	$[\text{C mol}^{-1}]$
h	element size	$[\text{m}]$
H	aggregate modulus	$[\text{N m}^{-2}]$
\mathbf{I}	unit tensor	$[-]$
J	relative volume change	$[-]$
\mathbf{J}	current density	$[\text{A m}^{-2}]$
k_e	electrokinetic coefficient	$[\text{V m}^2 \text{N}^{-1}]$

K	hydraulic permeability tensor	$[\text{m}^4 \text{N}^{-1} \text{s}^{-1}]$
L	length	$[\text{m}]$
m^β	mass of component β	$[\text{kg}]$
M^β	molar mass of ion β	$[\text{kg mol}^{-1}]$
n^α	volume fraction of phase α	$[-]$
n^β	volume fraction of component β	$[-]$
n	outward unit normal on a surface	$[-]$
p	fluid pressure	$[\text{N m}^{-2}]$
R	universal gas constant	$[\text{J mol}^{-1} \text{K}^{-1}]$
t	time	$[\text{s}]$
T	absolute temperature	$[\text{K}]$
\mathbf{T}^α	stress-tensor of phase α	$[\text{N m}^{-2}]$
u	displacement of the solid matrix	$[\text{m}]$
v	specific discharge	$[\text{m s}^{-1}]$
\mathbf{v}^α	velocity of phase α	$[\text{m s}^{-1}]$
\mathbf{v}^β	velocity of component β	$[\text{m s}^{-1}]$
V	representative elementary volume	$[\text{m}^3]$
V^α	volume of phase α	$[\text{m}^3]$
V^β	volume of component β	$[\text{m}^3]$
\bar{V}^β	molar volume of component β	$[\text{m}^3 \text{mol}^{-1}]$
W	energy equation	$[\text{J m}^{-3}]$
x^β	molar fraction of component β	$[-]$
x	position	$[\text{m}]$
z^β	valence of component β	$[-]$
Γ	boundary of a domain	
$\epsilon(\mathbf{u})$	strain-tensor	$[-]$
λ	Lagrange multiplier	$[\text{N m}^{-2}]$
λ_α	Lamé parameter of phase α	$[\text{N m}^{-2}]$
Λ_α	viscous stress parameter of phase α	$[\text{N s m}^{-2}]$
μ_α	Lamé parameter of phase α	$[\text{N m}^{-2}]$
μ^β	electro-chemical potential of component β	$[\text{N m}^{-2}]$
M_α	viscous stress parameter of phase α	$[\text{N s m}^{-2}]$
ξ	electrical potential	$[\text{V}]$
π	osmotic pressure	$[\text{N m}^{-2}]$
$\boldsymbol{\pi}^\alpha$	momentum interaction with phases other than α	$[\text{N m}^{-3}]$
ρ^α	intrinsic mass density of phase α	$[\text{kg m}^{-3}]$
$\boldsymbol{\sigma}^\alpha$	effective stress-tensor for phase α	$[\text{N m}^{-2}]$
ϕ^β	osmotic coefficient of component β	$[-]$
ω	subdomain	

Ω domain

Superscripts

D Dirichlet boundary
 f fluid
 fc fixed charge
 l liquid
 N Neumann boundary
 s solid
 tot total mixture
 $+$ cation
 $-$ anion

Subscripts

0 reference state
 f fluid
 h discrete space variable
 n discrete time variable
 p pressure
 s solid
 u displacement

1 Introduction

Cartilaginous tissues like, for example, intervertebral disc tissue, exhibit swelling or shrinking behaviour. The swelling of these tissues influences the behaviour of the cells. For example, the hydration of the extra-cellular matrix influences the metabolism of the chondrocytes [67]. This swelling is caused by mechanical, chemical or electrical mechanisms. An example of a *mechanical force* is the weight of the body applied on the human spine. A *chemical force* is for example a concentration difference over the tissue. An *electrical force* can be applied by an electrical potential field. In all cases, the macroscopic swelling and shrinking is caused by inflow or outflow of fluid. The forces cause a fluid flow, a solute flow and/or an electrical current. By the interaction between these fixed charges and the freely moving and electrically charged particles inside the tissue, physical phenomena occur, like osmosis, streaming potentials, diffusion potentials, electro-phoresis and electro-osmosis (table 1.1). These phenomena may influence the function of the tissue [16, 17, 20, 32, 55, 56]. In order to develop more insight into the mechanism, this swelling and compression behaviour has been modelled.

	Pressure gradient	Concentration gradient	Electrical potential
Fluid flow	Filtration	Osmosis	Electro-osmosis
Solute flow	Ultra-filtration	Diffusion	Electro-phoresis
Electrical current	Streaming current	Diffusion current	Electrical conduction

Table 1.1 Particle flow in porous media.

The behaviour of intervertebral disc is chosen to be studied. A reason for choosing this tissue is that the intervertebral disc is the most vulnerable structure of the human spine. Damage of the disc causes serious health problems, like hernia. In disc herniation, the fibre structure at the outer part of the disc is damaged in such way that the soft inner part is pushed outwards. When this tissue presses against the nerves, low back pain, radiating to the lower limbs, or even paralysis occurs. The intervertebral disc tissue is a soft biological tissue that is suitable for in vitro experiments: large samples (order of mm's) can be made. Furthermore, the tissue has no blood vessels and there are less cells than in other tissues. Therefore, the tissue does not deteriorate during swelling and compression experiments that last for 20 to 24 hours [23, 40, 41, 71].

1.1 Anatomy of the Intervertebral Disc

Intervertebral discs are located in the spine. The spine carries the load of the upper part of the human body and allows different postures. The human spine consists of bone segments, the vertebrae, that are mutually connected by intervertebral discs, ligaments and muscles. An intervertebral disc is located between two vertebral bodies. The tissue

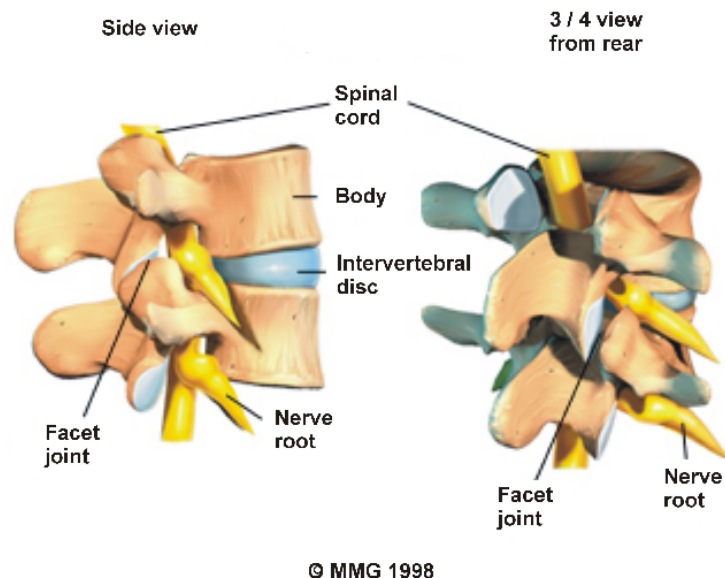


Figure 1.1 The motion segment (printed with permission from Medical Multimedia Group, Missoula, Montana, USA).

is softer than the vertebrae. The intervertebral discs have a shock absorbing function and they give some flexibility to the spine. In the human, the intervertebral discs are responsible for 20 – 33 % of the total height of the vertebral column [77]. The combination of two vertebrae and an intervertebral disc is called a *motion segment* (figure 1.1). An intervertebral disc consists of a soft inner part, the *nucleus pulposus*, and a stronger outer part, the *annulus fibrosus* (figure 1.2). The nucleus pulposus consists of a gelatinous material. In the annulus fibrosus, the main structures are a fibre network consisting of *collagen fibres* and *proteoglycan* molecules, freely moving charged particles (mainly ions and proteins), and an interstitial fluid. This network is arranged in lamellae. Within a lamella, the fibres lie parallel to each other.

A collagen fibre is a rod-like protein molecule built of long polypeptide chains of amino acids. A collagen fibre is composed of several smaller fibres, called *microfibrils* (figure 1.3). The fundamental unit of such fibril is a macromolecule, called *tropocollagen*, held together by covalent bonds. Tropocollagen consists of three polypeptide chains folded by hydrogen bounds in such way, that they form a triple helical configuration [9].

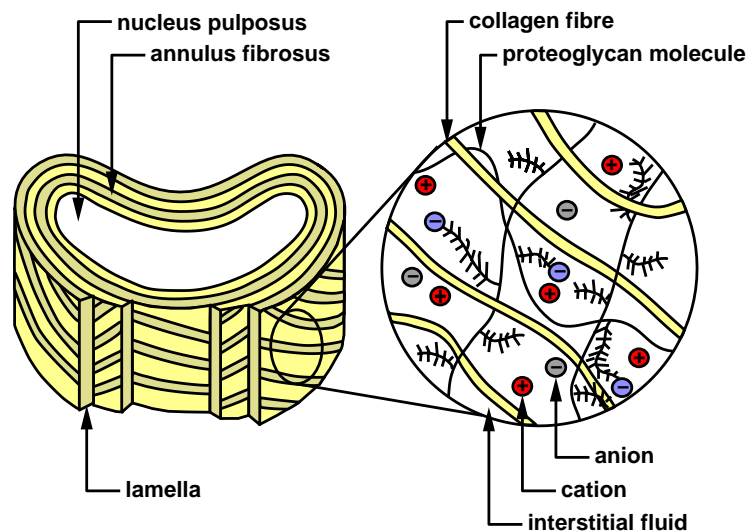


Figure 1.2 Schematic representation of the intervertebral disc tissue.

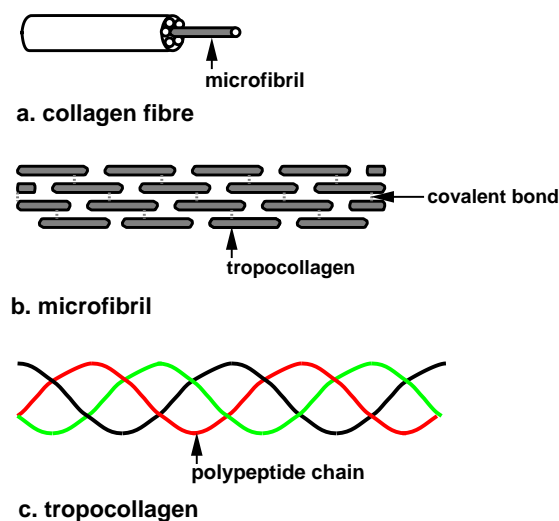


Figure 1.3 Schematic representation of a collagen fibre (a) built of microfibrils (b), that consist of polypeptide chains in a triple helical configuration (c).

Proteoglycans are large molecules consisting of many *glycosaminoglycans* (GAGs) linked to core proteins (figure 1.4). These glycosaminoglycans are made up of long chains of *polysaccharides*. A single core protein carries between 6 and 60 polysaccharide chains [9]. Via linker proteins, several proteoglycan units form a chain of hyaluronic acid. In this way, a three-dimensional network is formed. Due to the physiological pH and the ionic strength of the interstitial fluid, the carboxyl and sulfate groups of the polysaccharides are ionised. The density of these charges is called *fixed charge density*. Due to this ionisation the proteoglycans are capable of retaining water up to a 50-fold

of their own weight [19]. Thus, the fixed charges cause an osmotic pressure.

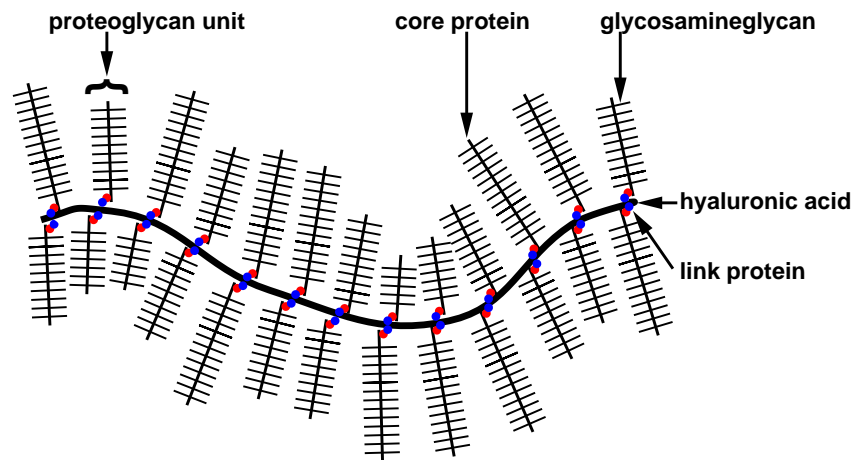


Figure 1.4 Schematic representation of proteoglycan aggregates.

From experiments [23, 28, 40, 71] it appears that chemical loads can invoke large deformations of the annulus fibrosus (osmosis). For example, when switching the bathing solution from the natural fluid to pure water, the volume of a sample of the nucleus pulposus, can increase to 200 % of the original volume [71]. Even in a physiological salt solution, the tissue swells substantially. These deformations can also be achieved by applying a mechanical load. Not only the geometry but also the composition of the tissue changes by swelling.

1.2 Models of Cartilaginous Tissues

The models that describe the behaviour of soft biological tissues, are split into two groups: *micromodels* and *macromodels*. In a micromodel, the tissue is described at molecular level. The macroscopic material behaviour is derived by the summation of all molecular behaviours. In a macromodel, an averaged structure is used.

First, we consider the micromodels. In physics, two important models are used for the water binding capacity of gel-like structures: the *DLVO-model*, derived by Derjaguin, Landau, Verwey and Overbeek [22, 76] and the Poisson-Boltzmann unit-cell model (*PB-model*).

In the DLVO-model, the major forces that operate between macromolecules or surfaces in fluids, are the attractive Van der Waals force and the repulsive electrical double-layer force [47]. The first force is always present. The second depends on the presence of charged surface groups. Double-layer forces are caused by fixed, negatively charged groups of the solid matrix. In order to maintain electro-neutrality, freely moving cations (positive ions) are attracted by those fixed charges and form electrical dipole layers, also

called double-layers. The double-layer forces are caused by the repulsion of equally charged particles of neighbouring double layers, thus forcing the fluid compartment to grow. The observation that even uncharged particles and molecules are often miscible in water, led to the postulation of an additional repulsive force [21], i.e. the hydration or structural force. This hydration force is caused by a bounded layer of water molecules to the surface. The layer prevents the surfaces or macromolecules from approaching closer than the thickness of two water molecules. When two surfaces or macromolecules approach closer, the relation between the force and the distance between the two surfaces or macromolecules is described by the DLVO-theory. This theory predicts that at long range (distance between the surfaces of macromolecules larger than 2.5 nm) the net repulsive force is due to the electrical double-layer force. This force increases exponentially with decreasing distance. For a shorter range, the attractive Van der Waals force is more important. The DLVO-theory predicts the forces well up to 2 nm [47]. Experiments have shown that when the distance becomes smaller, the hydration of smooth rigid surfaces gives rise to an oscillatory force [48]. The spatial period of oscillations corresponds to the size of the water molecules. Rough heterogeneous surfaces or biological surfaces, like a lipid bilayer, cause oscillations with a smaller range and magnitude [47].

In the Poisson-Boltzmann unit-cell model (PB-model), the repulsive forces between the glycosaminoglycans (GAGs) cause an electrostatic contribution to the tissue stiffness [14]. These repulsive forces are calculated from the fundamental laws of electrostatics and thermodynamics using the PB unit-cell as described by, for example, Marcus [57]. In the PB-model, the tissue consists of a large number of *unit-cells*. Each unit-cell is an idealised cylinder with in the centre one polyelectrolyte molecule (GAG) surrounded by a cylindrical space of aqueous electrolyte. The total macroscopic forces are derived by summing the microscopic forces of these unit-cells. The PB-model neglects hydration forces and Van der Waals forces, and does not apply for distances below 2.5 nm.

A drawback of the micromodels is that a precise description of the tissue material is needed. In general, the internal structure and the geometry are too complicated to use the micromodels. So, it is almost impossible to model the material behaviour in this way. Therefore, macromodels are used.

A macromodel is the *Donnan model*. As shown by Basser and Grodzinsky [4], this macroscopic model is an approximate solution of the PB-model using homogenisation and scaling methods. Homogenisation methods are mathematical procedures to simplify complicated equations by averaging them over a finite volume. The resulting equations are scaled by the Debye length (a characteristic molecular length). So, the macrocontinuum, thermodynamic Donnan model as well as the statistical, mechanical PB-model describe the electrostatic repulsion and attraction between charged groups. They differ however in the scaling length for the continuum (figure 1.5).

The *mixture theory* is a broad framework in which a wide variety of macromodels fit. In this theory, from the microstructure of the tissue, a continuum model is derived based on volume fractions of a *representative elementary volume* (figure 1.6). A representative elementary volume is chosen so that it is large enough, compared to the size of the pores, that it may be treated as homogeneous. At the same time it is small enough, compared

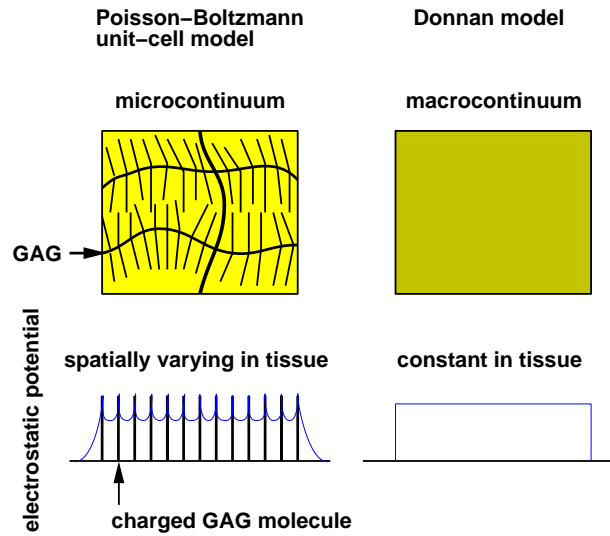


Figure 1.5 Schematic representation of the microcontinuum PB-model (left) and the macrocontinuum Donnan model (right). The macroscopic electrical potential in the PB-model is derived by summing the potentials of the unit-cells around the charged GAG molecules. In the Donnan model, the electrostatic potential is approximated by a homogenisation method.

to the macroscopic phenomena we are interested in, so that it may be considered as infinitesimal in the mathematical treatment. In this continuum theory, there is a fraction of every component in every point.

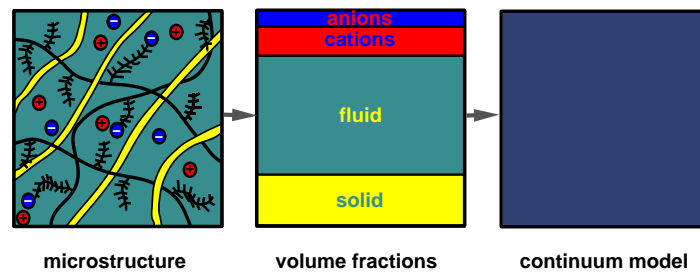


Figure 1.6 Continuum approach of the tissue.

The first concept for the mixture theory was introduced at the end of the 18th century by Woltman [78]. He introduced the concept of *volume fractions* in connection with a discussion on the mechanical behaviour of mud. He stated that the specific weight of the mud is described by

$$\frac{vP + up}{v + u - rv}, \quad (1.1)$$

where P and p are the weight of the loose earth and the water, respectively. The volumes are v for the loose earth and u for the added water. Finally, r is the ratio between the pore volume filled with water and the earth volume. So, rv is the volume of the added water that goes into the pores without increasing the total volume. If the mud does not contain more water than the spaces between the loose earth can hold, then the mud does not expand. For the water volume it holds that $u = rv$, and the weight of the mud is described by

$$\frac{vP + up}{v} = \frac{v(P + rp)}{v} = P + rp. \quad (1.2)$$

In this context, he spoke of a mixture.

In the 19th century, Fick, Darcy and Stefan laid the foundations of the mixture theory. Fick [25] studied the problem of diffusion of mixtures. He derived a differential equation of the diffusion stream in a channel along the x -direction with varying cross-section A :

$$\frac{\partial y}{\partial t} = -k \left(\frac{\partial^2 y}{\partial x^2} + \frac{1}{A} \frac{\partial A}{\partial x} \frac{\partial y}{\partial x} \right), \quad (1.3)$$

where y is the concentration of the component, t the time and k is a constant depending on the nature of the components. He stated that for constant cross-section, the equation simplifies to

$$\frac{\partial y}{\partial t} = -k \frac{\partial^2 y}{\partial x^2}. \quad (1.4)$$

Nowadays, this equation is known as *Fick's second law*.

In the same period, Darcy performed flow experiments through natural sand (figure 1.7). He observed a relation between the total water volume running through the sand sample, and the pressure loss over the sample. In this way, he experimentally found a relation between the pressure difference $P_2 - P_1$ and the fluid flow Q [18]:

$$\frac{Q}{A} = \frac{K(P_2 - P_1)}{L}, \quad (1.5)$$

where A the cross-sectional area, K the hydraulic permeability, and L the sample length. This result is essential for a continuum approach for the liquid flow in a porous medium.

Stefan [72] made another important step in developing the theory of mixtures. Based on the principles of mechanics founded by Maxwell, he presumed interaction forces between the constituents. In a mixture of two gases, equilibrium and motion equations were derived for each component. He stated that these equations are also valid for liquids and electrons in conductors. Later, he considered also a special case, i.e. the diffusion of a gas through a porous solid [72]. The porous solid was modelled as a gas with the property that the gas particles were fixed. This is the first mixture model of a porous medium.

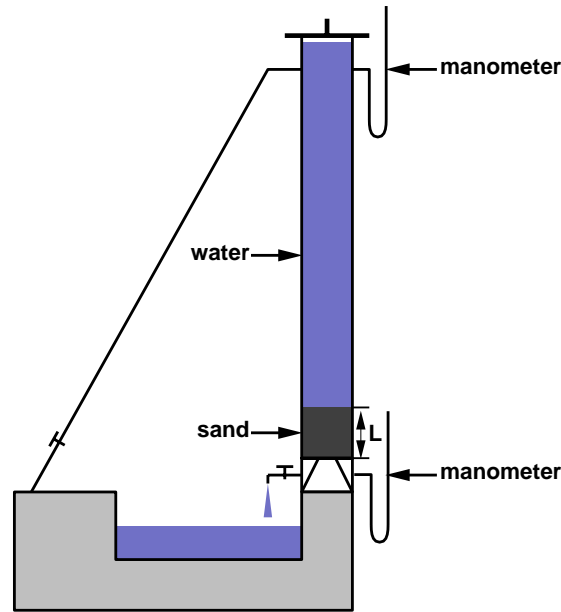


Figure 1.7 Darcy's experimental set-up.

In the previous theories, the solid was assumed to be rigid. Terzaghi [73, 74] extended the theory to a deformable porous solid that is saturated with a liquid. He considered the problem of consolidation. He performed experiments on the one-dimensional consolidation process in a thin clay layer. Using Darcy's law, the partial differential equation describing the problem of consolidation was derived:

$$\frac{k}{a} \frac{\partial^2 w}{\partial z^2} = \frac{\partial w}{\partial t}, \quad (1.6)$$

where k is the permeability, a is the compression number, w is the pore-water overpressure ($p_1 - p$, where p_1 represents a constant load), z is the position and t is the time. Later, the theory was extended by Biot [7, 8] and by Bowen [10, 11]. Biot generalised Terzaghi's one-dimensional theory to the three-dimensional case being able to handle any arbitrary load which may vary in time. Bowen considered finite deformation of the porous media. He derived the equations for the incompressible [10] and compressible [11] porous solids with any number of immiscible fluids. These *biphasic models* are still used in the field of civil engineering.

Since the 1980's, biphasic models are successfully used to model the compressive behaviour of soft biological tissues, like articular cartilage [60, 61], skin and subcutis [62, 64], and the left ventricle of the heart [42, 45, 46]. However, these models are not suited for modelling osmotic phenomena, since they do not take into account the charged proteoglycans. This tissue component causes the osmotic pre-stress of the tissue. Therefore, Lai et al. [51] developed a *triphasic theory* for soft hydrated tissues. They distinguished three components: a charged porous solid (collagen fibres and proteoglycans), a fluid, and the fluid miscible components (ions). Their theory combines

the physico-chemical theory for ionic and poly-ionic (proteoglycans) solutions with the biphasic mixture theory. Therefore, it is possible to describe the deformations and the stresses for cartilage for chemical and mechanical loads. In their theory, they neglect geometric non-linearities and hydration forces. Snijders [70] developed a finite element formulation of a simplified version of the triphasic theory, neglecting electrical fluxes and electrical potential gradients.

From confined compression experiments, performed by de Heus [19], Snijders [71] and Houben [40], and their triphasic finite element simulations, it appeared that fitting the experimental data required a diffusion coefficient for the ions, many times larger than the diffusion coefficient of the ions in water [63]. As the fixed charge density is large, the electrical effects inside the tissue may not be neglected. A *four-component mixture theory*, derived by Huyghe and Janssen [43], includes geometric non-linearity, electrical fluxes and potential gradients. In this mixture theory, four components are distinguished: a charged solid, a fluid, cations and anions. By the distinction between cations and anions, the electrical phenomena can be modelled. Huyghe and Janssen [43] introduce electro-neutrality as a restriction on the second law of thermodynamics, while Lai et al. [51] introduce the electrical potential as an external field. Thereby, Huyghe and Janssen introduce the electrical potential as a Lagrange multiplier and hence as a field intrinsic to the material. Following the approach developed by Lai et al. [51], Gu et al. [34] derived a mixture theory consisting of a solid phase, a fluid phase and n different species of mono- or multi-valent ions. They incorporated the electro-neutrality condition in their model. Achanta et al. [1] used a *hybrid mixture theory*, modelling the interfaces as separate continua. Therefore, the hydration layer is modelled as a separate component in the mixture.

In order to reduce the number of material parameters to a minimum, we do not distinguish between the hydration layer and the rest of the fluid as long as the experiments do not require such complex model.

1.3 Objectives

In this thesis, the four-component mixture theory is studied. The objectives of this study are:

- The development of a finite element description for the four-component mixture theory as derived by Huyghe and Janssen [43]. With this finite element model, we should be able to compute the deformations, the fluid and ion flows, the fluid pressure, the cation and anion concentrations and the electrical potential field.
- The verification of the four-component mixture theory with respect to the evolution in time of the deformations and the electrical potential field by confined swelling and compression experiments.

1.4 Outline of the Thesis

In chapter 2, we derive the four-component mixture theory from the balance equations and the constitutive equations for the solid matrix, the fluid flow and the ion flows. It is shown that this theory reduces to the biphasic theory when assuming that there are no particles dissolved in the fluid phase.

In chapter 3, the two-component mixture theory is considered. It is shown that the problem definition has a unique solution when making adequate assumptions on the behaviour of the displacements, fluid velocity and the fluid pressure. These assumptions are not in conflict with the physical problem we are interested in. Two ways of describing the problem are considered: the displacement-pressure formulation and the displacement-pressure-velocity formulation. From the first one, a conforming finite element method is derived. From the second one, a mixed-hybrid finite element method is derived. For both methods, the errors are considered that are caused by size of the elements and by the size of the time-steps.

In chapter 4, the two-component mixture model is extended to the four-component mixture model. A mixed finite element method is derived that results in a non-symmetric matrix-vector system. The displacements, the fluid and the ion flows, the fluid pressures, the ion concentrations and the electrical potentials are unknown. The finite element model is used to simulate the experiments described in chapters 5 and 6.

In chapter 5, the four-component mixture theory is tested in experiments on intervertebral disc tissue. Uniaxial confined swelling and compression experiments were performed on cylindrical samples made out of the annulus fibrosus part of intervertebral discs. The value of the material parameters were estimated by fitting the experiments with the finite element model of chapter 4. The theory was verified by comparing the estimated values to values reported by other studies.

In chapter 6, the four-component mixture theory was tested in experiments on a hydrogel. A hydrogel is an artificial material that has similar properties as cartilaginous tissues. Uniaxial confined swelling and compression experiments were performed again. This time we also measure the electrical phenomena: streaming potentials and diffusion potentials. These phenomena gave an extra possibility to check the theory. The values of the material parameters were estimated by the finite element model of chapter 4. The theory is verified by comparing the estimated values of the parameters to the values reported in other studies.

2 Modelling of Cartilaginous Tissues

Cartilaginous tissues mainly consist of four components: a fibre network (collagen fibres and proteoglycans), a fluid, and positively and negatively charged particles. Due to this consistency, physical effects as described in table 1.1 can occur. In order to describe these effects in a physical model, these four components have to be included.

The interactions of the components can be described by either a micromodel or a macromodel. In a micromodel, a detailed description of the tissue is needed. In general, this structure is too complex to describe. Therefore, we choose to use a macromodel based on a continuum approach. In this approach, the material is divided into representative elementary volumes that have a size such that they are large enough to be treated as homogeneous. At the same time, they are small enough to model the differences in material properties.

In each representative elementary volume, the structure properties are averaged and the volume fractions of each component are determined (figure 2.1). Next, the represen-

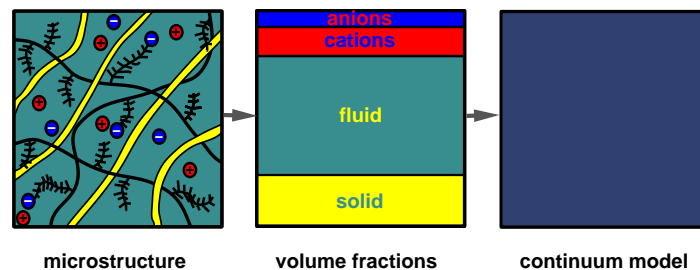


Figure 2.1 Continuum approach of the tissue.

tative elementary volume is considered to be a homogeneous material. This means that at every point in the material, a fraction of every component is present. In this way, the tissue is modelled as a continuum. We describe this continuum by a *four-component mixture theory*.

2.1 Four-Component Mixture Theory

In the four-component mixture theory, the material is modelled as a charged, porous solid (denoted by s) that is saturated with a fluid (denoted by f), in which some freely moving ions (cations (+) and anions (-)) are dissolved [28, 43]. The solid can shrink only by expelling the fluid into its surroundings, and swell only by attracting the fluid from its surroundings.

In this thesis, we distinguish components and phases. A *component* is a group of particles with the same properties. A *phase* is defined as a set of miscible components.

In the four-component mixture theory, there are four components: a solid (s), a liquid (l), cations (+) and anions (-). But there are only two phases: a solid (s) and a fluid (f). In this case, the fluid consists of three components: the liquid, the cations and the anions.

In the four-component mixture theory, the material behaviour is described by a set of coupled equations: balance equations and constitutive equations

2.1.1 Balance equations

For each phase α , the material fulfils the *momentum equation*

$$\nabla \cdot \mathbf{T}^\alpha + \boldsymbol{\pi}^\alpha = \mathbf{f}^\alpha, \quad \alpha = s, f, \quad (2.1)$$

where \mathbf{T}^α is the *stress-tensor* of phase α , $\boldsymbol{\pi}^\alpha$ represents the interaction with the phases other than α , and \mathbf{f}^α represents the inertial terms and the body forces, such as gravity. The stress-tensors are modelled by

$$\mathbf{T}^\alpha := -n^\alpha p \mathbf{I} + \boldsymbol{\sigma}^\alpha, \quad \alpha = s, f, \quad (2.2)$$

where n^α is the *volume fraction* of phase α , p is the fluid pressure, and $\boldsymbol{\sigma}^\alpha$ is the effective stress-tensor of phase α . The volume fractions are defined by

$$n^\alpha := \frac{V^\alpha}{V}, \quad \alpha = s, f, \quad (2.3)$$

where V is a representative volume of the mixture and V^α is the volume occupied by phase α inside volume V . Conservation of the momentum for the whole mixture leads to the restriction $\boldsymbol{\pi}^s + \boldsymbol{\pi}^f = \mathbf{0}$. So, the total momentum balance is simplified to

$$\nabla \cdot (\mathbf{T}^s + \mathbf{T}^f) = \mathbf{f}^s + \mathbf{f}^f, \quad (2.4)$$

or

$$\nabla \cdot (\boldsymbol{\sigma}^s + \boldsymbol{\sigma}^f) - \nabla \cdot ((n^s + n^f) p) = \mathbf{f}. \quad (2.5)$$

From now on, we neglect the inertial terms and the body forces, that are represented by \mathbf{f} . So, $\mathbf{f} = \mathbf{0}$. Further, we assume that the material is saturated, i.e.

$$n^s + n^f = 1. \quad (2.6)$$

In every representative elementary volume, the material has also to fulfil the *mass balances*:

$$\frac{\partial(n^\alpha \rho^\alpha)}{\partial t} + \nabla \cdot (n^\alpha \rho^\alpha \mathbf{v}^\alpha) = 0, \quad \alpha = s, f, \quad (2.7)$$

$$\frac{\partial(n^f M^\beta c^\beta)}{\partial t} + \nabla \cdot (n^f M^\beta c^\beta \mathbf{v}^\beta) = 0, \quad \beta = +, -, \quad (2.8)$$

where ρ^α , \mathbf{v}^α , M^β , c^β and \mathbf{v}^β are the *intrinsic density* of phase α , the velocity of phase α , the *molar mass* of ion β , the *concentration* of ion β per unit fluid volume, and the velocity of ion β , respectively. Here, the intrinsic density for phase α is defined by

$$\rho^\alpha := \frac{m^\alpha}{V^\alpha}, \quad \alpha = s, f, \quad (2.9)$$

where m^α is the mass of phase α in a representative elementary volume and V^α the volume occupied by this phase in the same elementary volume.

In equations (2.7) and (2.8), it is assumed that there are no sources or sinks. The first term in these equations is an accumulation term. This term accounts for the influence of the deformation of the solid. The second term in the mass balances accounts for the mass flow.

In this thesis, we assume that the phases are intrinsically incompressible (ρ^α is constant) and that the molar masses of the ions are constant (M^β is constant). So, the intrinsic density and the molar masses can be left out in the mass balances.

The total mass balance follows from the summation of all phase mass balances and the saturation assumption:

$$\nabla \cdot \mathbf{v}^s + \nabla \cdot (n^f (\mathbf{v}^f - \mathbf{v}^s)) = 0. \quad (2.10)$$

Here, the solid velocity \mathbf{v}^s is defined by

$$\mathbf{v}^s := \frac{\partial \mathbf{u}}{\partial t}, \quad (2.11)$$

where \mathbf{u} are the solid displacements and t is the time.

Finally, *electro-neutrality* is needed:

$$z^+ c^+ + z^- c^- + z^{fc} c^{fc} = 0, \quad (2.12)$$

where z^β is the value of the valence of the charged particles. For a mono-valent salt, its value is +1 for the cations and -1 for the anions. The superscript *fc* stands for fixed charge. A fixed charge is an electrically charged particle attached to the solid skeleton.

2.1.2 Constitutive equations

Also constitutive equations are needed. The first equations define the *effective stress-tensors* σ^α :

$$\sigma^\alpha := 2\mu_\alpha \boldsymbol{\epsilon}(\mathbf{u}) + \lambda_\alpha \nabla \cdot \mathbf{u} \mathbf{I} + 2M_\alpha \mathbf{d}(\mathbf{v}^\alpha) + \Lambda_\alpha \nabla \cdot \mathbf{v}^\alpha \mathbf{I}, \quad \alpha = s, f,$$

where $\boldsymbol{\epsilon}(\mathbf{u}) = \frac{1}{2}((\nabla \mathbf{u}) + (\nabla \mathbf{u})^T)$ is the strain tensor, μ_α and λ_α are Lamé parameters, and $\mathbf{d}(\mathbf{v}^\alpha) = \frac{1}{2}((\nabla \mathbf{v}^\alpha) + (\nabla \mathbf{v}^\alpha)^T)$ is the rate of strain tensor, and M_α and Λ_α are the viscous stress parameters.

The solid matrix is modelled as a linearly elastic material. This means that the viscous stress parameters M_s and Λ_s are equal to zero. So, the mechanical behaviour is described by *Hooke's law*:

$$\boldsymbol{\sigma}^s = 2\mu_s \boldsymbol{\epsilon}(\mathbf{u}) + \lambda_s \nabla \cdot \mathbf{u} \mathbf{I}, \quad (2.13)$$

where μ_s and λ_s are the Lamé parameters for the solid. These Lamé parameters depend on the Poisson's ratio and the stiffness of the solid material, see e.g. [12].

The fluid is modelled as a Newtonian viscous fluid. So, $\mu_f = 0$ and $\lambda_f = 0$, i.e.

$$\boldsymbol{\sigma}^f = 2M_f \mathbf{d}(\mathbf{v}^f) + \Lambda_f \nabla \cdot \mathbf{v}^f \mathbf{I}. \quad (2.14)$$

We now assume that the viscosity is negligible compared to the momentum transfer. So, $\|\boldsymbol{\sigma}^s\| \gg \|\boldsymbol{\sigma}^f\|$. This is usually the case except for very small layers of very permeable materials [2]. So, the momentum balance (2.5) is described by

$$\nabla \cdot \boldsymbol{\sigma} - \nabla p = \mathbf{0}, \quad (2.15)$$

where

$$\boldsymbol{\sigma} = 2\mu_s \boldsymbol{\epsilon}(\mathbf{u}) + \lambda_s \nabla \cdot \mathbf{u} \mathbf{I}. \quad (2.16)$$

The next constitutive equations describe the fluid flow and the ion flows. We assume that the average pore size (≈ 3.5 nm for cartilaginous tissues [30]) is large enough to neglect some boundary effects, such as the Knudsen diffusion and the Klinkenberg effect [39]. Then, the flows are described by an extended Darcy's law and an extended Fick's law. These extended laws are derived by Huyghe and Janssen [43, 44] such that the second law of thermodynamics is fulfilled. Therefore, Huyghe and Janssen [44] use *electrochemical potentials*. These potentials are continuous functions. They are defined by

$$\mu^\beta := p + \frac{z^\beta}{\bar{V}^\beta} F \xi + \frac{\partial W}{\partial n^\beta}, \quad \beta = l, +, -, \quad (2.17)$$

where \bar{V}^β is the volume occupied by one mole of component β , F is Faraday's constant, ξ the electrical potential, W is the energy, and l is the liquid component. Note that all electrochemical potentials are defined with respect to the components.

Now, the partial derivative of the energy equation is defined by [43]

$$\frac{\partial W}{\partial n^\beta} := \mu_0^\beta(T) + \frac{RT}{\bar{V}^\beta} \ln(f^\beta x^\beta), \quad (2.18)$$

where μ_0^β is a reference value for the electrochemical potential that may depend on the absolute temperature T , R is the universal gas constant, f^β is an *activity coefficient* of

component β ($0 \leq f^\beta \leq 1$) and x^β is the molar fraction of component β ($0 \leq x^\beta \leq 1$). The activity coefficients f^β are equal to one for an ideal solution. Further, they are defined such that $f^\beta \rightarrow 1$ if $x^\beta \rightarrow 1$.

The definition of the *energy equation* is based on the partial derivative to the volume fractions n^β . Therefore, the molar fractions are written as functions of the volume fractions. First, we derive a relation between the molar fractions and the concentrations:

$$x^\beta = \frac{x^\beta / V^f}{1/V^f} = \frac{x^\beta / V^f}{\sum_{\gamma=l,+,-} x^\gamma / V^f} = \frac{c^\beta}{\sum_{\gamma=l,+,-} c^\gamma}, \quad \beta = l, +, -. \quad (2.19)$$

Now, the relation between the concentrations and the volume fractions is given by

$$\bar{V}^\beta c^\beta = \frac{n^\beta}{n^f}, \quad \beta = l, +, -. \quad (2.20)$$

Substitution of (2.20) into (2.19) results in

$$x^\beta = \frac{c^\beta}{\sum_{\gamma=l,+,-} c^\gamma} = \frac{n^\beta / \bar{V}^\beta}{\sum_{\gamma=l,+,-} n^\gamma / \bar{V}^\gamma}. \quad (2.21)$$

So, the partial derivative of the energy equation W is defined by

$$\frac{\partial W}{\partial n^\beta} := \mu_0^\beta(T) + \frac{RT}{\bar{V}^\beta} \ln \left(\frac{f^\beta n^\beta / \bar{V}^\beta}{\sum_{\gamma=l,+,-} n^\gamma / \bar{V}^\gamma} \right), \quad \beta = l, +, -. \quad (2.22)$$

For the activity coefficients we choose

$$f^\beta := (n^\beta)^{1-\phi^\beta}, \quad \beta = l, +, -. \quad (2.23)$$

where ϕ^β is the *osmotic coefficient* for component β ($0 \leq \phi^\beta \leq 1$). The osmotic coefficients ϕ^β model the non-ideality of the material. In the case of an ideal material, the osmotic coefficients are equal to one. It holds that $f^\beta \rightarrow 1$ if $n^\beta \rightarrow 1$ and $f^\beta = 1$ for an ideal solution ($\phi^\beta = 1$). So, the activity coefficients f^β have the right properties.

We assume that $c^l + c^+ + c^-$ is constant. This means that number of particles inside the fluid stays the same. From these assumptions and equation (2.22) it follows that

$$\begin{aligned} W = W_0(\mathbf{u}, T) &+ \sum_{\beta=l,+,-} \mu_0^\beta(T) n^\beta + \sum_{\beta=l,+,-} RT \frac{n^\beta}{\bar{V}^\beta} \ln \left(\frac{n^\beta / \bar{V}^\beta}{\sum_{\gamma=l,+,-} n^\gamma / \bar{V}^\gamma} \right) \\ &+ \sum_{\beta=l,+,-} RT \frac{n^\beta}{\bar{V}^\beta} \ln(f^\beta) - \sum_{\beta=l,+,-} RT(1 - \phi^\beta) \frac{n^\beta}{\bar{V}^\beta}. \end{aligned} \quad (2.24)$$

Note that for an uncharged liquid ($z^l = 0$), the electrochemical potential μ^l is equal to the difference between the fluid pressure p and the *osmotic pressure* π [65], i.e. $\mu^l =$

$p - \pi$, assuming that the reference value is equal to zero, i.e. $\mu_0^f = 0$. Thus, the osmotic pressure is defined by

$$\pi := -\frac{\partial W}{\partial n^f}. \quad (2.25)$$

For an ideal dilute solution ($f^l = 1$, $n^+ \ll n^l$, and $n^- \ll n^l$), the osmotic pressure is approximated by

$$\begin{aligned} \pi &= -\frac{RT}{\bar{V}^l} \ln\left(\frac{n^l/\bar{V}^l}{\sum_{\beta=l,+,-} n^\beta/\bar{V}^\beta}\right) \\ &= -\frac{RT}{\bar{V}^l} \ln\left(\frac{c^l}{\sum_{\beta=l,+,-} c^\beta}\right) \\ &= -\frac{RT}{\bar{V}^l} \ln\left(1 - \frac{c^+ + c^-}{\sum_{\beta=l,+,-} c^\beta}\right) \\ &\approx \frac{RT}{\bar{V}^l} \frac{c^+ + c^-}{\sum_{\beta=l,+,-} c^\beta} \\ &\approx \frac{RT}{\bar{V}^l} \frac{c^+ + c^-}{c^l} \\ &= \frac{n^f}{n^l} RT(c^+ + c^-) \\ &\approx RT(c^+ + c^-). \end{aligned} \quad (2.26)$$

This is equal to the often used expression for the osmotic pressure, see e.g. [65].

From the definitions of the electrochemical potentials and the assumption that $c^l + c^+ + c^-$ is constant, it follows

$$\nabla \mu^\beta = \nabla p + z^\beta \frac{F}{\bar{V}^\beta} \nabla \xi + \frac{RT}{\bar{V}^\beta} \left(\frac{\nabla c^\beta}{c^\beta} + \frac{\nabla f^\beta}{f^\beta} \right). \quad (2.27)$$

Now, we combine relations (2.20) and (2.23) to

$$\frac{\nabla f^\beta}{f^\beta} = (1 - \phi^\beta) \left(\frac{\nabla n^\beta}{n^\beta} \right) = (1 - \phi^\beta) \left(\frac{\nabla c^\beta}{c^\beta} + \frac{\nabla n^f}{n^f} \right).$$

We assume small deformations. This means that

$$\frac{\nabla f^\beta}{f^\beta} \approx (1 - \phi^\beta) \frac{\nabla c^\beta}{c^\beta}.$$

So, we write for the gradient of the electrochemical potentials

$$\nabla \mu^\beta = \nabla p + z^\beta \frac{F}{\bar{V}^\beta} \nabla \xi + \frac{RT}{\bar{V}^\beta} (2 - \phi^\beta) \frac{\nabla c^\beta}{c^\beta}. \quad (2.28)$$

According to Huyghe and Janssen [43], the relation between the electrochemical potentials and the component velocities is given by

$$-n^\beta \nabla \mu^\beta = \sum_{\gamma=l,+,-} \mathbf{B}^{\beta\gamma} (\mathbf{v}^\gamma - \mathbf{v}^s), \quad \beta = l, +, -, \quad (2.29)$$

where $\mathbf{B}^{\beta\gamma}$ are *friction tensors* between components β and γ . They are defined by

$$\begin{aligned} \mathbf{B}^{++} &:= RTn^+ (\bar{\mathbf{V}}^+)^{-1} (\mathbf{D}^+)^{-1}, \\ \mathbf{B}^{--} &:= RTn^- (\bar{\mathbf{V}}^-)^{-1} (\mathbf{D}^-)^{-1}, \\ \mathbf{B}^{+-} &:= \mathbf{B}^{-+} = 0, \\ \mathbf{B}^{l+} &:= \mathbf{B}^{+l} = -\mathbf{B}^{++}, \\ \mathbf{B}^{l-} &:= \mathbf{B}^{-l} = -\mathbf{B}^{--}, \\ \mathbf{B}^{ll} &:= (n^l)^2 \mathbf{K}^{-1} - (\mathbf{B}^{l+} + \mathbf{B}^{l-}). \end{aligned}$$

Equation (2.29) can also be written as

$$\begin{pmatrix} \mathbf{v}^l - \mathbf{v}^s \\ \mathbf{v}^+ - \mathbf{v}^s \\ \mathbf{v}^- - \mathbf{v}^s \end{pmatrix} = - \begin{pmatrix} \frac{\mathbf{K}n^l}{(n^l)^2} & \frac{\mathbf{K}n^+}{(n^l)^2} & \frac{\mathbf{K}n^-}{(n^l)^2} \\ \frac{\mathbf{K}n^l}{(n^l)^2} & \frac{\mathbf{K}n^+}{(n^l)^2} + \frac{\bar{\mathbf{V}}^+ \mathbf{D}^+}{RT} & \frac{\mathbf{K}n^-}{(n^l)^2} \\ \frac{\mathbf{K}n^l}{(n^l)^2} & \frac{\mathbf{K}n^+}{(n^l)^2} & \frac{\mathbf{K}n^-}{(n^l)^2} + \frac{\bar{\mathbf{V}}^- \mathbf{D}^-}{RT} \end{pmatrix} \begin{pmatrix} \nabla \mu^l \\ \nabla \mu^+ \\ \nabla \mu^- \end{pmatrix},$$

or by

$$n^f (\mathbf{v}^l - \mathbf{v}^s) = -\frac{\mathbf{K}}{n^f} (n^l \nabla \mu^l + n^+ \nabla \mu^+ + n^- \nabla \mu^-), \quad (2.30)$$

$$c^\beta (\mathbf{v}^\beta - \mathbf{v}^l) = -\mathbf{D}^\beta \frac{\bar{\mathbf{V}}^\beta c^\beta}{RT} \nabla \mu^\beta, \quad \beta = +, -. \quad (2.31)$$

The equations (2.30) and (2.31) are the *extended Darcy's law* and the *extended Fick's law*, respectively.

The fluid velocity \mathbf{v}^f is a weighted average of the velocity of the liquid and the velocities of the ions. Since we are interested in the situation in which there are far more water molecules than ions, we approximate the velocity of the fluid by the velocity of the liquid: $\mathbf{v}^f \approx \mathbf{v}^l$. After substituting equations (2.28) into equation (2.30) and assuming $c^l + c^+ + c^-$ to be constant, the extended Darcy's law is given by

$$n^f (\mathbf{v}^f - \mathbf{v}^s) = -\mathbf{K} \left(\nabla p + (\phi^l - \phi^+) RT \nabla c^+ + (\phi^l - \phi^-) RT \nabla c^- - z^{fc} c^{fc} F \nabla \xi \right). \quad (2.32)$$

Note, that if there are no particles in the fluid ($c^+ = c^- = 0$) and there is no electrical potential field ($\xi = 0$), equation (2.32) results in the standard *Darcy's law* $n^f (\mathbf{v}^f - \mathbf{v}^s) = -\mathbf{K} \nabla p$.

After substituting equations (2.28) into equation (2.31) and assuming $c^l + c^+ + c^-$ to be constant, the extended Fick's law is given by

$$c^\beta(\mathbf{v}^\beta - \mathbf{v}^l) = -\mathbf{D}^\beta \left((2 - \phi^\beta) \nabla c^\beta + z^\beta \frac{F}{RT} c^\beta \nabla \xi + \frac{\bar{V}^\beta}{RT} c^\beta \nabla p \right), \quad \beta = +, -. \quad (2.33)$$

Note that if there is no pressure gradient, equation (2.33) is equal to the extended Fick's law as described by Barthel et al. [3]. If there is no liquid flow ($\mathbf{v}^l = \mathbf{0}$) and the particles have no charge ($z^\beta = 0$), and we have an ideal solution ($\phi^\beta = 1$), equation (2.33) is equal to Fick's first law $c^\beta \mathbf{v}^\beta = -\mathbf{D}^\beta \nabla c^\beta$ (see e.g. [39]).

2.1.3 Total set of equations

The material is described by the following equations:

$$\begin{aligned} \nabla \cdot \boldsymbol{\sigma} - \nabla p &= \mathbf{0}, \\ \frac{\partial n^\alpha}{\partial t} + \nabla \cdot (n^\alpha \mathbf{v}^\alpha) &= 0, \quad \alpha = s, f, \\ \frac{\partial (n^f c^\beta)}{\partial t} + \nabla \cdot (n^f c^\beta \mathbf{v}^\beta) &= 0, \quad \beta = +, -, \\ z^+ c^+ + z^- c^- + z^{fc} c^{fc} &= 0, \\ n^s + n^f &= 1, \end{aligned}$$

and

$$\begin{aligned} \boldsymbol{\sigma} &= 2\mu_s \boldsymbol{\epsilon}(\mathbf{u}) + \lambda_s \nabla \cdot \mathbf{u} \mathbf{I}, \\ n^f(\mathbf{v}^f - \mathbf{v}^s) &= -\mathbf{K} \left(\nabla p + (\phi^l - \phi^+) RT \nabla c^+ + (\phi^l - \phi^-) RT \nabla c^- - z^{fc} c^{fc} F \nabla \xi \right), \\ c^\beta(\mathbf{v}^\beta - \mathbf{v}^f) &= -\mathbf{D}^\beta \left((2 - \phi^\beta) \nabla c^\beta + z^\beta \frac{F}{RT} c^\beta \nabla \xi + \frac{\bar{V}^\beta}{RT} c^\beta \nabla p \right), \quad \beta = +, -, \\ \mathbf{v}^s &= \frac{\partial \mathbf{u}}{\partial t}, \end{aligned}$$

and some proper boundary conditions.

2.2 Reduction to a Two-Component Mixture Theory

In this section, the four-component mixture theory is reduced to the two-component mixture theory as described by, for example, Biot [7]. Therefore, we neglect the influence of all electrically charged particles. Then the electro-neutrality condition (2.12) is not relevant anymore. Furthermore, the mass balances for the ions (2.8) and Fick's law (2.33)

disappear. Darcy's law (2.32) is simplified by removing the concentration dependent terms. Thus, it holds:

$$\begin{aligned}\nabla \cdot \boldsymbol{\sigma} - \nabla p &= \mathbf{0}, \\ \frac{\partial n^\alpha}{\partial t} + \nabla \cdot (n^\alpha \mathbf{v}^\alpha) &= 0, \quad \alpha = s, f, \\ n^s + n^f &= 1,\end{aligned}$$

and

$$\begin{aligned}\boldsymbol{\sigma} &= 2\mu_s \boldsymbol{\varepsilon}(\mathbf{u}) + \lambda_s \nabla \cdot \mathbf{u} \mathbf{I}, \\ n^f (\mathbf{v}^f - \mathbf{v}^s) &= -\mathbf{K} \nabla p, \\ \mathbf{v}^s &= \frac{\partial \mathbf{u}}{\partial t},\end{aligned}$$

and some proper boundary conditions.

3 Two-Component Mixture Theory

3.1 Physical Model

In this chapter, the tissue is modelled by a *two-component mixture theory*, in literature also known as a biphasic theory [61], or as the theory of poroelasticity, see e.g. [2, 68, 69]. In the two-component mixture theory, the tissue is modelled as a porous solid saturated with a fluid. In the case of an intervertebral disc tissue, the porous solid skeleton represents the fibre network (collagen fibres and proteoglycans) and the fluid the interstitial fluid. For the sake of simplicity, we assume that the fluid is incompressible and Newtonian viscous, and the solid is linearly elastic. The solid can shrink only by expelling fluid into its surroundings, or swell only by attracting the fluid from its surroundings.

In the two-component mixture theory, the material behaviour is described by a set of coupled equations as described in chapter 2:

$$\begin{aligned} \nabla \cdot \boldsymbol{\sigma} - \nabla p &= \mathbf{0}, \\ \frac{\partial n^\alpha}{\partial t} + \nabla \cdot (n^\alpha \mathbf{v}^\alpha) &= 0, \quad \alpha = s, f, \\ n^s + n^f &= 1, \end{aligned} \quad (3.1)$$

and

$$\begin{aligned} \boldsymbol{\sigma} &= 2\mu_s \boldsymbol{\epsilon}(\mathbf{u}) + \lambda_s \nabla \cdot \mathbf{u} \mathbf{I}, \\ n^f (\mathbf{v}^f - \mathbf{v}^s) &= -\mathbf{K} \nabla p, \\ \mathbf{v}^s &= \frac{\partial \mathbf{u}}{\partial t}. \end{aligned} \quad (3.2)$$

The set of equations can be reduced by summing the mass balances for the solid and the fluid. This results in

$$\frac{\partial (n^s + n^f)}{\partial t} + \nabla \cdot (n^f (\mathbf{v}^f - \mathbf{v}^s)) + \nabla \cdot ((n^s + n^f) \mathbf{v}^s) = 0. \quad (3.3)$$

Using the saturation condition ($n^f + n^s = 1$) and the definition of the solid velocity, this

equation can be written as

$$\frac{\partial}{\partial t}(\nabla \cdot \mathbf{u}) + \nabla \cdot (n^f(\mathbf{v}^f - \mathbf{v}^s)) = 0. \quad (3.4)$$

In order to make the notation more compact, the *specific discharge* \mathbf{v} is introduced:

$$\mathbf{v} := n^f(\mathbf{v}^f - \mathbf{v}^s). \quad (3.5)$$

So, the total mass balance is described by

$$\frac{\partial}{\partial t}(\nabla \cdot \mathbf{u}) + \nabla \cdot \mathbf{v} = 0. \quad (3.6)$$

Further, the stress-strain relation is substituted into the momentum equation. Then, the two-component problem is described on domain Ω by the following set of equations

$$\begin{aligned} -\nabla \cdot (2\mu_s \boldsymbol{\epsilon}(\mathbf{u}) + \lambda_s \nabla \cdot \mathbf{u} \mathbf{I}) + \nabla p &= \mathbf{0} & \text{in } \Omega, \\ \mathbf{K}^{-1} \mathbf{v} + \nabla p &= \mathbf{0} & \text{in } \Omega, \\ \frac{\partial}{\partial t}(\nabla \cdot \mathbf{u}) + \nabla \cdot \mathbf{v} &= 0 & \text{in } \Omega. \end{aligned} \quad (3.7)$$

For the sake of simplicity, the following boundary conditions are considered:

$$\begin{aligned} \mathbf{u} &= \mathbf{0} & \text{on } \Gamma_u^D, \\ \mathbf{n} \cdot (2\mu_s \boldsymbol{\epsilon}(\mathbf{u}) + \lambda_s \nabla \cdot \mathbf{u} \mathbf{I} - p \mathbf{I}) &= \mathbf{g}_u^N & \text{on } \Gamma_u^N, \\ p &= 0 & \text{on } \Gamma_p^D, \\ \mathbf{n} \cdot \mathbf{v} &= \mathbf{g}_p^N & \text{on } \Gamma_p^N, \end{aligned}$$

where the Dirichlet boundaries Γ_α^D and the Neumann boundaries Γ_α^N are open portions of the total boundary Γ , such that $\Gamma_\alpha^D \cap \Gamma_\alpha^N = \emptyset$ and $\bar{\Gamma}_\alpha^D \cup \bar{\Gamma}_\alpha^N = \Gamma$. Other boundary conditions can also be considered, but they make the writing of the proofs more complicated. Furthermore, these boundary conditions are sufficient for describing compression experiments.

The porosity can be determined in the following way. We assume the components to be incompressible. Furthermore, we assume that there are no reactions by which solid is formed. Therefore the volume V^s of the solid in the deformed state is equal to the volume V_0^s of the solid in the reference state in a representative elementary volume:

$$V^s = V_0^s.$$

The tissue deformation is characterised by the *relative volume change*

$$J := \det(\nabla \mathbf{u}). \quad (3.8)$$

The mixture volume V^{tot} in the deformed state is described by

$$V^{tot} = J V_0^{tot}.$$

Now, the porosity in the deformed state is described by (figure 3.1)

$$\begin{aligned} n^f &:= \frac{V^f}{V^{tot}} = \frac{V^{tot} - V^s}{V^{tot}} = 1 - \frac{V^s}{V^{tot}} \\ &= 1 - \frac{V_0^s}{J V_0^{tot}} = 1 - \frac{n_0^s}{J} \\ &= 1 - \frac{1 - n_0^f}{J}. \end{aligned} \tag{3.9}$$

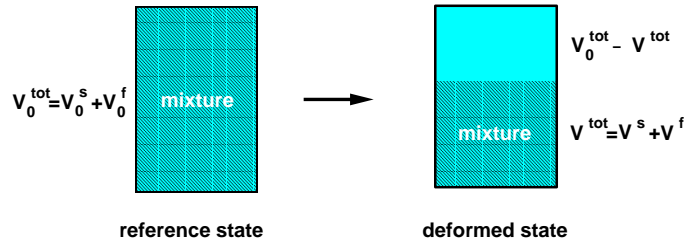


Figure 3.1 Schematic representation of the tissue deformation.

Throughout the thesis, Ω shall denote an open connected domain in \mathbb{R}^d ($d = 1, 2, 3$), with a Lipschitz continuous boundary Γ (see for example [12]).

3.2 Variational Formulation

In order to solve the coupled equations (3.7) by the finite element method, the problem is written in a variational form. Therefore, some *Hilbert spaces* and corresponding norms are needed. These spaces are defined by (see for example [12, 13, 37])

$$\begin{aligned} L_2(\Omega) &:= \{ \phi : \Omega \rightarrow \mathbb{R} \mid \int_{\Omega} \phi^2 dV < \infty \}, \\ \mathbf{L}_2(\Omega) &:= \{ \mathbf{u} : \Omega \rightarrow \mathbb{R}^d \mid \int_{\Omega} |\mathbf{u}|_2^2 dV < \infty \}, \quad d = 1, 2, 3, \\ H_1(\Omega) &:= \{ \phi \in L_2(\Omega) \mid \nabla \phi \in \mathbf{L}_2(\Omega) \}, \\ H_{1,0}(\Omega) &:= \{ \phi \in H_1(\Omega) \mid \phi = 0 \text{ on } \Gamma_p^D \}, \\ H_1(\Omega)^d &:= \{ \mathbf{u} = (u_1, u_2, \dots, u_d) \mid u_i \in H_1(\Omega), i = 1, 2, \dots, d \}, \\ H_{1,0}(\Omega)^d &:= \{ \mathbf{u} \in H_1(\Omega)^d \mid \mathbf{u} = \mathbf{0} \text{ on } \Gamma_u^D \}, \\ H(\text{div}, \Omega) &:= \{ \mathbf{u} \in \mathbf{L}_2(\Omega) \mid \nabla \cdot \mathbf{u} \in L_2(\Omega) \}, \\ H_0(\text{div}, \Omega) &:= \{ \mathbf{u} \in H(\text{div}, \Omega) \mid \mathbf{n} \cdot \mathbf{u} = 0 \text{ on } \Gamma_p^N \}. \end{aligned}$$

The corresponding norms are defined by

$$\begin{aligned}\|\phi\|_0 &:= \left(\int_{\Omega} \phi^2 d\mathbf{x} \right)^{\frac{1}{2}}, & \phi &\in L_2(\Omega), \\ \|\mathbf{u}\|_0 &:= \left(\int_{\Omega} |\mathbf{u}|_2^2 dV \right)^{\frac{1}{2}}, & \mathbf{u} &\in \mathbf{L}_2(\Omega), \\ \|\phi\|_1 &:= \left(\|\phi\|_0^2 + \|\nabla \phi\|_0^2 \right)^{\frac{1}{2}}, & \phi &\in H_1(\Omega), \\ \|\mathbf{u}\|_{\text{div}} &:= \left(\|\mathbf{u}\|_0^2 + \|\nabla \cdot \mathbf{u}\|_0^2 \right)^{\frac{1}{2}}, & \mathbf{u} &\in H(\text{div}, \Omega).\end{aligned}$$

3.2.1 Displacement-pressure formulation

The equations that describe the behaviour of a deformable two-component material, are often reduced to a set of equations with only the solid matrix displacements and the fluid pressure as unknowns. In this displacement-pressure formulation (u - p formulation), Darcy's law is substituted into the mass balance equation (3.6). In this way, the fluid fluxes are eliminated. So, the u - p problem can be described by the equations

$$\begin{aligned}-\nabla \cdot (2\mu_s \boldsymbol{\epsilon}(\mathbf{u}) + \lambda_s \nabla \cdot \mathbf{u} \mathbf{I}) + \nabla p &= \mathbf{0} & \text{in } \Omega, \\ \frac{\partial}{\partial t} (\nabla \cdot \mathbf{u}) - \nabla \cdot (\mathbf{K} \nabla p) &= 0 & \text{in } \Omega,\end{aligned}\tag{3.10}$$

with boundary conditions

$$\begin{aligned}\mathbf{u} &= \mathbf{0} & \text{on } \Gamma_u^D, \\ \mathbf{n} \cdot (2\mu_s \boldsymbol{\epsilon}(\mathbf{u}) + \lambda_s \nabla \cdot \mathbf{u} \mathbf{I} - p \mathbf{I}) &= \mathbf{g}_u^N & \text{on } \Gamma_u^N, \\ p &= 0 & \text{on } \Gamma_p^D, \\ -\mathbf{n} \cdot (\mathbf{K} \nabla p) &= \mathbf{g}_p^N & \text{on } \Gamma_p^N.\end{aligned}$$

These boundary conditions can depend on time. We assume that they do not depend on time, since we consider several stages in our experiments, as described in chapters 5 and 6, in which the boundary conditions do not change. Every stage can be considered as a new problem with a different initial condition depending on the previous stage.

In order to solve these equation by a finite element method, the first equation is multiplied by a vectorial test function \mathbf{w} and the second equation by a scalar test function q . The resulting equations are integrated over the domain Ω . In this way, a variational form is derived:

Problem 3.1 Find $(\mathbf{u}, p) \in H_{1,0}(\Omega)^d \times H_{1,0}(\Omega)$ such that

$$\begin{aligned}\mathbf{a}(\mathbf{u}, \mathbf{w}) + \mathbf{b}(\mathbf{w}, p) &= \langle \mathbf{g}_u^N, \mathbf{w} \rangle, \\ \frac{d}{dt} \mathbf{b}(\mathbf{u}, q) - \mathbf{c}(p, q) &= \langle \mathbf{g}_p^N, q \rangle,\end{aligned}\tag{3.11}$$

for every $\mathbf{w} \in H_{1,0}(\Omega)^d$ and $q \in H_{1,0}(\Omega)$.

Here

$$\begin{aligned}
a(\mathbf{u}, \mathbf{w}) &:= \int_{\Omega} 2\mu_s \boldsymbol{\epsilon}(\mathbf{u}) : \boldsymbol{\epsilon}(\mathbf{w}) + \lambda_s (\nabla \cdot \mathbf{u})(\nabla \cdot \mathbf{w}) \, dV, \\
b(\mathbf{w}, q) &:= - \int_{\Omega} \nabla \cdot \mathbf{w} \, q \, dV, \\
c(p, q) &:= \int_{\Omega} (\mathbf{K} \nabla p) \cdot \nabla q \, dV, \\
\langle \mathbf{g}_u^N, \mathbf{w} \rangle &:= \int_{\Gamma_u^N} \mathbf{g}_u^N \cdot \mathbf{w} \, dS, \\
\langle \mathbf{g}_p^N, q \rangle &:= \int_{\Gamma_p^N} \mathbf{g}_p^N \, q \, dS.
\end{aligned}$$

In these equations, a time derivative appears. The Euler implicit time discretisation is introduced, since it is a stable time discretisation. The problem to solve is now

Problem 3.2 Find $(\mathbf{u}_n, p_n) \in H_{1,0}(\Omega)^d \times H_{1,0}(\Omega)$ on time t_n , such that

$$\begin{aligned}
a(\mathbf{u}_n, \mathbf{w}) + b(\mathbf{w}, p_n) &= \langle \mathbf{g}_u^N, \mathbf{w} \rangle, \\
b(\mathbf{u}_n, q) - \Delta t \, c(q, p_n) &= b(\mathbf{u}_{n-1}, q) + \Delta t \langle \mathbf{g}_p^N, q \rangle,
\end{aligned} \tag{3.12}$$

for every $\mathbf{w} \in H_{1,0}(\Omega)^d$ and $q \in H_{1,0}(\Omega)$ and $\Delta t = t_n - t_{n-1} > 0$.

Here, the subscript $n - 1$ denotes the value of a parameter at time t_{n-1} , and the subscript n the value at the next time $t_n = t_{n-1} + \Delta t$.

A drawback of this formulation is that, when a finite element formulation is derived, the displacements and the fluid pressures are computed directly, but the fluid flux is computed a posteriori by Darcy's law. Therefore, the gradient of the pressure field is needed. This has to be approximated. So, the accuracy of the fluid flux will be less than when it is computed directly. Also, when there is locally a steep gradient in the permeability, the accuracy for the fluid flux will be poor since Darcy's law is approximated. A good accuracy can only be reached by using a locally very fine grid. This problem can be avoided by computing the fluid flux directly. This is done in the next section.

3.2.2 Displacement-pressure-velocity formulation

The displacement-pressure-velocity formulation (*u-p-v formulation*) of the two-component mixture theory employs the solid matrix displacements, the fluid pressure and the fluid flux as unknowns. The variational formulation is derived by multiplying the first equation of (3.7) by a vectorial test function \mathbf{w} , the second one by a vectorial test function \mathbf{s} and the third one by a scalar test function q . The resulting equations are integrated over the domain Ω . After applying the rules of partial integration, the variational form of two-component problem is given by

Problem 3.3 Find $(\mathbf{u}, \mathbf{v}, p) \in H_{1,0}(\Omega)^d \times H(\operatorname{div}, \Omega) \times L_2(\Omega)$ such that $\mathbf{n} \cdot \mathbf{v} = g_p^N$ on Γ_p^N and

$$\begin{aligned} a(\mathbf{u}, \mathbf{w}) &+ b(\mathbf{w}, p) &= \langle \mathbf{g}_u^N, \mathbf{w} \rangle, \\ c(\mathbf{v}, \mathbf{s}) &+ d(\mathbf{s}, p) &= 0, \\ \frac{d}{dt} b(\mathbf{u}, q) &+ d(\mathbf{v}, q) &= 0, \end{aligned} \quad (3.13)$$

for every $\mathbf{w} \in H_{1,0}(\Omega)^d$, $\mathbf{s} \in H_0(\operatorname{div}, \Omega)$, and $q \in L_2(\Omega)$.

Here

$$\begin{aligned} a(\mathbf{u}, \mathbf{w}) &:= \int_{\Omega} 2\mu_s \boldsymbol{\epsilon}(\mathbf{u}) : \boldsymbol{\epsilon}(\mathbf{w}) + \lambda_s (\nabla \cdot \mathbf{u})(\nabla \cdot \mathbf{w}) \, dV, \\ b(\mathbf{w}, q) &:= - \int_{\Omega} \nabla \cdot \mathbf{w} \, q \, dV, \\ c(\mathbf{v}, \mathbf{s}) &:= \int_{\Omega} (\mathbf{K}^{-1} \mathbf{v}) \cdot \mathbf{s} \, dV, \\ d(\mathbf{s}, q) &:= - \int_{\Omega} \nabla \cdot \mathbf{s} \, q \, dV, \\ \langle \mathbf{g}_u^N, \mathbf{w} \rangle &:= \int_{\Gamma_u^N} \mathbf{g}_u^N \cdot \mathbf{w} \, dS. \end{aligned}$$

In these equations a time derivative appears. Therefore a time discretisation is needed. A stable discretisation is the Euler implicit time discretisation. Now, the variational problem is given by

Problem 3.4 Find $(\mathbf{u}_n, \mathbf{v}_n, p_n) \in H_{1,0}(\Omega)^d \times H(\operatorname{div}, \Omega) \times L_2(\Omega)$ such that $\mathbf{n} \cdot \mathbf{v}_n = g_p^N$ on Γ_p^N and

$$\begin{aligned} a(\mathbf{u}_n, \mathbf{w}) &+ b(\mathbf{w}, p_n) &= \langle \mathbf{g}_u^N, \mathbf{w} \rangle, \\ \Delta t c(\mathbf{v}_n, \mathbf{s}) &+ \Delta t d(\mathbf{s}, p_n) &= 0, \\ b(\mathbf{u}_n, q) &+ \Delta t d(\mathbf{v}_n, q) &= b(\mathbf{u}_{n-1}, q), \end{aligned} \quad (3.14)$$

for every $\mathbf{w} \in H_{1,0}(\Omega)^d$, $\mathbf{s} \in H_0(\operatorname{div}, \Omega)$, $q \in L_2(\Omega)$, and $\Delta t = t_n - t_{n-1} > 0$.

Note that the relative fluid velocity \mathbf{v}_n can be written as

$$\mathbf{v}_n = \mathbf{v}_n^0 + \mathbf{v}_n^1, \quad (3.15)$$

where $\mathbf{v}_n^0 \in H_0(\operatorname{div}, \Omega)$ and $\mathbf{v}_n^1 \in H(\operatorname{div}, \Omega)$ such that $\mathbf{n} \cdot \mathbf{v}_n^1 = g_p^N$ on Γ_p^N . For the theoretical considerations in the following analysis, we assume that $g_p^N = 0$ without loss of generality.

In order to investigate the existence and uniqueness of the solution of the variational formulation of the two-component problem, the problem is rewritten as

Problem 3.5 Find $(\mathbf{u}_n, \mathbf{v}_n, p_n) \in H_{1,0}(\Omega)^d \times H_0(\operatorname{div}, \Omega) \times L_2(\Omega)$ such that

$$\begin{aligned} A(\mathbf{u}_n, \mathbf{v}_n; \mathbf{w}, \mathbf{s}) &+ B(\mathbf{w}, \mathbf{s}; p_n) &= F(\mathbf{w}), \\ B(\mathbf{u}_n, \mathbf{v}_n; q) &&= b(\mathbf{u}_{n-1}, q), \end{aligned} \quad (3.16)$$

for every $\mathbf{w} \in H_{1,0}(\Omega)^d$, $\mathbf{s} \in H_0(\operatorname{div}, \Omega)$ and $q \in L_2(\Omega)$.

Here

$$\begin{aligned} A(\mathbf{u}, \mathbf{v}; \mathbf{w}, \mathbf{s}) &:= a(\mathbf{w}, \mathbf{u}) + \Delta t c(\mathbf{v}, \mathbf{s}), \\ B(\mathbf{w}, \mathbf{s}; q) &:= b(\mathbf{w}, q) + \Delta t d(\mathbf{s}, q), \\ F(\mathbf{w}) &:= \langle \mathbf{g}_u^N, \mathbf{w} \rangle. \end{aligned} \quad (3.17)$$

This problem is a saddle point problem.

Lemma 3.6 *Problem 3.5 has a unique solution.*

Proof. In the proof of uniqueness of the solution, the norm on $H_{1,0}(\Omega)^d \times H_0(\operatorname{div}, \Omega)$ is used. This norm is defined by

$$\|\mathbf{w}, \mathbf{s}\|_{1,\operatorname{div}}^2 := \|\mathbf{w}\|_1^2 + \|\mathbf{s}\|_{\operatorname{div}}^2. \quad (3.18)$$

First, a general saddle point problem is considered. Then, the two-component mixture model is considered again.

In this proof, some additional definitions are needed. Let \mathcal{U} and \mathcal{P} be two Hilbert spaces, and suppose $a : \mathcal{U} \times \mathcal{U} \rightarrow \mathbb{R}$ and $b : \mathcal{P} \times \mathcal{P} \rightarrow \mathbb{R}$ are continuous bilinear forms, i.e.

$$\begin{aligned} \|a\| &:= \sup_{0 \neq \mathbf{u} \in \mathcal{U}, 0 \neq \mathbf{w} \in \mathcal{U}} \frac{|a(\mathbf{u}, \mathbf{w})|}{\|\mathbf{u}\|_{\mathcal{U}} \|\mathbf{w}\|_{\mathcal{U}}} < \infty, \\ \|b\| &:= \sup_{0 \neq \mathbf{w} \in \mathcal{U}, 0 \neq q \in \mathcal{P}} \frac{|b(\mathbf{w}, q)|}{\|\mathbf{w}\|_{\mathcal{U}} \|q\|_{\mathcal{P}}} < \infty. \end{aligned} \quad (3.19)$$

Before the problem 3.5 is considered, we recall some properties for a general saddle point problem. A general *saddle point problem* has the form

Problem 3.7 Find $(\mathbf{u}, p) \in \mathcal{U} \times \mathcal{P}$ with

$$\begin{aligned} a(\mathbf{u}, \mathbf{w}) + b(\mathbf{w}, p) &= \langle \mathbf{f}, \mathbf{w} \rangle_{\mathcal{U}' \times \mathcal{U}}, \\ b(\mathbf{u}, q) &= \langle \mathbf{g}, q \rangle_{\mathcal{P}' \times \mathcal{P}}, \end{aligned} \quad (3.20)$$

for every $\mathbf{w} \in \mathcal{U}$, and every $q \in \mathcal{P}$.

For this problem, the *kernels* of the operators B and B^t are defined by

$$\ker B := \{ \mathbf{w} \in \mathcal{U} \mid b(\mathbf{w}, q) = 0, \forall q \in \mathcal{P} \}, \quad (3.21)$$

$$\ker B^t := \{ q \in \mathcal{P} \mid b(\mathbf{w}, q) = 0, \forall \mathbf{w} \in \mathcal{U} \}. \quad (3.22)$$

The saddle point problem 3.7 has a unique solution if the following two conditions are satisfied (see for example [13]):

1. The bilinear form $a(\mathbf{u}, \mathbf{w})$ is *elliptic* on $\ker B$, i.e. there exists an $\alpha > 0$, such that

$$a(\mathbf{w}, \mathbf{w}) \geq \alpha \|\mathbf{w}\|_{\mathcal{U}}^2, \quad \forall \mathbf{w} \in \ker B. \quad (3.23)$$

2. The bilinear form $b(\mathbf{u}, q)$ satisfies the *inf-sup condition*, i.e.

$$\inf_{0 \neq q \in \mathcal{P} / \ker B^t} \sup_{0 \neq \mathbf{u} \in \mathcal{U}} \frac{b(\mathbf{u}, q)}{\|\mathbf{u}\|_{\mathcal{U}} \|q\|_{\mathcal{P}}} \geq \beta, \quad (3.24)$$

where $\beta > 0$.

Now, we return to the two-component mixture theory. Analogous to the general saddle point problem, the kernels are defined by

$$\ker B := \{(\mathbf{w}, \mathbf{s}) \in H_{1,0}(\Omega)^d \times H_0(\operatorname{div}, \Omega) \mid B(\mathbf{w}, \mathbf{s}; q) = 0, \forall q \in L_2(\Omega)\}, \quad (3.25)$$

$$\ker B^t := \{q \in L_2(\Omega) \mid B(\mathbf{w}, \mathbf{s}; q) = 0, \forall (\mathbf{w}, \mathbf{s}) \in H_{1,0}(\Omega)^d \times H_0(\operatorname{div}, \Omega)\}. \quad (3.26)$$

The two-component mixture model has a unique solution if the following two conditions are satisfied:

1. The bilinear form $A(\mathbf{u}, \mathbf{v}; \mathbf{w}, \mathbf{s})$ is elliptic on $\ker B$, i.e. there exists an $\alpha > 0$, such that

$$A(\mathbf{w}, \mathbf{s}; \mathbf{w}, \mathbf{s}) \geq \alpha \|\mathbf{w}, \mathbf{s}\|_{1,\operatorname{div}}^2, \quad \forall (\mathbf{w}, \mathbf{s}) \in \ker B. \quad (3.27)$$

2. The bilinear form $B(\mathbf{w}, \mathbf{s}; q)$ satisfies the *inf-sup condition*, i.e.

$$\inf_{0 \neq q \in L_2(\Omega) / \ker B^t} \sup_{0 \neq (\mathbf{w}, \mathbf{s}) \in H_{1,0}(\Omega)^d \times H_0(\operatorname{div}, \Omega)} \frac{B(\mathbf{w}, \mathbf{s}; q)}{\|\mathbf{w}, \mathbf{s}\|_{1,\operatorname{div}} \|q\|_0} \geq \beta, \quad (3.28)$$

where $\beta > 0$.

First, the ellipticity condition is considered. In the proof of this condition, some extra definitions with respect to the Lamé parameters and the permeability are needed:

$$\begin{aligned} \mu_{s,0} &:= \operatorname{ess\,inf}_{x \in \Omega} \mu_s > 0, \\ \lambda_{s,0} &:= \operatorname{ess\,inf}_{x \in \Omega} \lambda_s > 0, \\ K_o &:= \operatorname{ess\,sup}_{x \in \Omega} |\mathbf{K}|_2 < \infty. \end{aligned} \quad (3.29)$$

Furthermore, Korn's second inequality (see for example [12]) is needed:

Korn's second inequality *Let $\Omega \subset \mathbb{R}^d$ be an open bounded set with a piecewise smooth boundary. Then there exists a positive number $c = c(\Omega)$ such that*

$$\int_{\Omega} \boldsymbol{\epsilon}(\mathbf{w}) : \boldsymbol{\epsilon}(\mathbf{w}) \, dV \geq c \|\mathbf{w}\|_1^2, \quad \forall \mathbf{w} \in H_{1,0}(\Omega)^d. \quad (3.30)$$

Now, it is proven that $A(\mathbf{w}, \mathbf{s}; \mathbf{w}, \mathbf{s})$ fulfils the condition (3.27) using definitions (3.29) and Korn's second inequality. Let $(\mathbf{w}, \mathbf{s}) \in \ker B$, then

$$\begin{aligned}
A(\mathbf{w}, \mathbf{s}; \mathbf{w}, \mathbf{s}) &= a(\mathbf{w}, \mathbf{w}) + \Delta t c(\mathbf{s}, \mathbf{s}) \\
&\geq 2\mu_{s,o} \int_{\Omega} \boldsymbol{\epsilon}(\mathbf{w}) : \boldsymbol{\epsilon}(\mathbf{w}) \, dV + \lambda_{s,o} \int_{\Omega} (\nabla \cdot \mathbf{w})(\nabla \cdot \mathbf{w}) \, dV + \frac{\Delta t}{K_o} \int_{\Omega} \mathbf{s} \cdot \mathbf{s} \, dV \\
&\geq 2c\mu_{s,o} \|\mathbf{w}\|_1^2 + \lambda_{s,o} \|\nabla \cdot \mathbf{w}\|_0^2 + \frac{\Delta t}{K_o} \|\mathbf{s}\|_0^2 \\
&= 2c\mu_{s,o} \|\mathbf{w}\|_1^2 + \lambda_{s,o} (\Delta t)^2 \|\nabla \cdot \mathbf{s}\|_0^2 + \frac{\Delta t}{K_o} \|\mathbf{s}\|_0^2 \\
&\geq \min\left(2c\mu_{s,o}, \lambda_{s,o} (\Delta t)^2, \frac{\Delta t}{K_o}\right) \|\mathbf{w}, \mathbf{s}\|_{1,\text{div}}^2.
\end{aligned} \tag{3.31}$$

So, the ellipticity condition (3.27) is fulfilled with $\alpha = \min(2c\mu_{s,o}, \lambda_{s,o} (\Delta t)^2, \frac{\Delta t}{K_o})$.

Next, the *inf-sup* condition is considered. Before this condition is proven, the following problem is considered, see e.g. [13]:

Problem 3.8 Let $q \in L_2(\Omega)$, then there exists a unique $\phi_q \in H_{1,0}(\Omega)$ such that

$$\int_{\Omega} \nabla \phi_q \cdot \nabla \psi \, dV = \int_{\Omega} q \psi \, dV, \quad \forall \psi \in H_{1,0}(\Omega). \tag{3.32}$$

When choosing $\psi = \phi_q$, the following equation holds:

$$\|\nabla \phi_q\|_0^2 = \int_{\Omega} q \phi_q \, dV \leq \|q\|_0 \|\phi_q\|_0 \leq C(\Omega) \|q\|_0 \|\nabla \phi_q\|_0, \tag{3.33}$$

according to the *Poincaré-Friedrichs inequality*, see e.g. [12]:

$$\|\phi\|_0 \leq C(\Omega) \|\nabla \phi\|_0, \quad \forall \phi \in H_{1,0}(\Omega), \tag{3.34}$$

where $C(\Omega) > 0$.

So, we end with the inequality

$$\|\nabla \phi_q\|_0 \leq C(\Omega) \|q\|_0. \tag{3.35}$$

Note that $\nabla \phi_q \in H_0(\text{div}, \Omega)$. Now, we choose $\mathbf{s} = \nabla \phi_q$:

$$\begin{aligned}
\sup_{0 \neq (\mathbf{w}, \mathbf{s}) \in H_{1,0}(\Omega)^d \times H_0(\text{div}, \Omega)} \frac{B(\mathbf{w}, \mathbf{s}; q)}{\|\mathbf{w}, \mathbf{s}\|_{1,\text{div}}} &\geq \Delta t \sup_{0 \neq \mathbf{s} \in H_0(\text{div}, \Omega)} \frac{d(\mathbf{s}; q)}{\|\mathbf{s}\|_{\text{div}}} \\
&\geq \Delta t \frac{-\int_{\Omega} \Delta \phi_q q \, dV}{\|\nabla \phi_q\|_{\text{div}}} \\
&= \Delta t \frac{\|q\|_0^2}{(\|\nabla \phi_q\|_0^2 + \|q\|_0^2)^{1/2}} \\
&\geq \frac{\Delta t}{(1 + C(\Omega)^2)^{1/2}} \|q\|_0.
\end{aligned} \tag{3.36}$$

So, condition (3.28) holds with $\beta = \Delta t(1 + C(\Omega)^2)^{-1/2}$.

Since conditions (3.27) and (3.28) are fulfilled, the continuous variational formulation of the two-component mixture theory has a unique solution. Note that α and β depend on Δt . ■

3.3 Finite Element Models

Both variational formulations described in the previous section, can be used to derive a finite element model.

3.3.1 Displacement-pressure finite element model

The displacement-pressure equations (3.12) are solved numerically by means of the finite element method. In order to do so, the total domain Ω is split up into a number of subdomains $\omega \in \Omega_h$.

We refer to the *polynomial spaces* $P^n(\Omega_h)$ as a set of piecewise polynomials of degree $\leq n$. $P_0^n(\Omega_h)$ means that the value of the piecewise polynomials of degree $\leq n$ is zero at the Dirichlet boundary.

The problem to solve is:

Problem 3.9 Find $(\mathbf{u}_h, p_h) \in P_0^1(\Omega_h)^d \times P_0^1(\Omega_h)$, i.e. $\mathbf{u}_h = \mathbf{0}$ on Γ_u^D and $p_h = 0$ on Γ_p^D , such that at time t_n , for every $\mathbf{w}_h \in P_0^1(\Omega_h)^d$ and for every $q_h \in P_0^1(\Omega_h)$, it holds that

$$\begin{aligned} a(\mathbf{u}_{h,n}, \mathbf{w}_h) + b(\mathbf{w}_h, p_{h,n}) &= \langle \mathbf{g}_u^N, \mathbf{w}_h \rangle, \\ b(\mathbf{u}_{h,n}, q_h) - \Delta t c(p_{h,n}, q_h) &= b(\mathbf{u}_{h,n-1}, q_h) + \Delta t \langle \mathbf{g}_p^N, q_h \rangle. \end{aligned} \quad (3.37)$$

The functions \mathbf{u}_h and p_h , and their basis functions are expressed as

$$\begin{aligned} \mathbf{u}_h(\mathbf{x}, t) &:= \sum_{i=1}^I \tilde{u}_i(t) \mathbf{w}_i(\mathbf{x}), \\ p_h(\mathbf{x}, t) &:= \sum_{j=1}^J \tilde{p}_j(t) q_j(\mathbf{x}). \end{aligned}$$

In this way, problem 3.9 can be written in a matrix-vector notation:

$$\begin{bmatrix} \mathbf{A} & \mathbf{B} \\ \mathbf{B}^T & -\Delta t \mathbf{C} \end{bmatrix} \begin{bmatrix} \mathbf{u}_n \\ p_n \end{bmatrix} = \begin{bmatrix} \mathbf{F}_1 \\ \mathbf{B}^T \mathbf{u}_{n-1} + \Delta t \mathbf{F}_2 \end{bmatrix}, \quad (3.38)$$

where

$$\begin{aligned}
\mathbf{u} &:= [\tilde{\mathbf{u}}_1 \ \tilde{\mathbf{u}}_2 \ \cdots \ \tilde{\mathbf{u}}_I]^T, \\
\mathbf{p} &:= [\tilde{p}_1 \ \tilde{p}_2 \ \cdots \ \tilde{p}_J]^T, \\
\mathbf{A}_{ij} &:= \int_{\Omega} 2\mu_s \boldsymbol{\epsilon}(\mathbf{w}_j) : \boldsymbol{\epsilon}(\mathbf{w}_i) + \lambda_s (\nabla \cdot \mathbf{w}_j) (\nabla \cdot \mathbf{w}_i) \, dV, \\
\mathbf{B}_{ij} &:= - \int_{\Omega} \nabla \cdot \mathbf{w}_i q_j \, dV, \\
\mathbf{C}_{ij} &:= \int_{\Omega} (\mathbf{K} \nabla q_j) \cdot (\nabla q_i) \, dV, \\
\mathbf{F}_{1,i} &:= \int_{\Gamma_u^N} \mathbf{g}_u^N \cdot \mathbf{w}_i \, dS, \\
\mathbf{F}_{2,i} &:= \int_{\Gamma_p^N} \mathbf{g}_p^N q_i \, dS.
\end{aligned}$$

A drawback of this u - p formulation, is that the mass balance of the system is not enforced, because an extra error is made by the computation, a posteriori, for the fluid flow. This error arises in the approximating of the derivatives of the fluid pressure field, which are used to compute the fluid flow via Darcy's law. This extra error can be large if there are large differences in the values for the permeabilities [50]. This error can be avoided by a mixed finite element method as shown in the next section.

3.3.2 Mixed finite element model

Problem 3.3 is used to derive a mixed finite element model of the two-component mixture model. In this finite element model, the infinite-dimensional spaces $H_{1,0}(\Omega)^d$, $H_0(\text{div}, \Omega)$ and $L_2(\Omega)$ are approximated by finite-dimensional spaces \mathcal{U}_h , \mathcal{V}_h and \mathcal{P}_h . Therefore, the total domain Ω is split up into a number of subdomains $\omega \in \Omega_h$. We introduce a collection $e \in E_h$ of edges of subdomains $\omega \in \Omega_h$ in the two-dimensional case or the collection $e \in E_h$ of faces of subdomains $\omega \in \Omega_h$ in the three-dimensional case. The subdomains are chosen such that Γ_p^N is described by a number of edges or faces.

In this way, the variational problem 3.4 is approximated by

Problem 3.10 Find $(\mathbf{u}_h, \mathbf{v}_h, p_h) \in \mathcal{U}_h \times \mathcal{V}_h \times \mathcal{P}_h$ such that for every $(\mathbf{w}_h, \mathbf{s}_h, q_h) \in \mathcal{U}_h \times \mathcal{V}_h \times \mathcal{P}_h$,

$$\begin{aligned}
a(\mathbf{u}_{h,n}, \mathbf{w}_h) &+ b(\mathbf{w}_h, p_{h,n}) &= \langle \mathbf{g}_u^N, \mathbf{w}_h \rangle, \\
\Delta t c(\mathbf{v}_{h,n}, \mathbf{s}_h) &+ \Delta t d(\mathbf{s}_h, p_{h,n}) &= \mathbf{0}, \\
b(\mathbf{u}_{h,n}, q_h) &+ \Delta t d(\mathbf{v}_{h,n}, q_h) &= b(\mathbf{u}_{h,n-1}, q_h).
\end{aligned}$$

Now, we are looking for the lowest order finite element spaces \mathcal{U}_h , \mathcal{V}_h and \mathcal{P}_h such that the approximated problem also has a unique solution. For the theoretical consideration in the following analysis, we assume that $\mathbf{g}_p^N = \mathbf{0}$ without loss of generality.

In order to do so, some finite element spaces have to be introduced. The first ones are called *Raviart-Thomas spaces* [13]. The Raviart-Thomas space $RT^0(\omega)$ is the space of linear vectorial functions \mathbf{u} on ω , such that $\mathbf{n} \cdot \mathbf{u}$ is constant on edges or faces. Now, some other Raviart-Thomas spaces are defined by

$$\begin{aligned} RT_{-1}^0(\Omega_h) &:= \{\mathbf{u} \in \mathbf{L}_2(\Omega) \mid \mathbf{u}|_\omega \in RT^0(\omega), \quad \forall \omega \in \Omega_h\}, \\ RT_0^0(\Omega_h) &:= \{\mathbf{u} \in RT_{-1}^0(\Omega_h) \mid \text{the normal component of } \mathbf{u} \text{ is continuous} \\ &\quad \text{across the interelement boundaries}\} \\ &= RT_{-1}^0(\Omega_h) \cap H(\text{div}, \Omega), \\ RT_{0,0}^0(\Omega_h) &:= \{\mathbf{u} \in RT_0^0(\Omega_h) \mid \mathbf{n} \cdot \mathbf{u} = 0 \text{ on } \Gamma_p^N\} \\ &= RT_{-1}^0(\Omega_h) \cap H_0(\text{div}, \Omega). \end{aligned} \tag{3.39}$$

The finite dimensional space $RT_{0,0}^0(\Omega_h)$ is spanned by linearly independent vectorial basis functions \mathbf{v}_i , $i = 1, \dots, I$, such that

$$\int_{e_j} \mathbf{n}_j \cdot \mathbf{v}_i dS = \delta_{ij}, \quad i, j = 1, \dots, I,$$

where \mathbf{n}_j is the normal vector of edge or face e_j . The normal is directed outwards when its on the Dirichlet edge or face.

Other spaces we need, are called multiplier spaces [13]. The multiplier space $M^0(\omega)$ is the one-dimensional space on constant scalar functions on $\omega \in \Omega_h$. Then, another multiplier space is defined by

$$M_{-1}^0(\Omega_h) := \{p \in L_2(\Omega) \mid p|_\omega \in M^0(\omega), \quad \forall \omega \in \Omega_h\}. \tag{3.40}$$

The finite dimensional space $M_{-1}^0(\Omega_h)$ is spanned by linearly independent scalar basis functions ψ_j , $j = 1, \dots, J$, such that

$$\psi_i(\mathbf{x}) = \delta_{ij}, \quad \mathbf{x} \in \Omega_j, \quad i, j = 1, \dots, J.$$

Lemma 3.11 *The approximated variational problem 3.10 has a unique solution if $\mathcal{U}_h = P_0^1(\Omega_h)^d$, $\mathcal{V}_h = RT_{0,0}^0(\Omega_h)$, and $\mathcal{P}_h = M_{-1}^0(\Omega_h)$.*

Proof. In order to prove this lemma, it has to be checked whether the discrete ellipticity condition is fulfilled and whether the discrete *inf-sup* condition, also called *LBB-condition*, is fulfilled.

First, the discrete ellipticity condition is checked. Therefore, the kernels of the discrete operators B_h and B_h^t are defined by

$$\ker B_h := \{(\mathbf{w}_h, \mathbf{s}_h) \in P_0^1(\Omega_h)^d \times RT_{0,0}^0(\Omega_h) \mid B(\mathbf{w}_h, \mathbf{s}_h; q)_h = 0, \quad \forall q_h \in M_{-1}^0(\Omega_h)\}, \tag{3.41}$$

$$\ker B_h^t := \{q \in M_{-1}^0(\Omega_h) \mid B(\mathbf{w}_h, \mathbf{s}_h; q)_h = 0, \quad \forall (\mathbf{w}_h, \mathbf{s}_h) \in P_0^1(\Omega_h)^d \times RT_{0,0}^0(\Omega_h)\}. \tag{3.42}$$

Next, a projection is used with the property that for every $q \in L_2(\Omega)$ there is a $\Pi_h q \in M_{-1}^0(\Omega_h)$ such that

$$\int_{\Omega} (q - \Pi_h q) r \, dV = 0, \quad \forall r \in M_{-1}^0(\Omega_h). \quad (3.43)$$

Let $(\mathbf{w}, \mathbf{s}) \in P_0^1(\Omega_h)^d \times RT_{0,0}^0(\Omega_h)$ and $q \in L_2(\Omega)$, then $\nabla \cdot \mathbf{w} \in M_{-1}^0(\Omega_h)$ and $\nabla \cdot \mathbf{s} \in M_{-1}^0(\Omega_h)$. So,

$$\int_{\Omega} \nabla \cdot \mathbf{w} q \, dV + \Delta t \int_{\Omega} \nabla \cdot \mathbf{s} q \, dV = \int_{\Omega} \nabla \cdot \mathbf{w} \Pi_h q \, dV + \Delta t \int_{\Omega} \nabla \cdot \mathbf{s} \Pi_h q \, dV. \quad (3.44)$$

This means that $\ker B_h \subset \ker B$. Thus, $A(\mathbf{w}_h, \mathbf{s}_h; \mathbf{w}_h, \mathbf{s}_h)$ is elliptic on $\ker B_h$, since $A(\mathbf{w}, \mathbf{s}; \mathbf{w}, \mathbf{s})$ is elliptic on $\ker B$.

Next, the LBB-condition is considered. A projection is used for \mathbf{s} : for every $\mathbf{s} \in H_0(\text{div}; \Omega)$ there exists a $\Pi_h \mathbf{s} \in RT_{0,0}^0(\Omega_h)$, such that

$$\int_e \mathbf{n} \cdot (\mathbf{s} - \Pi_h \mathbf{s}) \, dS = 0, \quad \forall e \in E_h. \quad (3.45)$$

Furthermore it holds that

$$\int_{\omega} \nabla \cdot (\mathbf{s} - \Pi_h \mathbf{s}) \, dV = \int_{\partial\omega} \mathbf{n} \cdot (\mathbf{s} - \Pi_h \mathbf{s}) \, dS = 0, \quad \forall \omega \in \Omega_h. \quad (3.46)$$

Since

$$\int_{\omega} \nabla \cdot \mathbf{s} - \Pi_h(\nabla \cdot \mathbf{s}) \, dV = 0, \quad (3.47)$$

it holds that

$$\nabla \cdot (\Pi_h \mathbf{s}) = \Pi_h(\nabla \cdot \mathbf{s}). \quad (3.48)$$

For the projection Π_h it holds that

$$\|\Pi_h \mathbf{s}\|_{\text{div}} \leq C_p \|\mathbf{s}\|_{\text{div}}. \quad (3.49)$$

Next, the proof is analogous to section 3.2.2. The following problem is considered:

Problem 3.12 Let $q_h \in M_{-1}^0(\Omega_h)$, then there exists a unique $\phi_h \in H_{1,0}(\Omega)$ such that

$$\int_{\Omega} \nabla \phi_h \cdot \nabla \psi \, dV = \int_{\Omega} q_h \psi \, dV, \quad \forall \psi \in H_{1,0}(\Omega). \quad (3.50)$$

When choosing $\psi = \phi_h$, it follows

$$\|\nabla \phi_h\|_0 \leq C(\Omega) \|q_h\|_0, \quad (3.51)$$

where $C(\Omega) \geq 0$.

Note that $\nabla \phi_h \in H_0(\text{div}, \Omega)$. Further,

$$\int_{\Omega} \Delta \phi_h r \, dV = \int_{\Omega} \nabla \cdot (\Pi_h(\nabla \phi_h)) r \, dV, \quad r \in M_{-1}^0(\Omega_h). \quad (3.52)$$

Now, we choose $\mathbf{s}_h = \Pi_h(\nabla \phi_h)$:

$$\begin{aligned} \sup_{0 \neq (\mathbf{w}_h, \mathbf{s}_h) \in P_0^1(\Omega_h)^d \times RT_{0,0}^0(\text{div}, \Omega)} \frac{B(\mathbf{w}_h, \mathbf{s}_h; \mathbf{q}_h)}{\|\mathbf{w}_h, \mathbf{s}_h\|_{1, \text{div}}} &\geq \Delta t \sup_{0 \neq \mathbf{s}_h \in RT_{0,0}^0(\text{div}, \Omega)} \frac{d(\mathbf{s}_h; \mathbf{q}_h)}{\|\mathbf{s}_h\|_{\text{div}}} \\ &\geq \Delta t \frac{-\int_{\Omega_h} \nabla \cdot (\Pi_h(\nabla \phi_h)) \mathbf{q}_h \, dV}{\|\Pi_h(\nabla \phi_h)\|_{\text{div}}} \\ &\geq \Delta t \frac{-\int_{\Omega_h} \Delta \phi_h \mathbf{q}_h \, dV}{C_p \|\nabla \phi_h\|_{\text{div}}} \\ &= \Delta t \frac{\|\mathbf{q}_h\|_0^2}{C_p (\|\nabla \phi_h\|_0^2 + \|\mathbf{q}_h\|_0^2)^{1/2}} \\ &\geq \frac{\Delta t}{C_p (1 + C(\Omega)^2)^{1/2}} \|\mathbf{q}\|_0. \end{aligned} \quad (3.53)$$

So, condition (3.28) holds with $\beta = \Delta t C_p^{-1} (1 + C(\Omega)^2)^{-1/2}$.

Since conditions (3.27) and (3.28) are fulfilled, the continuous variational formulation of the two-component mixture theory has a unique solution. Note that α and β depend on Δt . \blacksquare

The function $\mathbf{u}_h \in P_0^1(\Omega_h)^d$, $\mathbf{v}_h \in RT_{0,0}^0(\Omega_h)$ and $p_h \in M_{-1}^0(\Omega_h)$, and their basis functions are expressed as

$$\begin{aligned} \mathbf{u}_h(\mathbf{x}, t) &:= \sum_{i=1}^I \tilde{\mathbf{u}}_i(t) \mathbf{w}_i(\mathbf{x}), \\ \mathbf{v}_h(\mathbf{x}, t) &:= \sum_{j=1}^J \tilde{\mathbf{v}}_j(t) \mathbf{s}_j(\mathbf{x}), \\ p_h(\mathbf{x}, t) &:= \sum_{k=0}^K \tilde{p}_k(t) q_k(\mathbf{x}). \end{aligned}$$

Substitution in the discrete variational formulation leads to

$$\begin{bmatrix} \mathbf{A} & \mathbf{0} & \mathbf{B} \\ \mathbf{0} & \Delta t \mathbf{C} & \Delta t \mathbf{D} \\ \mathbf{B}^T & \Delta t \mathbf{D}^T & \mathbf{0} \end{bmatrix} \begin{bmatrix} \mathbf{u}_n \\ \mathbf{v}_n \\ \mathbf{p}_n \end{bmatrix} = \begin{bmatrix} \mathbf{F}_1 \\ \mathbf{0} \\ \mathbf{B}^T \mathbf{u}_{n-1} \end{bmatrix}, \quad (3.54)$$

where,

$$\begin{aligned}
\mathbf{u} &:= [\tilde{u}_1 \ \tilde{u}_2 \ \dots \ \tilde{u}_I]^T, \\
\mathbf{v} &:= [\tilde{v}_1 \ \tilde{v}_2 \ \dots \ \tilde{v}_J]^T, \\
\mathbf{p} &:= [\tilde{p}_1 \ \tilde{p}_2 \ \dots \ \tilde{p}_K]^T, \\
A_{ij} &= \int_{\Omega} 2\mu_s \boldsymbol{\epsilon}(\mathbf{w}_j) : \boldsymbol{\epsilon}(\mathbf{w}_i) + \lambda_s (\nabla \cdot \mathbf{w}_j)(\nabla \cdot \mathbf{w}_i) \, dV, \\
B_{ij} &:= - \int_{\Omega} (\nabla \cdot \mathbf{w}_i) q_j \, dV, \\
C_{ij} &:= \int_{\Omega} (\mathbf{K}^{-1} \mathbf{s}_j) \cdot \mathbf{s}_i \, dV, \\
D_{ij} &:= - \int_{\Omega} \nabla \cdot \mathbf{s}_j q_i \, dV, \\
F_{1,i} &:= \int_{\Gamma_N} \mathbf{g}_u^N \cdot \mathbf{w}_i \, dS.
\end{aligned}$$

The disadvantage of modelling the two-component mixture theory in this mixed finite element method is that it results in very large and sparse matrices A , B , C and D , especially if the domain is three-dimensional. We would like to reduce the system without losing the advantages of the displacement-pressure-velocity formulation. Therefore, we introduce a mixed-hybrid finite element model that is discussed in the next section.

3.3.3 Mixed-hybrid finite element model

In the mixed-hybrid finite element model a Lagrange multiplier is introduced, that enforces the continuity of the normal component of the fluxes \mathbf{v} across the inter element boundaries. Therefore, an approximation of the Dirichlet boundary condition is defined by

$$\int_e (g_h^D - g^D) \, dS = 0, \quad \forall e \in E_h. \quad (3.55)$$

Now, some additional multiplier spaces are defined, see e.g. [50]:

$$\begin{aligned}
M_{-1}^0(E_h) &:= \{\lambda \in H^{1/2}(\bigcup_{e \in E_h} e) \mid \lambda_e \in M^0(e), \quad \forall e \in E_h\}, \\
M_{-1,0}^0(E_h) &:= \{\lambda \in M_{-1}^0(E_h) \mid \lambda = 0 \text{ on } \Gamma_p^D\}.
\end{aligned} \quad (3.56)$$

It follows that if $\mathbf{v} \in RT_{-1}^0(\Omega_h)$, then $\mathbf{v} \in RT_{0,0}^0(\Omega_h)$ if, and only if,

$$\sum_{\omega \in \Omega_h} \int_{\partial\omega} \mathbf{n} \cdot \mathbf{v} \, \mu \, dS = 0, \quad \forall \mu \in M_{-1,0}^0(E_h), \quad (3.57)$$

where \mathbf{n} is the outward normal to $\partial\omega$.

So, the mixed-hybrid finite element model of the two-component mixture theory is as follows

Problem 3.13 Find $(\mathbf{u}_h, \mathbf{v}_h, p_h, \lambda_h) \in P_0^1(\Omega_h)^d \times RT_{-1}^0(\Omega_h) \times M_{-1}^0(\Omega_h) \times M_{-1,0}^0(E_h)$ such that for every $(\mathbf{w}_h, \mathbf{s}_h, q_h, \mu_h) \in P_0^1(\Omega_h)^d \times RT_{-1}^0(\Omega_h) \times M_{-1}^0(\Omega_h) \times M_{-1,0}^0(E_h)$,

$$\begin{aligned} a(\mathbf{u}_{h,n}, \mathbf{w}_h) &+ b(\mathbf{w}_h, p_{h,n}) &= f_1(\mathbf{w}_h), \\ b(\mathbf{u}_{h,n}, \mathbf{q}_h) &+ \Delta t c(\mathbf{v}_{h,n}, \mathbf{s}_h) + \Delta t d(\mathbf{s}_h, p_{h,n}) + \Delta t e(\mathbf{s}_h, \lambda_h) &= \mathbf{0}, \\ &+ \Delta t d(\mathbf{v}_{h,n}, q_h) &= b(\mathbf{u}_{h,n-1}, q_h), \\ &+ \Delta t e(\mathbf{v}_{h,n}, \mu_h) &= \Delta t f_2(\mu_h), \end{aligned}$$

where,

$$\begin{aligned} a(\mathbf{u}_h, \mathbf{w}_h) &:= \int_{\Omega} 2\mu_s \boldsymbol{\epsilon}(\mathbf{u}_h) : \boldsymbol{\epsilon}(\mathbf{w}_h) + \lambda_s (\nabla \cdot \mathbf{u}_h) (\nabla \cdot \mathbf{w}_h) dV, \\ b(\mathbf{w}_h, p_h) &:= - \int_{\Omega} \nabla \cdot \mathbf{w}_h p_h dV, \\ c(\mathbf{v}_h, \mathbf{s}_h) &:= \int_{\Omega} (\mathbf{K}^{-1} \mathbf{v}_h) \cdot \mathbf{s}_h dV, \\ d(\mathbf{s}_h, p_h) &:= - \sum_{\omega \in \Omega_h} \int_{\omega} \nabla \cdot \mathbf{s}_h p_h dV, \\ e(\mathbf{s}_h, \lambda_h) &:= \sum_{\omega \in \Omega_h} \int_{\partial \omega} \mathbf{n} \cdot \mathbf{s}_h \lambda_h dS, \\ f_1(\mathbf{w}_h) &:= \int_{\Gamma_u^N} \mathbf{g}_u^N \cdot \mathbf{w}_h dS, \\ f_2(\mu_h) &:= \int_{\Gamma_p^N} \mathbf{g}_p^N \mu_h dS. \end{aligned}$$

Now, the discrete form of the functions \mathbf{u}_h , \mathbf{v}_h , p_h and λ_h and their corresponding basis functions are introduced. These functions can be expressed as

$$\begin{aligned} \mathbf{u}_h(\mathbf{x}, t) &:= \sum_{i=1}^I \tilde{u}_i(t) \mathbf{w}_i(\mathbf{x}), \\ \mathbf{v}_h(\mathbf{x}, t) &:= \sum_{j=1}^J \tilde{v}_j(t) \mathbf{s}_j(\mathbf{x}), \\ p_h(\mathbf{x}, t) &:= \sum_{k=1}^K \tilde{p}_k(t) q_k(\mathbf{x}), \\ \lambda_h(\mathbf{x}, t) &:= \sum_{l=1}^L \tilde{\lambda}_l(t) \mu_l(\mathbf{x}). \end{aligned}$$

By substituting these functions into the variational formulation, the following system is

derived

$$\begin{bmatrix} \mathbf{A} & \mathbf{0} & \mathbf{B} & \mathbf{0} \\ \mathbf{0} & \Delta t \mathbf{C} & \Delta t \mathbf{D} & \Delta t \mathbf{E} \\ \mathbf{B}^T & \Delta t \mathbf{D}^T & \mathbf{0} & \mathbf{0} \\ \mathbf{0} & \Delta t \mathbf{E}^T & \mathbf{0} & \mathbf{0} \end{bmatrix} \begin{bmatrix} \mathbf{u}_n \\ \mathbf{v}_n \\ \mathbf{p}_n \\ \lambda_n \end{bmatrix} = \begin{bmatrix} \mathbf{F}_1 \\ \mathbf{0} \\ \mathbf{B}^T \mathbf{u}_{n-1} \\ \Delta t \mathbf{F}_2 \end{bmatrix}, \quad (3.58)$$

where

$$\begin{aligned} \mathbf{u} &:= [\tilde{\mathbf{u}}_1 \ \tilde{\mathbf{u}}_2 \ \dots \ \tilde{\mathbf{u}}_I]^T, \\ \mathbf{v} &:= [\tilde{\mathbf{v}}_1 \ \tilde{\mathbf{v}}_2 \ \dots \ \tilde{\mathbf{v}}_J]^T, \\ \mathbf{p} &:= [\tilde{\mathbf{p}}_1 \ \tilde{\mathbf{p}}_2 \ \dots \ \tilde{\mathbf{p}}_K]^T, \\ \lambda &:= [\tilde{\lambda}_1 \ \tilde{\lambda}_2 \ \dots \ \tilde{\lambda}_L]^T, \\ \mathbf{A}_{ij} &:= \int_{\Omega} 2\mu_s \boldsymbol{\epsilon}(\mathbf{w}_i) : \boldsymbol{\epsilon}(\mathbf{w}_j) \, dV + \int_{\Omega} \lambda_s (\nabla \cdot \mathbf{w}_i) (\nabla \cdot \mathbf{w}_j) \, dV, \\ \mathbf{B}_{ij} &:= - \int_{\Omega} (\nabla \cdot \mathbf{w}_i) q_j \, dV, \\ \mathbf{C}_{ij} &:= \int_{\Omega} (\mathbf{K}^{-1} \mathbf{s}_j) \cdot \mathbf{s}_i \, dV, \\ \mathbf{D}_{ij} &:= - \int_{\omega_j} \nabla \cdot \mathbf{s}_i \, dV, \\ \mathbf{E}_{ij} &:= \int_{\partial \omega_j} \mathbf{n} \cdot \mathbf{s}_i \, dS, \\ \mathbf{F}_{1,i} &:= \int_{\Gamma_u^N} \mathbf{g}_u^N \cdot \mathbf{w}_i \, dS, \\ \mathbf{F}_{2,i} &:= \int_{\Gamma_p^N} \mathbf{g}_p^N \mu_i \, dS. \end{aligned}$$

\mathbf{C} is a symmetric positive definite block-matrix. So, it has an element-wise inverse \mathbf{C}^{-1} . Using this property, it follows:

$$\mathbf{v}_n = \mathbf{C}^{-1}(-\mathbf{D} \mathbf{p}_n - \mathbf{E} \lambda_n). \quad (3.59)$$

This can be substituted into the system of coupled equations:

$$\begin{bmatrix} \mathbf{A} & \mathbf{B} & \mathbf{0} \\ \mathbf{B}^T & -\Delta t \mathbf{D}^T \mathbf{C}^{-1} \mathbf{D} & -\Delta t \mathbf{D}^T \mathbf{C}^{-1} \mathbf{E} \\ \mathbf{0} & -\Delta t \mathbf{E}^T \mathbf{C}^{-1} \mathbf{D} & -\Delta t \mathbf{E}^T \mathbf{C}^{-1} \mathbf{E} \end{bmatrix} \begin{bmatrix} \mathbf{u}_n \\ \mathbf{p}_n \\ \lambda_n \end{bmatrix} = \begin{bmatrix} \mathbf{F}_1 \\ \mathbf{B}^T \mathbf{u}_{n-1} \\ \Delta t \mathbf{F}_2 \end{bmatrix}. \quad (3.60)$$

Note that $\mathbf{D}^T \mathbf{C}^{-1} \mathbf{D}$ is a diagonal matrix with positive diagonal entries.

Eventually, we obtain

$$\mathbf{p}_n = (\mathbf{D}^T \mathbf{C}^{-1} \mathbf{D})^{-1} \left(\frac{\mathbf{B}^T}{\Delta t} \mathbf{u}_n - \frac{\mathbf{B}^T}{\Delta t} \mathbf{u}_{n-1} - (\mathbf{D}^T \mathbf{C}^{-1} \mathbf{E}) \lambda_n \right). \quad (3.61)$$

So, the system that has to be solved reduces to

$$\begin{bmatrix} \mathbf{A}_* & \mathbf{B}_* \\ \mathbf{B}_*^T & -\Delta t \mathbf{C}_* \end{bmatrix} \begin{bmatrix} \mathbf{u}_n \\ \lambda_n \end{bmatrix} = \begin{bmatrix} \tilde{\mathbf{F}}_*^1 \\ \tilde{\mathbf{F}}_*^2 \end{bmatrix}, \quad (3.62)$$

where

$$\begin{aligned} \mathbf{A}_* &:= \mathbf{A} + \frac{1}{\Delta t} \mathbf{B}(\mathbf{D}^T \mathbf{C}^{-1} \mathbf{D})^{-1} \mathbf{B}^T, \\ \mathbf{B}_* &:= -\mathbf{B}(\mathbf{D}^T \mathbf{C}^{-1} \mathbf{D})^{-1} (\mathbf{D}^T \mathbf{C}^{-1} \mathbf{E}), \\ \mathbf{C}_* &:= -(\mathbf{E}^T \mathbf{C}^{-1} \mathbf{D})(\mathbf{D}^T \mathbf{C}^{-1} \mathbf{D})^{-1} (\mathbf{D}^T \mathbf{C}^{-1} \mathbf{E}) + \mathbf{E}^T \mathbf{C}^{-1} \mathbf{E}, \\ \tilde{\mathbf{F}}_*^1 &:= \mathbf{F}_1 + \frac{1}{\Delta t} \mathbf{B}(\mathbf{D}^T \mathbf{C}^{-1} \mathbf{D})^{-1} \mathbf{B}^T \mathbf{u}_{n-1}, \\ \tilde{\mathbf{F}}_*^2 &:= \Delta t \mathbf{F}_2 - \mathbf{B}(\mathbf{D}^T \mathbf{C}^{-1} \mathbf{D})^{-1} (\mathbf{D}^T \mathbf{C}^{-1} \mathbf{E}) \mathbf{u}_{n-1}. \end{aligned}$$

The matrices \mathbf{A}_* and \mathbf{C}_* are positive definite matrices (see [50]).

3.4 Examples

3.4.1 One-dimensional example

A one-dimensional confined compression experiment is considered (figure 3.2). In such experiment, a force is applied by an impermeable piston at one side of the sample. At the other side, the fluid can flow out freely, but solid displacements are not possible. The rest of the cylindrical sample is enclosed in an impermeable ring. So, the experiment can be described by a one-dimensional model.

The boundary conditions are as follows (figure 3.2): the first boundary condition is a Dirichlet boundary condition for the displacements: $u(0, t) = 0$. The second boundary condition is $p(0, t) = 0$. So, the material fixed at $x = 0$ and there is a free fluid outlet at $x = 0$. At $x = L$ (at the other side of the material), a force F is applied. At that side, no fluid flux is allowed.

The behaviour of the solution is analysed by letting the time step going to zero ($\Delta t \rightarrow 0$). This may cause problems, since for example the ellipticity condition (3.27) depends on Δt . From earlier studies, it appeared that when Δt was chosen smaller than a critical value, oscillations in the solution occurred. For the sake of simplicity, it is assumed that the material parameters (the permeability K and the Lamé parameters μ_s and λ_s) have the same value over the whole domain. Further, it is assumed that these parameters do not depend on the deformation of the solid matrix. A uniform mesh is used with element length h .

Displacement-pressure finite element model

Since a one-dimensional model is used, problem 3.9 reduces to

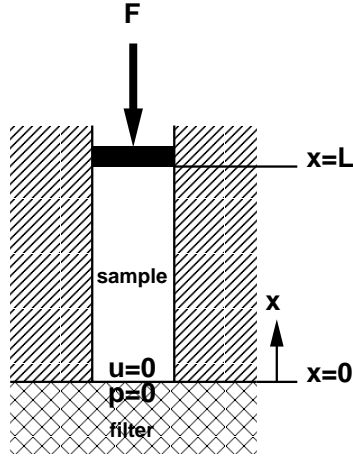


Figure 3.2 Schematic representation of the confined compression experiment.

Problem 3.14 Find $(u_h, p_h) \in P_0^1(\Omega_h) \times P_0^1(\Omega_h)$ such that on time t_n , for every $w_h \in P_0^1(\Omega_h)$ and for every $q_h \in P_0^1(\Omega_h)$,

$$\begin{aligned} a(u_{h,n}, w_h) + b(w_h, p_{h,n}) &= \langle \mathbf{g}_u^N, w_h \rangle, \\ b(u_{h,n}, q_h) - \Delta t c(q_h, p_{h,n}) &= b(u_{h,n-1}, q_h) + \Delta t \langle \mathbf{g}_p^N, q_h \rangle, \end{aligned} \quad (3.63)$$

where,

$$\begin{aligned} \Delta t &:= t_n - t_{n-1}, \\ a(u_h, w_h) &:= (2\mu_s + \lambda_s) \int_0^L \left(\frac{d}{dx} u_h \frac{d}{dx} w_h \right) dx, \\ b(w_h, p_h) &:= - \int_0^L p_h \frac{d}{dx} w_h dx, \\ c(q_h, p_h) &:= K \int_0^L \frac{d}{dx} q_h \frac{d}{dx} p_h dx, \\ \langle \mathbf{g}_u^N, w_h \rangle &:= \mathbf{g}_u^N, \\ \langle \mathbf{g}_p^N, q_h \rangle &:= \mathbf{g}_p^N, \end{aligned}$$

and L is the size of the material.

The functions u_h and p_h , and their basis functions are expressed as

$$\begin{aligned} u_h(x, t) &:= \sum_{i=1}^I \tilde{u}_i(t) w_i(x), \\ p_h(x, t) &:= \sum_{j=1}^J \tilde{p}_j(t) q_j(x). \end{aligned}$$

In this way, problem 3.14 can be written in matrix-vector notation

$$\begin{bmatrix} \mathbf{A} & \mathbf{B} \\ \mathbf{B}^T & -\Delta t \mathbf{C} \end{bmatrix} \begin{bmatrix} \mathbf{u}_n \\ \mathbf{p}_n \end{bmatrix} = \begin{bmatrix} \mathbf{F}_1 \\ \Delta t \mathbf{F}_2 + \mathbf{B}^T \mathbf{u}_{n-1} \end{bmatrix}, \quad (3.64)$$

where

$$\begin{aligned} \mathbf{u} &:= [\tilde{u}_1 \tilde{u}_2 \cdots \tilde{u}_I]^T, \\ \mathbf{p} &:= [\tilde{p}_1 \tilde{p}_2 \cdots \tilde{p}_J]^T, \\ A_{ij} &:= (2\mu_s + \lambda_s) \int_0^L \left(\frac{d}{dx} w_j \frac{d}{dx} w_i \right) dx, \\ B_{ij} &:= - \int_0^L \frac{d}{dx} w_i q_j dx, \\ C_{ij} &:= K \int_0^L \frac{d}{dx} q_j \frac{d}{dx} q_i dx, \\ F_{1,i} &:= g_u^N, \\ F_{2,i} &:= g_p^N. \end{aligned}$$

The material is divided up into N uniform elements with element size $h = L/N$. Then, the following $N \times N$ matrices are established:

$$\begin{aligned} \mathbf{A} &= \frac{2\mu_s + \lambda_s}{h} \begin{bmatrix} 2 & -1 & & & & & & & \\ -1 & 2 & -1 & & & & & & \\ & -1 & 2 & -1 & & & & & \\ & & & \ddots & \ddots & \ddots & & & \\ & & & & -1 & 2 & -1 & & \\ & & & & & & & -1 & 1 \end{bmatrix}, \quad \mathbf{B} = \frac{1}{2} \begin{bmatrix} 0 & 1 & & & & & & & \\ -1 & 0 & 1 & & & & & & \\ & -1 & 0 & 1 & & & & & \\ & & & \ddots & \ddots & \ddots & & & \\ & & & & & -1 & 0 & 1 & \\ & & & & & & & -1 & -1 \end{bmatrix}, \\ \mathbf{C} &= \frac{K}{h} \begin{bmatrix} 2 & -1 & & & & & & & \\ -1 & 2 & -1 & & & & & & \\ & -1 & 2 & -1 & & & & & \\ & & & \ddots & \ddots & \ddots & & & \\ & & & & & -1 & 2 & -1 & \\ & & & & & & & -1 & 1 \end{bmatrix}. \end{aligned}$$

Now, the numerical properties are investigated, which are related to the size of the time steps (Δt) and the element size (h). Therefore, the matrix notation of equation (3.64) is rewritten by eliminating the displacements \mathbf{u}_n . The resulting equation is

$$(\mathbf{B}^T \mathbf{A}^{-1} \mathbf{B} + \Delta t \mathbf{C}) \mathbf{p}_n = \Delta t \mathbf{F}_2 + \mathbf{B}^T \mathbf{u}_{n-1} - \mathbf{B}^T \mathbf{A}^{-1} \mathbf{F}_1.$$

The matrix on the left is now written out completely:

$$(\mathbf{B}^T \mathbf{A}^{-1} \mathbf{B} + \Delta t \mathbf{C}) = \frac{h}{4(2\mu_s + \lambda_s)} \begin{bmatrix} 2 & 1 & & & & \\ 1 & 2 & 1 & & & \\ & 1 & 2 & 1 & & \\ & & \ddots & \ddots & \ddots & \\ & & & 1 & 2 & 1 \\ & & & & 1 & 1 \end{bmatrix} + \Delta t \frac{K}{h} \begin{bmatrix} 2 & -1 & & & & \\ -1 & 2 & -1 & & & \\ & -1 & 2 & -1 & & \\ & & \ddots & \ddots & \ddots & \\ & & & -1 & 2 & -1 \\ & & & & -1 & 1 \end{bmatrix}.$$

In order to investigate the numerical behaviour when using small time steps, the definition of an *M-matrix* [66] is needed.

Definition 3.15 A matrix \mathbf{A} is an *M-matrix* if its entries a_{ij} satisfy $a_{ij} \leq 0$ for $i \neq j$ and $a_{ii} > 0$, and its inverse \mathbf{A}^{-1} exists with $\mathbf{A}^{-1} \geq 0$.

The matrix $\mathbf{B}^T \mathbf{A}^{-1} \mathbf{B} + \Delta t \mathbf{C}$ is an M-matrix if

$$\Delta t > \Delta t_{crit} = \frac{h^2}{4K(2\mu_s + \lambda_s)}. \quad (3.65)$$

This critical step size Δt_{crit} is important for the occurrence of oscillations in the solution: if $\Delta t < \Delta t_{crit}$ then oscillations can occur in the solution. If $\Delta t > \Delta t_{crit}$ then no oscillations will occur.

The same critical step size can be derived by eliminating the pressures p_n :

$$(\mathbf{B} \mathbf{C}^{-1} \mathbf{B}^T + \Delta t \mathbf{A}) \mathbf{u}_n = -\Delta t \mathbf{F}_1 + \mathbf{B} \mathbf{C}^{-1} \mathbf{u}_{n-1} - \mathbf{B} \mathbf{C}^{-1} \mathbf{F}_2. \quad (3.66)$$

The matrix on the left is now written out completely:

$$\mathbf{B} \mathbf{C}^{-1} \mathbf{B}^T + \Delta t \mathbf{A} = \frac{h}{4K} \begin{bmatrix} 2 & 1 & & & & & -4 \\ 1 & 2 & 1 & & & & -4 \\ & 1 & 2 & 1 & & & -4 \\ & & \ddots & \ddots & \ddots & \ddots & \vdots \\ & & & 1 & 2 & 1 & -4 \\ & & & & 1 & 2 & -3 \\ -4 & -4 & -4 & \cdots & -4 & -3 & 4N-3 \end{bmatrix} +$$

$$\Delta t \frac{2\mu_s + \lambda_s}{h} \begin{bmatrix} 2 & -1 & & & & & \\ -1 & 2 & -1 & & & & \\ & -1 & 2 & -1 & & & \\ & & \ddots & \ddots & \ddots & & \\ & & & -1 & 2 & -1 & \\ & & & & -1 & 2 & -1 \\ & & & & & -1 & 1 \end{bmatrix}.$$

Oscillations in the solution can occur when matrix $\mathbf{B} \mathbf{C}^{-1} \mathbf{B}^T + \Delta t \mathbf{A}$ is not an M-matrix. The matrix $\mathbf{B} \mathbf{C}^{-1} \mathbf{B}^T + \Delta t \mathbf{A}$ is an M-matrix if

$$\Delta t > \Delta t_{crit} = \frac{h^2}{4K(2\mu_s + \lambda_s)}.$$

This gives of course the same result as by elimination of the displacements.

From simulations, it appears that oscillations occur when $\Delta t < \Delta t_{crit}$. Figure 3.3 shows the results for $\Delta t = 0.5 \Delta t_{crit}$ and $\Delta t = 1.5 \cdot \Delta t_{crit}$. These values are chosen, because then the oscillations are visible. For every other $\Delta t < \Delta t_{crit}$ oscillations will occur also.

Also the convergence of the solution of this problem is considered. The computed displacements are compared to the analytical solution for the confined compression experiment as described by Terzaghi [74]. The maximum norm for the global error in the displacement solution is put in the table 3.1. The parameters have the values $K = 1$ (permeability), $t = 0.01$ (final time), $\mu_s = 0.400$ and $\lambda_s = 0.267$. All errors are considered at the final time. From table 3.1, it appears that the error is $O(\Delta t)$ and $O(h^2)$.

Mixed-hybrid finite element method

The same confined compression experiment is solved by the mixed-hybrid finite element method. The boundary conditions are applied to the matrix system (3.62). Then, the Lagrange multipliers λ_n are eliminated. We derive

$$(\mathbf{A}_* + \frac{1}{\Delta t} \mathbf{B}_* \mathbf{C}_*^{-1} \mathbf{B}_*^T) \mathbf{u}_n = \tilde{\mathbf{F}}_*^1 + \frac{1}{\Delta t} \mathbf{B}_* \mathbf{C}_*^{-1} \tilde{\mathbf{F}}_*^2,$$

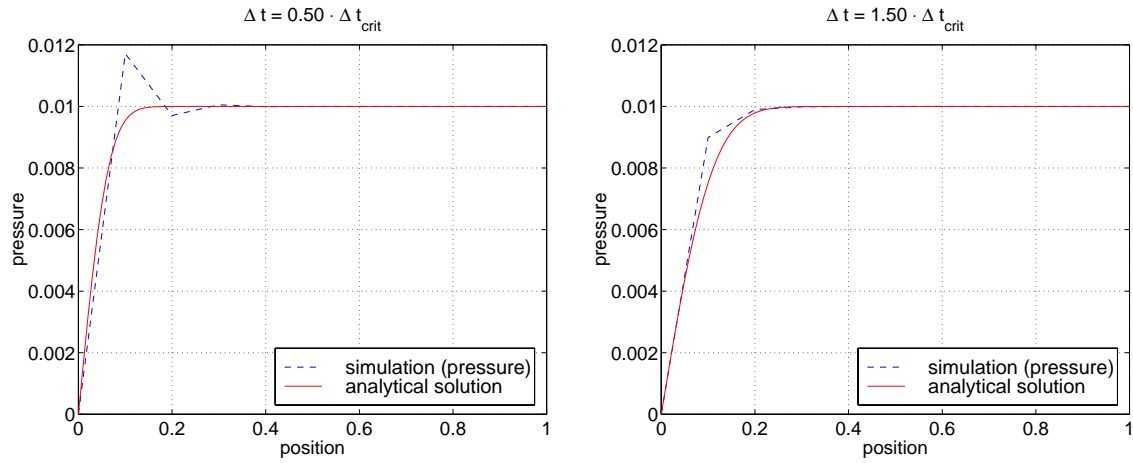


Figure 3.3 Simulated data for a confined compression experiment for $\Delta t = 0.5 \Delta t_{crit}$ (left) and for $\Delta t = 1.5 \Delta t_{crit}$ (right).

Number of Elements	Number of Time Steps							
	2	4	8	16	32	64	128	256
2	3.76e-04	4.09e-04	4.28e-04	4.38e-04	4.43e-04	4.46e-04	4.47e-04	4.48e-04
4	1.59e-04	1.66e-04	1.69e-04	1.71e-04	1.71e-04	1.72e-04	1.72e-04	1.72e-04
8	6.56e-05	3.93e-05	4.02e-05	4.45e-05	4.66e-05	4.77e-05	4.82e-05	4.85e-05
16	6.56e-05	3.35e-05	1.69e-05	9.99e-06	1.08e-05	1.14e-05	1.16e-05	1.18e-05
32	6.56e-05	3.35e-05	1.69e-05	8.50e-06	4.26e-06	2.52e-06	2.71e-06	2.86e-06
64	6.56e-05	3.35e-05	1.69e-05	8.50e-06	4.26e-06	2.13e-06	1.07e-06	6.32e-07
128	6.56e-05	3.35e-05	1.69e-05	8.50e-06	4.26e-06	2.13e-06	1.07e-06	5.33e-07
256	6.56e-05	3.35e-05	1.69e-05	8.50e-06	4.26e-06	2.13e-06	1.07e-06	5.33e-07

Table 3.1 Maximum norm for the global error in the displacements for the u - p finite element formulation.

where

$$A_* = \left(\frac{2\mu_s + \lambda_s}{h} + \frac{h}{12K\Delta t} \right) \begin{bmatrix} 2 & -1 & & & & & & & \\ -1 & 2 & -1 & & & & & & \\ & -1 & 2 & -1 & & & & & \\ & & \ddots & \ddots & \ddots & & & & \\ & & & -1 & 2 & -1 & & & \\ & & & & -1 & 2 & -1 & & \\ & & & & & -1 & 1 & & \end{bmatrix}$$

and

$$\frac{1}{\Delta t} \mathbf{B}_* \mathbf{C}_*^{-1} \mathbf{B}_*^T = \frac{h}{4K\Delta t} \begin{bmatrix} 2 & 1 & & & & & -4 \\ 1 & 2 & 1 & & & & -4 \\ & 1 & 2 & 1 & & & -4 \\ & & \ddots & \ddots & \ddots & & \vdots \\ & & & 1 & 2 & 1 & -4 \\ & & & & 1 & 2 & -3 \\ -4 & -4 & -4 & \dots & -4 & -3 & 4N-3 \end{bmatrix}.$$

Oscillations in the solution can occur when matrix $\mathbf{A}_* + \frac{1}{\Delta t}(\mathbf{B}_* \mathbf{C}_*^{-1} \mathbf{B}_*^T)$ is not an M-matrix. This matrix is an M-matrix if

$$\frac{2\mu_s + \lambda_s}{h} + \frac{h}{12K\Delta t} > \frac{h}{4K\Delta t},$$

i.e.

$$\Delta t > \Delta t_{crit} = \frac{h^2}{6K(2\mu_s + \lambda_s)}.$$

This means that the critical time step size Δt_{crit} is $\frac{1}{2}$ times smaller than in the u - p formulation.

From simulations, it appears that oscillations occur when $\Delta t < \Delta t_{crit}$. Figure 3.4 shows the results for $\Delta t = 0.5 \Delta t_{crit}$ and $\Delta t = 1.5 \Delta t_{crit}$. These values are chosen, because then the oscillations are visible. For every other $\Delta t < \Delta t_{crit}$ oscillations will occur also. The convergence of the solution of this problem is considered also. The computed

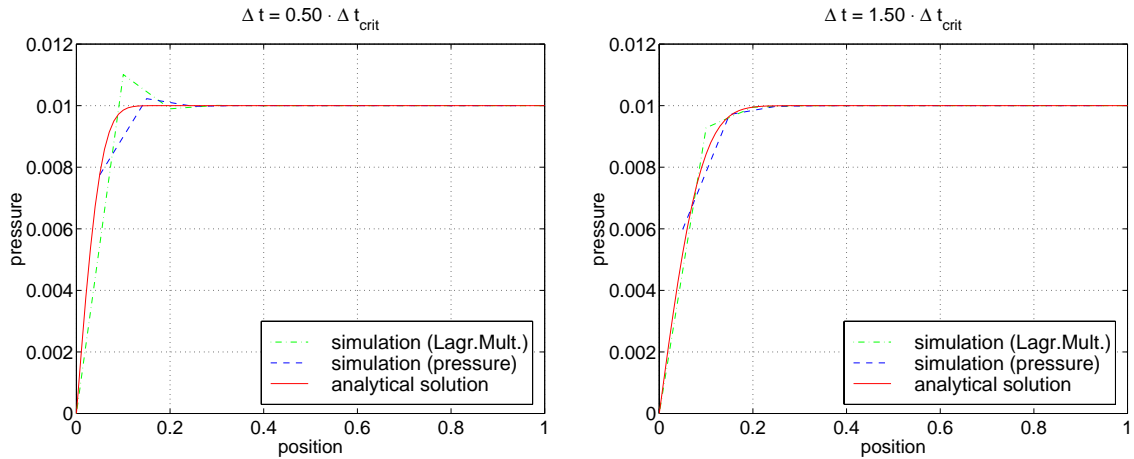


Figure 3.4 Simulated data for a confined compression experiment for $\Delta t = 0.5 \Delta t_{crit}$ (left) and for $\Delta t = 1.5 \Delta t_{crit}$ (right).

displacements are compared to the analytical solution for the confined compression experiment as described by Terzaghi [74]. The maximum norm for the global error in the displacement solution is put in the table 3.2. The parameters have the values $K = 1$ (permeability), $t = 0.01$ (final time), $\mu_s = 0.400$ and $\lambda_s = 0.267$. All errors are considered at the final time.

Number of Elements	Number of Time Steps							
	2	4	8	16	32	64	128	256
2	3.76e-04	4.09e-04	4.28e-04	4.38e-04	4.43e-04	4.46e-04	4.47e-04	4.48e-04
4	1.60e-04	1.66e-04	1.69e-04	1.71e-04	1.71e-04	1.72e-04	1.72e-04	1.72e-04
8	6.56e-05	3.93e-05	4.02e-05	4.45e-05	4.66e-05	4.77e-05	4.82e-05	4.85e-05
16	6.56e-05	3.35e-05	1.69e-05	9.99e-06	1.08e-05	1.14e-05	1.16e-05	1.18e-05
32	6.56e-05	3.35e-05	1.69e-05	8.50e-06	4.26e-06	2.52e-06	2.71e-06	2.86e-06
64	6.56e-05	3.35e-05	1.69e-05	8.50e-06	4.26e-06	2.13e-06	1.07e-06	6.32e-07
128	6.56e-05	3.35e-05	1.69e-05	8.50e-06	4.26e-06	2.13e-06	1.07e-06	5.33e-07
256	6.56e-05	3.35e-05	1.69e-05	8.50e-06	4.26e-06	2.13e-06	1.07e-06	5.33e-07

Table 3.2 Maximum norm for the global error in the displacements for the mixed-hybrid finite element formulation.

From table 3.2, it appears that the error is $O(\Delta t)$ and $O(h^2)$.

3.4.2 Two-dimensional example

Mixed-hybrid finite element method

Also a two-dimensional example is investigated. A two-dimensional version of the squeezing a sponge (plane strain) is considered [49]. In this problem, the sponge is squeezed in x - and y -direction over distance u_0 (figure 3.5). Because of the symmetry of the problem, we consider the part $x \geq 0$ and $y \geq 0$. The x -axis and the y -axis are considered to be impermeable and only displacements along the direction of the axes are allowed.

The analytical solution for the displacements in i -direction is given by [49]

$$u(x_i) = \frac{u_0}{L} x_i + \sum_{k=1}^{\infty} L \gamma_k \sin\left(\frac{k\pi x_i}{L}\right) \exp\left(\frac{-k^2 \pi t}{C}\right), \quad i = 1, 2, \quad (3.67)$$

where

$$\gamma_k = \frac{2(-1)^k}{k\pi L} u_0,$$

$$C = \frac{L^2}{(2\mu_s + \lambda_s)K}.$$

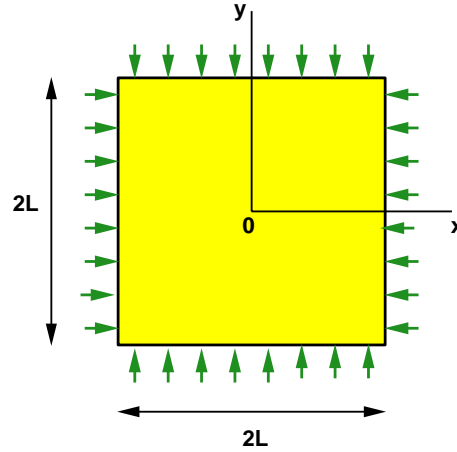


Figure 3.5 Schematic representation of the two-dimensional squeezing experiment.

The fluid pressure p and the fluid velocity \mathbf{v} are described by

$$p = (2\mu_s + \lambda_s) \sum_{k=1}^{\infty} k\pi\gamma_k \sum_{i=1}^2 \cos\left(\frac{k\pi x_i}{L}\right) \exp\left(\frac{-k^2\pi t}{C}\right), \quad (3.68)$$

and

$$v(x_i) = -L \sum_{k=1}^{\infty} \frac{\gamma_k k^2 x_i}{C} \sin\left(\frac{k\pi x_i}{L}\right) \exp\left(\frac{-k^2\pi t}{C}\right), \quad i = 1, 2. \quad (3.69)$$

These analytical solutions are compared to the mixed-hybrid finite element solutions. The parameters have the values $K = 1$ (permeability), $\mu_s = 0.400$, $\lambda_s = 0.267$ and $L = 1$. In figures 3.6 and 3.7, the analytical solutions for the displacements and fluid pressures are compared to the mixed-hybrid finite element solutions at $t = 0.01$. The displacements that are shown, are a combination of the displacements in x -direction, u_x , and the displacements in y -direction, u_y :

$$u(\mathbf{x}) = \sqrt{u_x^2(\mathbf{x}) + u_y^2(\mathbf{x})}.$$

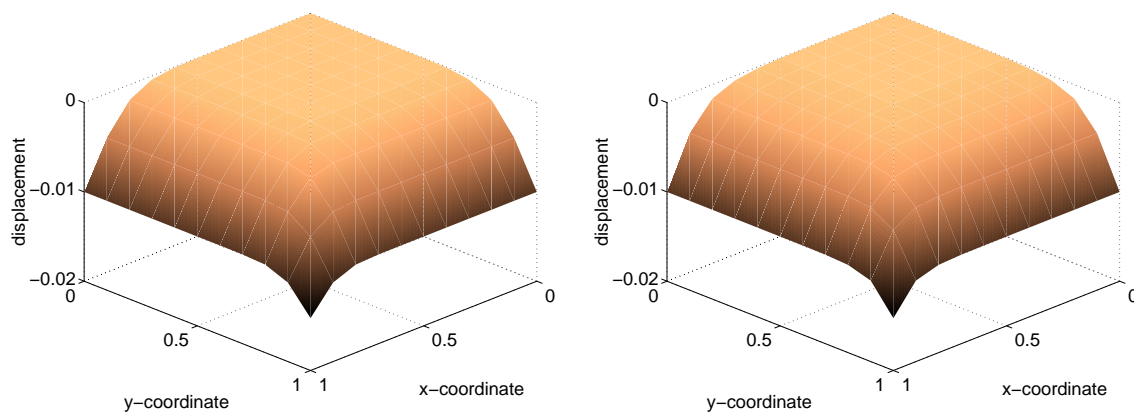


Figure 3.6 Analytical solution (left) and FEM solution (right) for the displacements at $t = 0.01$.

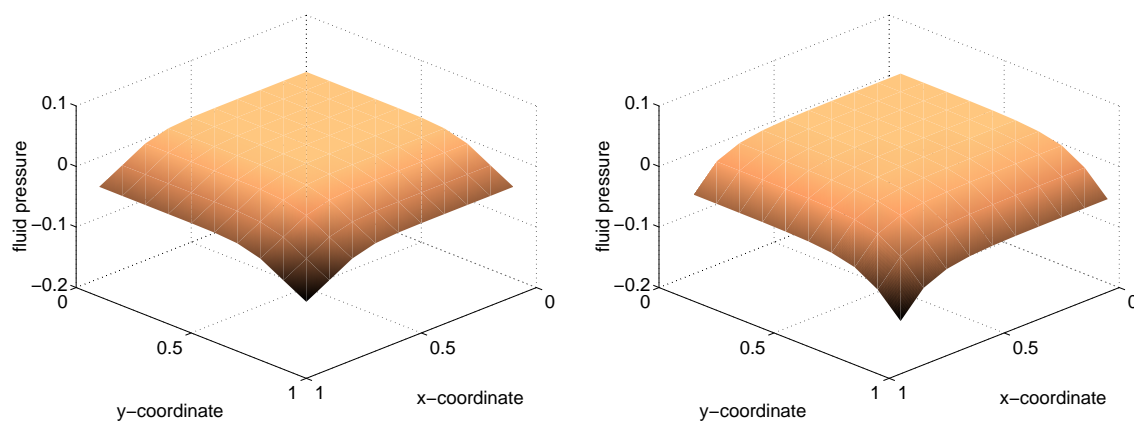


Figure 3.7 Analytical solution (left) and FEM solution (right) for the fluid pressure at $t = 0.01$.

In figure 3.8 the analytical evolution in time of the solid displacements and the fluid flow are compared to the computed evolution in time at several positions in the sample.

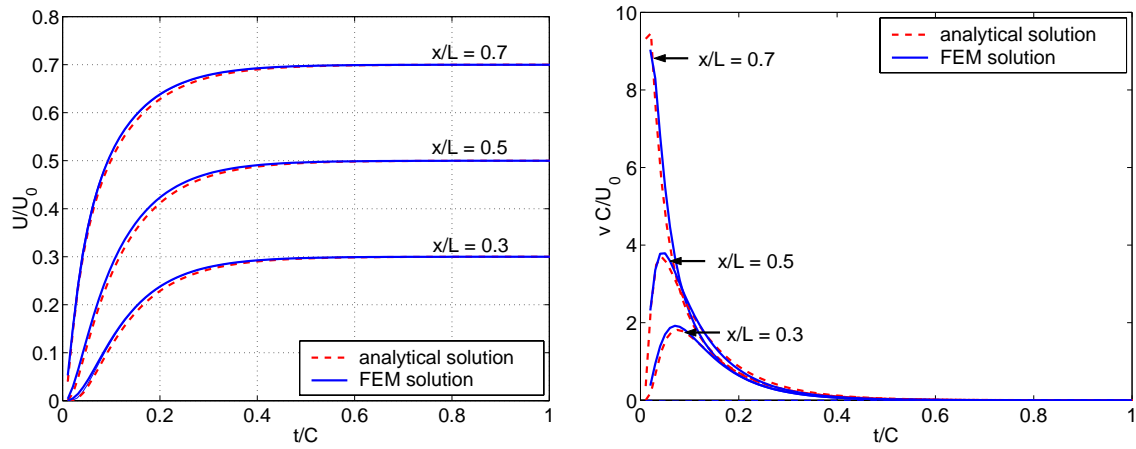


Figure 3.8 The evolution in time of the solid displacements (left) and the fluid flow (right) at several positions in the sample.

When the time-step size is smaller than the critical size Δt_{crit} , derived for the one-dimensional case, oscillations in the solution occur too (figure 3.9).

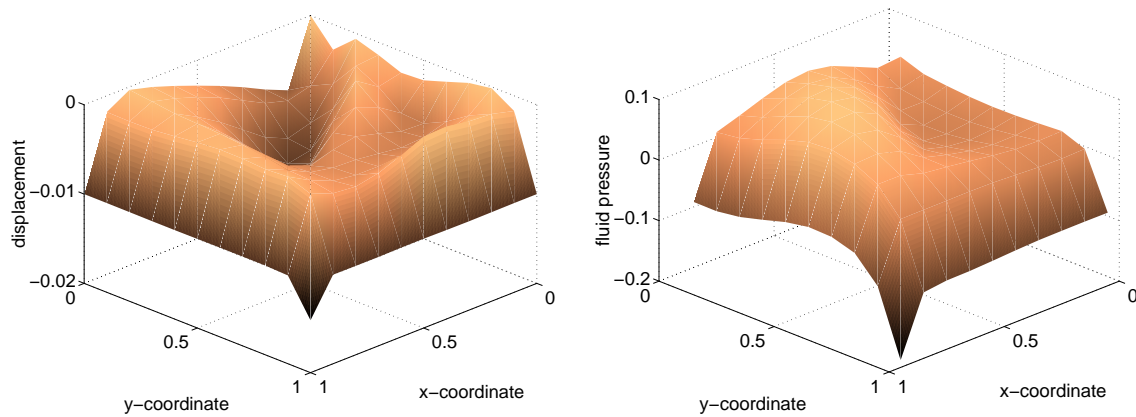


Figure 3.9 Computed solutions for the solid displacements (left) and for the fluid pressure (right) at $t = 0.6 \Delta t_{crit}$.

3.4.3 Discussion and conclusions

In the u - p formulation and the mixed-hybrid formulation, oscillations can occur when the time steps are chosen too small. In the one-dimensional case, the critical time step size Δt_{crit} is related to the square of the element size h . The critical time step size in the

mixed-hybrid formulation however is $1\frac{1}{2}$ times smaller than in the u - p formulation. Furthermore, the fluxes can be computed more accurately in the mixed-hybrid formulation than in the u - p formulation, especially when there are large gradients in the permeability. In the one-dimensional examples this is not notable, since the fluid can only flow in one direction. The errors for both methods are about the same in the one-dimensional examples. Advantages of the mixed-hybrid finite element method to the mixed finite element are that the matrix size is reduced without loss of accuracy and that the matrix-vector system in the mixed-hybrid finite element method has a form for which more iterative methods are available. So, for computing the fluid flux in a two- or three-dimensional situation with a large gradient in the permeability, it is better to choose the mixed-hybrid finite element method. A drawback for the mixed and the mixed-hybrid methods is that it is more expensive to compute the matrices.

It appears that in the u - p formulation and in the u - p - v formulation the error is $O(\Delta t)$ and $O(h^2)$.

From the *inf-sup* condition and the LBB-condition, it follows that the uniqueness depends only on $d(\mathbf{s}, q)$ or $d(\mathbf{s}_h, q_h)$ and not on $b(\mathbf{w}, q)$ or $b(\mathbf{w}_h, q_h)$. This means that there are more choices for the finite element space for \mathbf{w}_h without losing the uniqueness of the solution. The finite element space for \mathbf{w}_h has only to fulfil the discrete ellipticity condition and does not have to fulfil the LBB-condition.

4 Four-Component Mixture Theory

4.1 Physical Model

The two-component mixture theory of chapter 3 is not able to describe the swelling and compression behaviour of the tissues, that is caused by chemical and/or electrical loads. Therefore the theory is extended to a four-component mixture theory. In the four-component mixture theory, the material is modelled as a porous medium that is saturated with a fluid in which ions are dissolved. In the case of an intervertebral disc tissue, the porous solid skeleton represents the fibre network (collagen fibres and proteoglycans), the fluid represents the interstitial fluid and the ions represent the freely moving positively and negatively charged particles. For the sake of simplicity, we assume that the fluid is incompressible and Newtonian viscous, and the solid is linearly elastic. The solid can shrink only by expelling fluid into its surroundings, or swell only by attracting fluid from its surroundings.

According to chapter 2, the material behaviour is described by

$$\nabla \cdot \boldsymbol{\sigma} - \nabla p = \mathbf{0}, \quad (4.1)$$

$$\frac{\partial n^\alpha}{\partial t} + \nabla \cdot (n^\alpha \mathbf{v}^\alpha) = 0, \quad \alpha = s, f, \quad (4.2)$$

$$\frac{\partial (n^f c^\beta)}{\partial t} + \nabla \cdot (n^f c^\beta \mathbf{v}^\beta) = 0, \quad \beta = +, -, \quad (4.3)$$

$$z^+ c^+ + z^- c^- + z^{fc} c^{fc} = 0, \quad (4.4)$$

$$n^s + n^f = 1, \quad (4.5)$$

$$\boldsymbol{\sigma} = 2\mu_s \boldsymbol{\epsilon}(\mathbf{u}) + \lambda_s \nabla \cdot \mathbf{u} \mathbf{I}, \quad (4.6)$$

$$n^f (\mathbf{v}^f - \mathbf{v}^s) = -\mathbf{K} \left(\nabla p + (\phi^l - \phi^+) RT \nabla c^+ + (\phi^l - \phi^-) RT \nabla c^- - z^{fc} c^{fc} F \nabla \xi \right), \quad (4.7)$$

$$c^\beta (\mathbf{v}^\beta - \mathbf{v}^f) = -\mathbf{D}^\beta \left((2 - \phi^\beta) \nabla c^\beta + z^\beta \frac{F}{RT} c^\beta \nabla \xi + \frac{\bar{V}^\beta}{RT} c^\beta \nabla p \right), \quad \beta = +, -, \quad (4.8)$$

$$\mathbf{v}^s = \frac{\partial \mathbf{u}}{\partial t}. \quad (4.9)$$

Now, the mass balances for the phases, equations (4.2), are summed, the saturation

equation (4.5) and the definition of the solid velocity (4.9) are substituted into the equation. Furthermore, the constitutive equation for the stress (4.6) is substituted into the momentum equation (4.1) and the extended Darcy's law (4.7) and the extended Fick's laws (4.8) are substituted into the mass balances for the ions (4.3).

The material behaviour is now described by

$$\begin{aligned}
& \nabla \cdot (2\mu_s \boldsymbol{\epsilon}(\mathbf{u}) + \lambda_s \nabla \cdot \mathbf{u} \mathbf{I}) - \nabla p = \mathbf{0}, \\
\mathbf{v} = & -\mathbf{K} \left(\nabla p + (\phi^l - \phi^+) RT \nabla c^+ + (\phi^l - \phi^-) RT \nabla c^- - z^{fc} c^{fc} F \nabla \xi \right), \\
\mathbf{j}^\beta = & -\mathbf{D}^\beta \left((2 - \phi^\beta) \nabla c^\beta + z^\beta \frac{F}{RT} c^\beta \nabla \xi + \frac{\bar{V}^\beta}{RT} c^\beta \nabla p \right), \quad \beta = +, -, \\
& \frac{\partial}{\partial t} (\nabla \cdot \mathbf{u}) = -\nabla \cdot \mathbf{v}, \\
\frac{\partial (n^f c^\beta)}{\partial t} = & -\nabla \cdot (n^f \mathbf{j}^\beta) - \nabla \cdot (c^\beta \mathbf{v}) - \nabla \cdot (c^\beta n^f \frac{\partial \mathbf{u}}{\partial t}), \quad \beta = +, -, \\
& z^+ c^+ + z^- c^- + z^{fc} c^{fc} = 0,
\end{aligned} \tag{4.10}$$

where $\mathbf{v} := n^f (\mathbf{v}^f - \mathbf{v}^s)$ is the *fluid flux* relatively to the solid velocity and $\mathbf{j}^\beta := c^\beta (\mathbf{v}^\beta - \mathbf{v}^f)$ is the *ion flux* relatively to the fluid flow. The stress $\boldsymbol{\sigma}$ and the solid velocity \mathbf{v}^s can be derived a posteriori by the relations (4.6) and (4.9). The porosity n^f is a function of the deformation. We assume that solid is incompressible. So, the total volume can only change by expelling or attracting the fluid. Then, the porosity n^f is described by (3.9):

$$n^f := \frac{V^f}{V^{tot}} = 1 - \frac{1 - n_0^f}{J}, \tag{4.11}$$

where n_0^f is the initial porosity and $J := \det(\nabla \mathbf{u})$ is the relative volume change.

For the sake of simplicity, the following boundary conditions are considered

$$\begin{aligned}
\mathbf{u} &= \mathbf{0} && \text{on } \Gamma_u^D, \\
p &= p_{in} && \text{on } \Gamma_p^D, \\
c^+ &= c_{in}^+ && \text{on } \Gamma_p^D, \\
c^- &= c_{in}^- && \text{on } \Gamma_p^D, \\
\xi &= \xi_{in} && \text{on } \Gamma_p^D, \\
\mathbf{n} \cdot (2\mu_s \boldsymbol{\epsilon}(\mathbf{u}) + \lambda_s \nabla \cdot \mathbf{u} \mathbf{I} - p \mathbf{I}) &= \mathbf{g}_u^N && \text{on } \Gamma_u^N, \\
\mathbf{n} \cdot \mathbf{v} &= 0 && \text{on } \Gamma_p^N, \\
\mathbf{n} \cdot \mathbf{j}^+ &= 0 && \text{on } \Gamma_p^N, \\
\mathbf{n} \cdot \mathbf{j}^- &= 0 && \text{on } \Gamma_p^N,
\end{aligned}$$

where the Dirichlet boundaries Γ_α^D and the Neumann boundaries Γ_α^N are open portions of the total boundary Γ , such that $\Gamma_\alpha^D \cap \Gamma_\alpha^N = \emptyset$ and $\bar{\Gamma}_\alpha^D \cup \bar{\Gamma}_\alpha^N = \Gamma$. Other boundary

conditions can also be considered, but they make the formulae even more complex. We assume that the Dirichlet boundaries Γ_p^D are the same for the fluid pressure, the cation concentration, the anion concentration and the electrical potential. In that case, the sample is in contact with a bathing solution (figure 4.1). So, the the fluid pressure, the cation concentration, the anion concentration and the electrical potential are prescribed. On the boundary Γ_p^N , the sample is in contact with an insulating, impermeable wall. So, no fluxes are allowed over that boundary. These boundary conditions are sufficient for

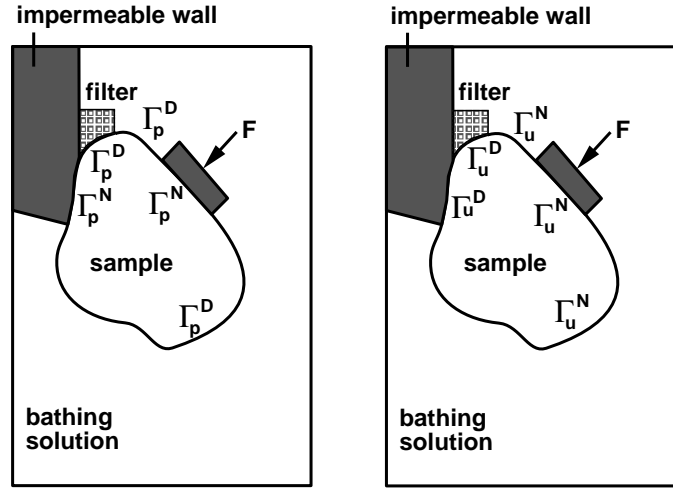


Figure 4.1 Schematic representation of the boundary conditions.

describing the swelling and compression experiments of chapters 5 and 6.

Since there is a jump over the boundary, the values for the fluid pressure p_{in} , the cations concentration c_{in}^+ , the anion concentration c_{in}^- and the electrical potential ξ_{in} are prescribed inside the sample. We assume that the outer part of the sample is in equilibrium with the bathing solution. Then, the ion concentration for a mono-valent salt solution is given by the *Donnan equilibrium*, see e.g. [28, 43]:

$$c_{in}^+ = -\frac{1}{2}z^{fc}c^{fc} + \frac{1}{2}\sqrt{(z^{fc}c^{fc})^2 + \frac{f_{out}^+f_{out}^-}{f_{in}^+f_{in}^-}(c_{out}^+ + c_{out}^-)^2}, \quad (4.12)$$

$$c_{in}^- = +\frac{1}{2}z^{fc}c^{fc} + \frac{1}{2}\sqrt{(z^{fc}c^{fc})^2 + \frac{f_{out}^+f_{out}^-}{f_{in}^+f_{in}^-}(c_{out}^+ + c_{out}^-)^2}, \quad (4.13)$$

where the c_{out}^β and f_{out}^β are the concentrations and the activity coefficients of ion β in the bathing solution and f_{in}^β is the activity coefficient of ion β inside the sample. Note that the concentrations always fulfil the electro-neutrality condition (4.4):

$$c_{in}^+ - c_{in}^- + z^{fc}c^{fc} = 0. \quad (4.14)$$

This means that c_{in}^+ and c_{in}^- can not be chosen independently. The jump in the fluid pressure is equal to the jump in the osmotic pressure, see e.g. [28, 43]:

$$p_{in} - p_{out} = \pi_{in} - \pi_{out} = -\frac{RT}{\bar{V}^l} \ln\left(f_{in}^l \left(1 - \frac{c_{in}^+ + c_{in}^-}{\sum_{\gamma=l,+,-} c_{in}^\gamma}\right)\right) + \frac{RT}{\bar{V}^l} \ln\left(f_{out}^l \left(1 - \frac{c_{out}^+ + c_{out}^-}{\sum_{\gamma=l,+,-} c_{out}^\gamma}\right)\right), \quad (4.15)$$

where the definition of the osmotic pressure (2.25) is used. When $c^+ \ll c^l$ and $c^- \ll c^l$, this equation is approximated by

$$p_{in} - p_{out} = \pi_{in} - \pi_{out} \approx RT((c_{in}^+ + c_{in}^-) - (c_{out}^+ + c_{out}^-)). \quad (4.16)$$

The jump on the electrical potential is described by the *Nernst potential* ξ_N , e.g. [35, 38]:

$$\xi_{in} - \xi_{out} = \xi_N = -\frac{RT}{z^\beta F} \ln\left(\frac{f_{in}^\beta c_{in}^\beta}{f_{out}^\beta c_{out}^\beta}\right), \quad \beta = +, -. \quad (4.17)$$

4.2 Variational Formulation

Equations (4.10) are solved by a finite element method. Therefore, the equations are written in a variational form. Hence, the equations are multiplied by test functions and integrated over the volume Ω . Further Gauss' theorem is used. We assume that we can choose the same spaces for the ion concentrations and the electrical potential as we use for the fluid pressure in the two-component mixture theory (chapter 3), since they act in the same way. Further, we assume that the fluid and ion fluxes behave in the same way as the fluid flux in two-component mixture theory. The material behaviour is now described by

Problem 4.1 Find $(\mathbf{u}, \mathbf{v}, \mathbf{j}^+, \mathbf{j}^-, p, c^+, c^-, \xi) \in H_{1,0}(\Omega)^d \times H_0(\text{div}, \Omega) \times H_0(\text{div}, \Omega) \times H_0(\text{div}, \Omega) \times L_2(\Omega) \times L_2(\Omega) \times L_2(\Omega) \times L_2(\Omega) \times L_2(\Omega)$ such that

$$\begin{aligned} a(\mathbf{u}, \mathbf{w}) &+ b(\mathbf{w}, p) &&= F^u, \\ c(\mathbf{v}, \mathbf{r}) &+ d(\mathbf{r}, p) + e(\mathbf{r}, c^+) + e(\mathbf{r}, c^-) + f(\mathbf{r}, \xi) &= F^f, \\ g(\mathbf{j}^+, \mathbf{s}^+) &+ h(\mathbf{s}^+, p) + i(\mathbf{s}^+, c^+) &+ j(\mathbf{s}^+, \xi) &= F^+, \\ g(\mathbf{j}^-, \mathbf{s}^-) &+ h(\mathbf{s}^-, p) &+ i(\mathbf{s}^-, c^-) + j(\mathbf{s}^-, \xi) &= F^-, \\ \frac{d}{dt} b(\mathbf{u}, q) + d(\mathbf{v}, q) &&&= 0, \\ k\left(\frac{\partial}{\partial t} \mathbf{u}, d^+\right) + l(\mathbf{v}, d^+) + m(\mathbf{j}^+, d^+) &+ \frac{d}{dt} n(d^+, c^+) &&= 0, \\ k\left(\frac{\partial}{\partial t} \mathbf{u}, d^-\right) + l(\mathbf{v}, d^-) + m(\mathbf{j}^-, d^-) &+ \frac{d}{dt} n(d^-, c^-) &&= 0, \\ &o(\mathbf{r}, c^+) + o(\mathbf{r}, c^-) &&= F^\xi, \end{aligned}$$

for every $\mathbf{w} \in H_{1,0}(\Omega)^d$, $\mathbf{r} \in H_0(\text{div}, \Omega)$, $\mathbf{s}^+ \in H_0(\text{div}, \Omega)$, $\mathbf{s}^- \in H_0(\text{div}, \Omega)$, $q \in L_2(\Omega)$, $d^+ \in L_2(\Omega)$, $d^- \in L_2(\Omega)$, and $r \in L_2(\Omega)$.

Here,

$$\begin{aligned}
a(\mathbf{u}, \mathbf{w}) &:= \int_{\Omega} 2(\mu_s \boldsymbol{\epsilon}(\mathbf{u}) : \boldsymbol{\epsilon}(\mathbf{w}) + \lambda_s (\nabla \cdot \mathbf{u})(\nabla \cdot \mathbf{w})) dV, \\
b(\mathbf{w}, p) &:= - \int_{\Omega} \nabla \cdot \mathbf{w} p dV, \\
c(\mathbf{v}, \mathbf{r}) &:= \int_{\Omega} (\mathbf{K}^{-1} \mathbf{v}) \cdot \mathbf{r} dV, \\
d(\mathbf{r}, p) &:= - \int_{\Omega} \nabla \cdot \mathbf{r} p dV, \\
e(\mathbf{r}, c^\beta) &:= - \int_{\Omega} \nabla \cdot \mathbf{r} (\phi^l - \phi^\beta) RT c^\beta dV, \\
f(\mathbf{r}, \xi) &:= \int_{\Omega} \nabla \cdot \mathbf{r} z^{fc} c^{fc} F \xi dV, \\
g(\mathbf{j}^\beta, \mathbf{s}^\beta) &:= \int_{\Omega} (\mathbf{D}^\beta)^{-1} \mathbf{j}^\beta \cdot \mathbf{s}^\beta dV, \\
h(\mathbf{s}^\beta, p) &:= - \int_{\Omega} \nabla \cdot (c^\beta \mathbf{s}^\beta) \frac{\bar{V}^\beta}{RT} p dV, \\
i(\mathbf{s}^\beta, c^\beta) &:= - \int_{\Omega} \nabla \cdot \mathbf{s}^\beta (2 - \phi^\beta) c^\beta dV, \\
j(\mathbf{s}^\beta, \xi) &:= \int_{\Omega} \nabla \cdot (c^\beta \mathbf{s}^\beta) z^\beta \frac{F}{RT} \xi dV, \\
k\left(\frac{\partial}{\partial t} \mathbf{u}, d^\beta\right) &:= \int_{\Omega} \nabla \cdot (c^\beta n^f \frac{\partial}{\partial t} \mathbf{u}) d^\beta dV, \\
l(\mathbf{v}, d^\beta) &:= \int_{\Omega} \nabla \cdot (c^\beta \mathbf{v}) d^\beta dV, \\
m(\mathbf{j}^\beta, d^\beta) &:= \int_{\Omega} \nabla \cdot (n^f \mathbf{j}^\beta) d^\beta dV, \\
n(d^\beta, c^\beta) &:= \int_{\Omega} d^\beta n^f c^\beta dV, \\
o(\mathbf{r}, c^\beta) &:= \int_{\Omega} r z^\beta c^\beta dV, \\
F^u(\mathbf{w}) &:= \int_{\Gamma_u^N} \mathbf{g}_u^N \cdot \mathbf{w} dS, \\
F^f(\mathbf{r}) &:= - \int_{\Gamma_p^p} \mathbf{n} \cdot \mathbf{r} p_{in} dS - \int_{\Gamma_p^p} \mathbf{n} \cdot \mathbf{r} (\phi^l - \phi^+) RT c_{in}^+ dS \\
&\quad - \int_{\Gamma_p^p} \mathbf{n} \cdot \mathbf{r} (\phi^l - \phi^-) RT c_{in}^- dS + \int_{\Gamma_p^p} \mathbf{n} \cdot \mathbf{r} z^{fc} c^{fc} F \xi_{in} dS, \\
F^+(s^+) &:= - \int_{\Gamma_p^p} (\mathbf{n} \cdot \mathbf{s}^+ (2 - \phi^+) c_{in}^+ + \mathbf{n} \cdot \mathbf{s}^+ z^+ \frac{F}{RT} c_{in}^+ \xi_{in} + \mathbf{n} \cdot \mathbf{s}^+ \frac{\bar{V}^+}{RT} c_{in}^+ p_{in}) dS, \\
F^-(s^-) &:= - \int_{\Gamma_p^p} (\mathbf{n} \cdot \mathbf{s}^- (2 - \phi^-) c_{in}^- + \mathbf{n} \cdot \mathbf{s}^- z^- \frac{F}{RT} c_{in}^- \xi_{in} + \mathbf{n} \cdot \mathbf{s}^- \frac{\bar{V}^-}{RT} c_{in}^- p_{in}) dS,
\end{aligned}$$

$$F^{\xi}(r) := - \int_{\Omega} r z^{fc} c^{fc} dV.$$

Note that this problem reduces to problem 3.3 (page 35), when there are no charged particles inside the fluid. The problem is non-linear since, for example, $h(\mathbf{s}^{\beta}, p)$ contains two unknowns: c^{β} and p . Also $j(\mathbf{s}^{\beta}, p)$, $k(\frac{\partial}{\partial t} \mathbf{u}, d^{\beta})$, $l(\mathbf{v}, d^{\beta})$, $m(\mathbf{s}^{\beta}, d^{\beta})$ and $n(d^{\beta}, c^{\beta})$ contain more than one unknown.

4.3 Mixed Finite Element Model

Now, the variational problem is approximated by finite elements. Therefore, we choose the finite element spaces $(\mathbf{u}_h, \mathbf{v}_h, \mathbf{j}_h^+, \mathbf{j}_h^-, p_h, c_h^+, c_h^-, \xi_h) \in P_0^1(\Omega)^d \times RT_{0,0}^0(\Omega_h) \times RT_{0,0}^0(\Omega_h) \times RT_{0,0}^0(\Omega_h) \times M_{-1}^0(\Omega_h) \times M_{-1}^0(\Omega_h) \times M_{-1}^0(\Omega_h) \times M_{-1}^0(\Omega_h)$. These spaces are defined in chapter 3. So, the finite element formulation of the problem is:

$$\begin{aligned} a(\mathbf{u}_h, \mathbf{w}_h) &+ b(\mathbf{w}_h, p_h) &&= F_h^u, \\ c(\mathbf{v}_h, \mathbf{r}_h) &+ d(\mathbf{r}_h, p_h) + e(\mathbf{r}_h, c_h^+) + e(\mathbf{r}_h, c_h^-) + f(\mathbf{r}_h, \xi_h) &= F_h^f, \\ g(\mathbf{j}_h^+, \mathbf{s}_h^+) &+ h(\mathbf{s}_h^+, p_h) + i(\mathbf{s}_h^+, c_h^+) &+ j(\mathbf{s}_h^+, \xi_h) &= F_h^+, \\ g(\mathbf{j}_h^-, \mathbf{s}_h^-) &+ h(\mathbf{s}_h^-, p_h) + i(\mathbf{s}_h^-, c_h^-) + j(\mathbf{s}_h^-, \xi_h) &= F_h^-, \\ \frac{d}{dt} b(\mathbf{u}_h, q_h) + d(\mathbf{v}_h, q_h) &&&= 0, \\ k(\frac{\partial}{\partial t} \mathbf{u}_h, d_h^+) + l(\mathbf{v}_h, d_h^+) + m(\mathbf{j}_h^+, d_h^+) &+ \frac{d}{dt} n(d_h^+, c_h^+) &&= 0, \\ k(\frac{\partial}{\partial t} \mathbf{u}_h, d_h^-) + l(\mathbf{v}_h, d_h^-) + m(\mathbf{j}_h^-, d_h^-) &+ \frac{d}{dt} n(d_h^-, c_h^-) &&= 0, \\ &o(r, c_h^+) + o(r, c_h^-) &&= F_h^{\xi}. \end{aligned}$$

The functions $\mathbf{u}_h, \mathbf{v}_h, \mathbf{j}_h^+, \mathbf{j}_h^-, p_h, c_h^+, c_h^-$ and ξ_h are expressed as

$$\begin{aligned} \mathbf{u}_h(\mathbf{x}, t) &:= \sum_{i=1}^I \tilde{u}_i(t) \mathbf{w}_i(\mathbf{x}), \\ \mathbf{v}_h(\mathbf{x}, t) &:= \sum_{j=1}^J \tilde{v}_j(t) \mathbf{s}_j(\mathbf{x}), \\ \mathbf{j}_h^+(\mathbf{x}, t) &:= \sum_{j=1}^J \tilde{j}_j^+(t) \mathbf{s}_j^+(\mathbf{x}), \\ \mathbf{j}_h^-(\mathbf{x}, t) &:= \sum_{j=1}^J \tilde{j}_j^-(t) \mathbf{s}_j^-(\mathbf{x}), \\ p_h(\mathbf{x}, t) &:= \sum_{k=1}^K \tilde{p}_k(t) q_k(\mathbf{x}), \\ c_h^+(\mathbf{x}, t) &:= \sum_{k=1}^K \tilde{c}_k^+(t) d_k^+(\mathbf{x}), \end{aligned}$$

$$c_h^-(\mathbf{x}, t) := \sum_{k=1}^K \tilde{c}_k^-(t) d_k^-(\mathbf{x}),$$

$$\xi_h(\mathbf{x}, t) := \sum_{k=1}^K \tilde{\xi}_k(t) r_k(\mathbf{x}).$$

Substitution in the discrete variational formulation leads to

$$\begin{aligned}
& \begin{bmatrix} 0 & 0 & 0 & 0 & 0 & 0 & 0 & 0 \\ 0 & 0 & 0 & 0 & 0 & 0 & 0 & 0 \\ 0 & 0 & 0 & 0 & 0 & 0 & 0 & 0 \\ 0 & 0 & 0 & 0 & 0 & 0 & 0 & 0 \\ \mathbf{B}^T & 0 & 0 & 0 & 0 & 0 & 0 & 0 \\ \mathbf{K}^+ & 0 & 0 & 0 & 0 & \mathbf{N}^+ & 0 & 0 \\ \mathbf{K}^- & 0 & 0 & 0 & 0 & 0 & \mathbf{N}^- & 0 \\ 0 & 0 & 0 & 0 & 0 & 0 & 0 & 0 \end{bmatrix} \frac{d}{dt} \begin{bmatrix} \mathbf{u} \\ \mathbf{v} \\ \mathbf{j}^+ \\ \mathbf{j}^- \\ \mathbf{p} \\ \mathbf{c}^+ \\ \mathbf{c}^- \\ \xi \end{bmatrix} \\
& + \begin{bmatrix} \mathbf{A} & 0 & 0 & 0 & \mathbf{B} & 0 & 0 & 0 \\ 0 & \mathbf{C} & 0 & 0 & \mathbf{D} & \mathbf{E}^+ & \mathbf{E}^- & \mathbf{F} \\ 0 & 0 & \mathbf{G}^+ & 0 & \mathbf{H}^+ & \mathbf{I}^+ & 0 & \mathbf{J}^+ \\ 0 & 0 & 0 & \mathbf{G}^- & \mathbf{H}^- & 0 & \mathbf{I}^- & \mathbf{J}^- \\ 0 & \mathbf{D}^T & 0 & 0 & 0 & 0 & 0 & 0 \\ 0 & \mathbf{L}^+ & \mathbf{M}^+ & 0 & 0 & 0 & 0 & 0 \\ 0 & \mathbf{L}^- & 0 & \mathbf{M}^- & 0 & 0 & 0 & 0 \\ 0 & 0 & 0 & 0 & 0 & \mathbf{O}^+ & \mathbf{O}^- & 0 \end{bmatrix} \begin{bmatrix} \mathbf{u} \\ \mathbf{v} \\ \mathbf{j}^+ \\ \mathbf{j}^- \\ \mathbf{p} \\ \mathbf{c}^+ \\ \mathbf{c}^- \\ \xi \end{bmatrix} = \begin{bmatrix} \mathbf{F}^u \\ \mathbf{F}^f \\ \mathbf{F}^+ \\ \mathbf{F}^- \\ \mathbf{0} \\ \mathbf{0} \\ \mathbf{0} \\ \mathbf{F}^\xi \end{bmatrix}, \tag{4.18}
\end{aligned}$$

where,

$$\begin{aligned}
\mathbf{u} &:= [\tilde{u}_1 \ \tilde{u}_2 \ \dots \ \tilde{u}_I]^T, \\
\mathbf{v} &:= [\tilde{v}_1 \ \tilde{v}_2 \ \dots \ \tilde{v}_J]^T, \\
\mathbf{j}^+ &:= [\tilde{j}_1^+ \ \tilde{j}_2^+ \ \dots \ \tilde{j}_J^+]^T, \\
\mathbf{j}^- &:= [\tilde{j}_1^- \ \tilde{j}_2^- \ \dots \ \tilde{j}_J^-]^T, \\
\mathbf{p} &:= [\tilde{p}_1 \ \tilde{p}_2 \ \dots \ \tilde{p}_K]^T, \\
\mathbf{c}^+ &:= [\tilde{c}_1^+ \ \tilde{c}_2^+ \ \dots \ \tilde{c}_K^+]^T, \\
\mathbf{c}^- &:= [\tilde{c}_1^- \ \tilde{c}_2^- \ \dots \ \tilde{c}_K^-]^T, \\
\xi &:= [\tilde{\xi}_1 \ \tilde{\xi}_2 \ \dots \ \tilde{\xi}_K]^T, \\
\mathbf{A}_{ij} &:= \int_{\Omega} 2(\mu_s \boldsymbol{\epsilon}(\mathbf{w}_j) : \boldsymbol{\epsilon}(\mathbf{w}_i) + \lambda_s (\nabla \cdot \mathbf{w}_j)(\nabla \cdot \mathbf{w}_i)) dV, \\
\mathbf{B}_{ij} &:= - \int_{\Omega} \nabla \cdot \mathbf{w}_i q_j dV, \\
\mathbf{C}_{ij} &:= \int_{\Omega} (\mathbf{K}^{-1} \mathbf{r}_j) \cdot \mathbf{r}_i dV, \\
\mathbf{D}_{ij} &:= - \int_{\Omega} \nabla \cdot \mathbf{r}_i q_j dV,
\end{aligned}$$

$$\begin{aligned}
\mathbf{E}_{ij}^\beta &:= - \int_{\Omega} \nabla \cdot \mathbf{r}_i (\phi^l - \phi^\beta) RT d_j^\beta dV, \\
\mathbf{F}_{ij} &:= \int_{\Omega} \nabla \cdot \mathbf{r}_i z^{fc} c^{fc} Fr_j dV, \\
\mathbf{G}_{ij}^\beta &:= \int_{\Omega} ((\mathbf{D}^\beta)^{-1} \mathbf{s}_j^\beta) \cdot \mathbf{s}_i^\beta dV, \\
\mathbf{H}_{ij} &:= - \int_{\Omega} \nabla \cdot (c^\beta \mathbf{s}_i^\beta) \frac{\bar{V}^\beta}{RT} q_j dV, \\
\mathbf{I}_{ij}^\beta &:= - \int_{\Omega} \nabla \cdot \mathbf{s}_i^\beta (2 - \phi^\beta) d_j^\beta dV, \\
\mathbf{J}_{ij}^\beta &:= \int_{\Omega} \nabla \cdot (c^\beta \mathbf{s}_i^\beta) z^\beta \frac{F}{RT} r_j dV, \\
\mathbf{K}_{ij}^\beta &:= \int_{\Omega} \nabla \cdot (c^\beta n^f \mathbf{w}_j) d_i^\beta dV, \\
\mathbf{L}_{ij}^\beta &:= \int_{\Omega} \nabla \cdot (c^\beta \mathbf{r}_j) d_i^\beta dV, \\
\mathbf{M}_{ij}^\beta &:= \int_{\Omega} \nabla \cdot (n^f \mathbf{s}_j^\beta) d_i^\beta dV, \\
\mathbf{N}_{ij}^\beta &:= \int_{\Omega} d_i^\beta n^f d_j^\beta dV, \\
\mathbf{O}_{ij}^\beta &:= \int_{\Omega} \mathbf{r}_i z^\beta d_j^\beta dV, \\
\mathbf{F}_i^u &:= \int_{\Gamma_u^N} \mathbf{g}_u^N \cdot \mathbf{w}_i dS, \\
\mathbf{F}_i^f &:= - \int_{\Gamma_p^D} \mathbf{n} \cdot \mathbf{r}_i p_{in} dS - \int_{\Gamma_p^D} \mathbf{n} \cdot \mathbf{r}_i (\phi^l - \phi^+) RT c_{in}^+ dS - \\
&\quad \int_{\Gamma_p^D} \mathbf{n} \cdot \mathbf{r}_i (\phi^l - \phi^-) RT c_{in}^- dS + \int_{\Gamma_p^D} \mathbf{n} \cdot \mathbf{r}_i z^{fc} c^{fc} F \xi_{in} dS, \\
\mathbf{F}_i^+ &:= - \int_{\Gamma_p^D} (\mathbf{n} \cdot \mathbf{s}_i^+ (2 - \phi^+) c_{in}^+ + \mathbf{n} \cdot \mathbf{s}_i^+ z^+ \frac{F}{RT} c_{in}^+ \xi_{in} + \mathbf{n} \cdot \mathbf{s}_i^+ \frac{\bar{V}^+}{RT} c_{in}^+ p_{in}) dS, \\
\mathbf{F}_i^- &:= - \int_{\Gamma_p^D} (\mathbf{n} \cdot \mathbf{s}_i^- (2 - \phi^-) c_{in}^- + \mathbf{n} \cdot \mathbf{s}_i^- z^- \frac{F}{RT} c_{in}^- \xi_{in} + \mathbf{n} \cdot \mathbf{s}_i^- \frac{\bar{V}^-}{RT} c_{in}^- p_{in}) dS, \\
\mathbf{F}_i^\xi &:= - \int_{\Omega} \mathbf{r}_i z^{fc} c^{fc} dV.
\end{aligned}$$

This system of equations is solved by an Euler implicit time discretisation.

For the non-linear terms in the matrices, the values of the parameters at the previous time-step are used, assuming that the values do not change much in between the time steps.

The non-linear terms do not cause problems in the finite element formulation, because in \mathbf{H}^+ , \mathbf{H}^- , \mathbf{J}^+ , \mathbf{J}^- , \mathbf{K}^+ , \mathbf{K}^- , \mathbf{L}^+ , and \mathbf{L}^- , the gradient of a piecewise constant function for c^β times a piecewise linear function is used. This results in a gradient of a piecewise linear function, that can be computed easily.

4.4 Electrochemical Potentials

A disadvantage of this set of equations is that the concentrations c^+ and c^- , the fluid pressure p , and the electrical potential ξ are discontinuous functions. So, it is more complicated to prescribe the boundary conditions. This is caused by the presence of the fixed charges. When there is a discontinuity of the fixed charges, for example over the boundary between a sample and the bathing solution, there is a discontinuity for the ion concentrations (because of electro-neutrality), the fluid pressure (because of an osmotic pressure) and the electrical potentials (because of a Nernst potential). From the electro-neutrality condition (4.4) it follows that

$$c^+ = -\frac{z^-}{z^+}c^- - \frac{z^{fc}}{z^+}c^{fc}. \quad (4.19)$$

So, when the fixed charged density c^{fc} shows a jump, the ion concentration c^+ shows a jump too. The same holds for the anion concentration.

The jump in the fluid pressure is described by (4.16). Since the concentrations are discontinuous, the osmotic pressure is discontinuous. The electrical potential difference over the boundary of a sample is described by (4.17) and is discontinuous too.

Therefore, Huyghe and Janssen [44] use electrochemical potentials. These potentials are continuous functions. They are defined by equations (2.17) and (2.18):

$$\mu^\beta := \mu_0^\beta(T) + p + \frac{z^\beta}{V^\beta}F\xi + \frac{RT}{V^\beta} \ln\left(f^\beta \frac{c^\beta}{\sum_{\gamma=l,+,-} c^\gamma}\right), \quad \beta = l, +, -. \quad (4.20)$$

The extended Darcy's law (2.30) and the extended Fick's law (2.31) are given by

$$\begin{aligned} n^f(\mathbf{v}^l - \mathbf{v}^s) &= -\frac{\mathbf{K}}{n^f} (n^l \nabla \mu^l + n^+ \nabla \mu^+ + n^- \nabla \mu^-), \\ c^\beta(\mathbf{v}^\beta - \mathbf{v}^l) &= -\mathbf{D}^\beta \frac{\bar{V}^\beta c^\beta}{RT} \nabla \mu^\beta, \quad \beta = +, -. \end{aligned}$$

The four-component mixture theory is described by (4.10). Now, the discontinuous fluid pressure p , the cation concentration c^+ , the anion concentration c^- and the electrical potential ξ are replaced by the continuous electrochemical potentials. In a special case, these unknowns can be expressed as algebraic functions of the electrochemical potentials μ^l , μ^+ and μ^- . Therefore, we have to make some assumptions:

- We consider a mono-valent salt-solution ($z^+ = +1$ and $z^- = -1$).
- The number of ions is small compared to the number of liquid molecules: $c^+ \ll c^l$ and $c^- \ll c^l$. This means also that $n^+ \ll n^f$, $n^- \ll n^f$ and $c^l = \frac{1}{V^l} \frac{n^f}{n^f + n^+ + n^-} \approx \frac{1}{V^l}$.
- The activity coefficients f^+ and f^- do not depend on the ion concentrations.

- In the electrochemical potentials for the ions, the fluid pressure can be neglected compared to the concentration and the electrical potential terms:

$$\mu^\beta \approx \mu_0^\beta(T) + z^\beta \frac{F}{\bar{V}^\beta} \xi + \frac{RT}{\bar{V}^\beta} \ln \left(f^\beta \frac{c^\beta}{\sum_{\gamma=l,+,-} c^\gamma} \right), \quad \beta = +, -. \quad (4.21)$$

Now, the equations (4.21) are multiplied by \bar{V}^β and then summed:

$$RT \ln \left(\frac{f^+ c^+ f^- c^-}{\left(\sum_{\gamma=l,+,-} c^\gamma \right)^2} \right) = \bar{V}^+ (\mu^+ - \mu_0^+) + \bar{V}^- (\mu^- - \mu_0^-). \quad (4.22)$$

Then, the condition of electro-neutrality (4.4) is used:

$$\begin{aligned} c^- (c^- - z^{fc} c^{fc}) &= \frac{\left(\sum_{\gamma=l,+,-} c^\gamma \right)^2}{f^+ f^-} \exp \left(\frac{\bar{V}^+ (\mu^+ - \mu_0^+) + \bar{V}^- (\mu^- - \mu_0^-)}{RT} \right) \\ &\approx \frac{1}{(\bar{V}^l)^2} \frac{1}{f^+ f^-} \exp \left(\frac{\bar{V}^+ (\mu^+ - \mu_0^+) + \bar{V}^- (\mu^- - \mu_0^-)}{RT} \right). \end{aligned}$$

From this equation and the electro-neutrality condition, it follows that

$$c^- = +\frac{1}{2} z^{fc} c^{fc} + \frac{1}{2} \sqrt{\left(z^{fc} c^{fc} \right)^2 + 4 \frac{1}{(\bar{V}^l)^2} \frac{1}{f^+ f^-} \exp \left(\frac{\bar{V}^+ (\mu^+ - \mu_0^+) + \bar{V}^- (\mu^- - \mu_0^-)}{RT} \right)}, \quad (4.23)$$

$$c^+ = -\frac{1}{2} z^{fc} c^{fc} + \frac{1}{2} \sqrt{\left(z^{fc} c^{fc} \right)^2 + 4 \frac{1}{(\bar{V}^l)^2} \frac{1}{f^+ f^-} \exp \left(\frac{\bar{V}^+ (\mu^+ - \mu_0^+) + \bar{V}^- (\mu^- - \mu_0^-)}{RT} \right)}. \quad (4.24)$$

The relations for the ions have to be substituted into equation (4.20) for $\beta = l$:

$$\begin{aligned} p &= \mu^l - \mu_0^l - \frac{RT}{\bar{V}^l} \ln \left(f^l \left(1 - \frac{c^+ + c^-}{\sum_{\gamma=l,+,-} c^\gamma} \right) \right) \\ &\approx \mu^l - \mu_0^l - \frac{RT}{\bar{V}^l} \ln \left(f^l \left(1 - \bar{V}^l (c^+ + c^-) \right) \right). \end{aligned} \quad (4.25)$$

Furthermore, the relations for the ions have to be substituted into relation (4.21):

$$\begin{aligned} \xi &= \frac{1}{F} \left(\bar{V}^+ (\mu^+ - \mu_0^+) - RT \ln \left(f^+ \frac{c^+}{\sum_{\gamma=l,+,-} c^\gamma} \right) \right) \\ &\approx \frac{1}{F} \left(\bar{V}^+ (\mu^+ - \mu_0^+) - RT \ln (\bar{V}^l f^+ c^+) \right). \end{aligned} \quad (4.26)$$

The functions $p = p(\mu^l, \mu^+, \mu^-)$ and $\xi = \xi(\mu^+, \mu^-)$ are highly non-linear. These functions are substituted into equations (4.10). In this way four discontinuous unknowns are replaced by three continuous unknowns. The electro-neutrality condition can be removed from the set of equations, since this condition is already used in order to express the fluid pressure, the cation and anion concentrations and the electrical potential as functions of the electrochemical potentials.

The advantages of this set of equations compared to the set of equations of section 4.1 are:

- The equations to solve contain less unknowns (15 unknowns in 3D: \mathbf{u} , \mathbf{v} , \mathbf{j}^+ , \mathbf{j}^- , μ^l , μ^+ and μ^-) than in the set of equations of section 4.1 (16 unknowns in 3D: \mathbf{u} , \mathbf{v} , \mathbf{j}^+ , \mathbf{j}^- , p , c^+ , c^- and ξ).
- All unknowns are continuous over the boundary.

The disadvantages are:

- The equations are highly non-linear.
- The electrochemical potentials do not have a direct physical meaning. It is easier to interpret the fluid pressure, the ion concentrations and the electrical potential, than the electrochemical potentials.

This formulation has advantages for the three-component mixture theory [51, 70]. For the four-component mixture theory, the disadvantages are bigger than the advantages for the description with electrochemical potentials. Therefore, we consider only the set of equations of section 4.1.

5 Experiments on Intervertebral Discs

5.1 Introduction

Connective tissues, like articular cartilage and intervertebral disc tissue, swell or shrink due to mechanical, chemical and electrical loads. The tissue behaviour has been modelled by mixture theories [15, 28, 29, 43, 45, 51, 61, 70]. We consider the four-component mixture model derived by Huyghe and Janssen [43]. Here, four components are distinguished: a charged porous solid, a fluid, cations and anions. As described in table 1.1, the fluid flow, the solute flow and the electrical current can be induced by a pressure gradient, a concentration gradient and an electrical potential field. In order to describe these phenomena by the four-component mixture theory, we need to determine the stiffness, the permeability, the diffusion coefficients for the ions and the osmotic coefficients. The values of these parameters are determined by experiments.

Previously, the material parameters were determined by one-dimensional permeation experiments [33, 35] or by uniaxial experiments. In permeation experiments, a pressure gradient is applied across a sample. In this way, a fluid flow and a streaming potential are generated [33, 58]. The uniaxial experiments can be split into two groups. In the first group of experiments, the deformation of the sample is allowed and measured in one direction. The deformation may be due to mechanical loads only [45, 61] or to a combination of mechanical and chemical loads [24, 28, 29, 40, 41, 63]. In the second group of experiments, the deformation is kept constant and the resulting swelling pressure is measured [23, 63].

The goals of this study are the verification of the four-component mixture theory and the determination of the material parameters of the intervertebral disc tissue by confined swelling and compression experiments. The parameters are determined by fitting the measurements to the four-component mixture theory. The mixture model is verified by comparing the values estimated by parameter fitting to the values reported in other studies [6, 23, 36, 59].

5.2 Intervertebral Disc Tissue

An intervertebral disc is a cartilaginous structure that is located between two vertebral bodies (figure 5.1). The tissue consists of a gelatinous centre, the nucleus pulposus, surrounded by several concentrically arranged lamellae, the annulus fibrosus. In these lamellae, fibre networks can be seen. The orientation of these fibres differs per lamella. Obviously, these fibres make the material anisotropic.

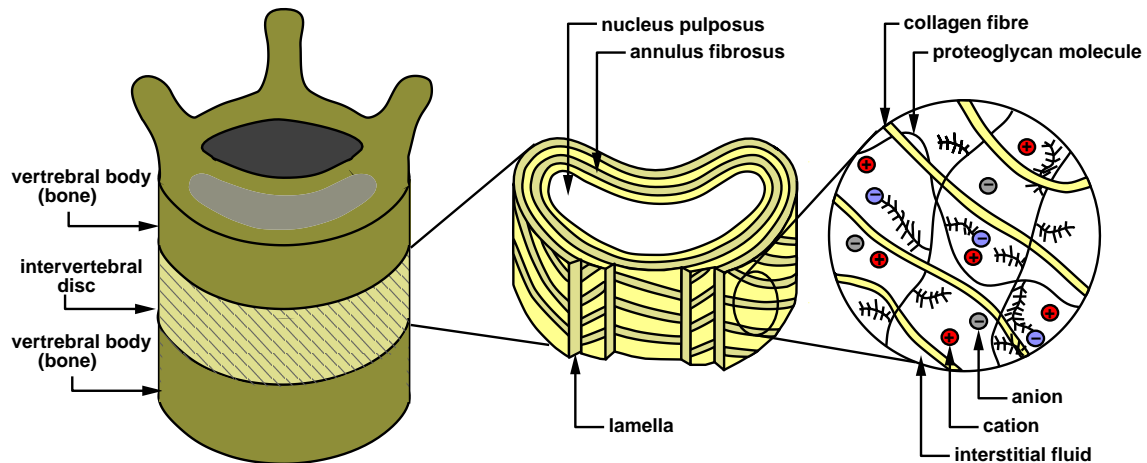


Figure 5.1 Intervertebral disc tissue.

The material mainly consists of a collagen network embedded in a hydrated proteoglycan gel. Collagen is a rod-like protein molecule built of long polypeptide chains. Proteoglycans are large molecules consisting of many glycosaminoglycans linked to core proteins. These glycosaminoglycans are made up of long chains of polysaccharides. Due to the physiological pH and the ionic strength of the interstitial fluid, the carboxyl and sulfate groups of the polysaccharides are ionised. The density of these charges is the fixed charge density. Due to this ionisation the proteoglycans are capable of retaining water up to a 50-fold of their own weight [19].

Because the proteoglycans are relatively fixed to the collagen network, osmotic phenomena occur under physiological conditions. The osmotic pressure within the disc ensures that the fibres of the annulus fibrosus are mainly subjected to tensile stresses, although the disc transfers compressive stresses from vertebral body to vertebral body. To understand this osmotic contribution, we subject samples to non-physiological changes in the external salt concentration. The chemical load to the sample changes with the salt concentration of the bathing solution. The osmotic swelling pressure in the disc highly depends on the proteoglycan content [23].

The tissue can also deform because of a mechanical force. The evolution in time of the deformation depends on the permeability and the stiffness of the matrix [41, 61].

The disc also contains cells. Since the cell density is low (5800 cells/mm^3) and the cell volume is less than 1% of the total volume [75], we assume that the cells hardly contribute to the mechanical behaviour of the total material. Meanwhile, the cells are

responsible for maintaining and remodelling the solid matrix. Their activity is vital for the health of the disc [75]. It is believed that mechanisms controlling the cellular metabolism depend on mechanical, physicochemical and electrical events in the tissue during deformation (see e.g. [26, 33]). Therefore, it is important to understand the relation between these events and the external forces.

5.3 Material and Methods

5.3.1 Sample preparation

The samples were made out of the annulus fibrosus part of the intervertebral disc tissue. They were prepared according to Houben [40, 41]. Here a short description is given. Intervertebral discs were obtained from the lumbar spines of 3 German Shepherds (2 males, 1 female, weight: 25 – 40 kg, age: 1 – 3 years), which were previously used for cardiac experiments. We assumed that the operations and the drugs did not influence the mechanical properties of the intervertebral discs. The lumbar part of the spine (L1 – S1) was removed within 3 hours after death. The muscle tissue and the ligaments were cut off while avoiding damage of the disc surface. The spines were sealed in plastic bags and placed in a freezer at $-65\text{ }^{\circ}\text{C}$. Within two weeks, rectangular slabs were sawed out of the annulus fibrosus part of the frozen discs L4-L5 to L7-S1, while cooling by liquid nitrogen ($-196\text{ }^{\circ}\text{C}$). Out of these slabs, 79 cylindrical samples (diameter 3.9 mm, height approximately 1 mm) were made using a lathe, while cooling again by liquid nitrogen. Each sample was put in an aluminium cup and kept in the freezer for maximally 21 days. During all stages of preparation the tissue was kept frozen.

5.3.2 Experimental set-up

In a uniaxial *confined swelling and compression experiment*, a cylindrical sample was enclosed in an impermeable confining ring made out of stainless steel (figure 5.2). A mechanical load was applied on top of the sample via a stainless steel loading piston. At the bottom of the sample was a glass filter through which a NaCl solution flowed. The permeability of the glass filter (pore size 16 – 40 μm , permeability $10^{-12}\text{ m}^4\text{N}^{-1}\text{s}^{-1}$) was much larger than the permeability of the sample. Thus, the boundary conditions were well defined for the fluid flow and for the ion concentrations along the filter-sample interface. A chemical load was applied by altering the salt concentration of the bathing solution.

During the experiments, the displacement of the piston was recorded via a linear variable displacement transducer (LVDT, Schaevitz, USA) interfaced by a Labmaster 12 bit AD converter (Scientific Solutions Inc., USA) to an IBM-AT. The data acquisition sampling frequency was 0.125 Hz. A vibrator was attached to the set-up, in order to overcome the sticking of the piston to the wall. This device vibrated intermittently at 50

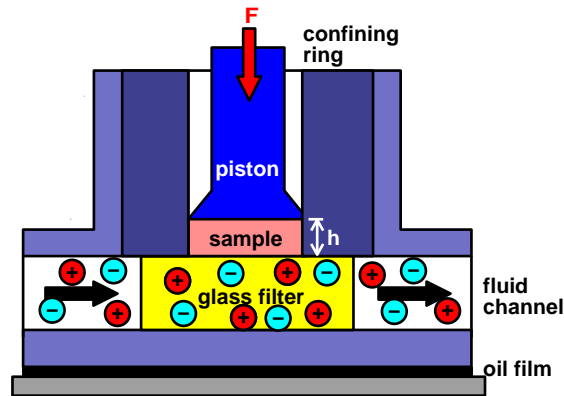


Figure 5.2 Schematic representation of the experimental set-up. The sample is enclosed in an impermeable confining ring.

Hz during 2 seconds. The vibration started 2 seconds after the data-acquisition. Lateral forces on the piston were minimised by allowing free lateral motion of the measuring chamber floating on a silicon oil film. Furthermore, the piston was greased with vaseline to prevent leakage between the wall and the piston.

5.3.3 Experimental protocol

Before starting the experiment, the irregularities of the frozen sample were removed by a scalpel. Then, the sample was placed in the loading chamber and the piston was put on top of it. Air in the set-up was removed by a vacuum pump. The temperature was kept at 22 ± 1 °C. The sample was loaded by the protocol of table 5.1 [28]. The duration of each stage was chosen such that an equilibrium was reached at the end of each stage. An equilibrium was considered to be reached when the sample height did not change more than 1% for the last hour. The duration of each stage depended on the size of the sample and its original position in the disc. The first stage, the conditioning stage, was used to get a well defined starting situation.

stage	conditioning	swelling	consolidation	control
mechanical load [MPa]	0.078	0.078	0.195	0.078
concentration [mol l^{-1}]	0.469 ± 0.026	0.159 ± 0.014	0.159 ± 0.014	0.469 ± 0.026

Table 5.1 Experimental protocol.

Note that the boundary conditions of the first and last stage were the same. This was done to check whether the material properties were maintained during the experiments.

5.3.4 Data analysis

Successful experiments were selected for further analysis. An experiment was considered successful, when no visible leakage occurred over the piston, no parts of bones or blood were included in the samples and the sample height after the first and the fourth stage differed less than 5%.

The material parameters were obtained by fitting the second and third stage. We assumed that the values of the parameters did not depend on the deformation. We fitted the experiments in the following way. In first approximation, the osmotic pressure was the same at the end of both stages, since there was no change in the concentration of the bathing solution, only a change in the fixed charged density. So, the value for the aggregate modulus $H := 2\mu_s + \lambda_s$ was determined from the increase of the mechanical load $\Delta\sigma$ and the strain ϵ of the sample:

$$H := \frac{\Delta\sigma}{\epsilon}, \quad (5.1)$$

with

$$\epsilon := \frac{h_2 - h_3}{h_3}, \quad (5.2)$$

where h_2 and h_3 were respectively the sample heights at the end of the second and the third stage.

The porosity of a sample was measured afterwards by freeze drying [40]. In this method, the weight of wet sample was measured directly after the experiment. The wet sample is the sample saturated with fluid. Also, the weight of the dried sample was measured. The difference in weight determined the amount of fluid that had disappeared. We assumed that the density of the fluid is equal to the density of water. Then, we computed the volume of the fluid V^f . Since we knew the total sample volume V^{tot} , we computed the porosity at the end of the experiment by

$$n^f = \frac{V^f}{V^{tot}}. \quad (5.3)$$

The fixed charge density c^{fc} was measured by a tracer cation method [40]. Here, the amount of fixed charges was measured. Since we knew the amount of fluid, the fixed charge density was computed.

Next, the osmotic coefficients were fitted. According to the momentum balance (4.1) and Hooke's law (4.6), the equilibrium height depends on the aggregate modulus H and the fluid pressure p . In equilibrium, the fluid and ion flows are equal to zero and the fluid pressure p is coupled to the osmotic coefficients ϕ^l , ϕ^+ and ϕ^- , the ion concentrations c^+ and c^- and the electrical potential field ξ , according to the extended Darcy's law (4.7) and the extended Fick's law (4.8). The aggregate modulus H was determined already. We assumed that the osmotic coefficients for the fluid, the cations, and the anions were the same:

$$\phi^l = \phi^+ = \phi^- = \phi. \quad (5.4)$$

The value for the osmotic coefficient in a free NaCl solution depends on the concentration. However, in the range from 0.15 M to 0.50 M it is almost constant [40, 63]. So, we assumed a constant osmotic coefficient ϕ in the bathing solution: $\phi = 0.924$. The value inside the sample was estimated by a fitting procedure such that the absolute error between the measured and computed equilibrium height of the second stage was minimised. Therefore, the experiments were simulated by a finite element code of the four-component mixture theory (chapter 4). We assumed that there was no leakage over the electrode filter and that the material parameters did not depend on the tissue deformation. The mechanical loads at the top of the sample were prescribed (figure 5.3). There were no ion and fluid flows at the top. At the bottom the ion concentrations, the

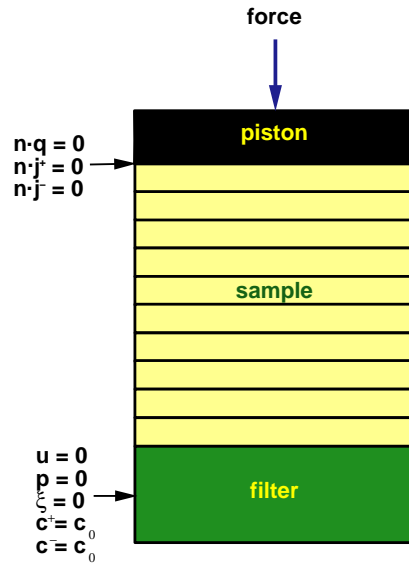


Figure 5.3 Boundary conditions for the uniaxial confined swelling and compression experiment.

fluid pressure ($p = 0$: free outflow) and the electrical potential ($\xi = 0$) were prescribed. Since these values had to be described in the middle of an element, we assumed that the element closest to the filter was immediately in equilibrium with the bathing solution. We checked this assumption by estimating the time constant τ . Since the convection is slower than the diffusion, the biphasic time constant is used:

$$\tau := \frac{h^2}{HK}, \quad (5.5)$$

where h is the distance to the boundary and K is the hydraulic permeability. The total sample height is about 1 mm. We divided the sample in 10 uniform elements. Thus, $h \approx 0.05$ mm. The aggregate modulus H is about 1 MPa and the permeability K is about $2.5 \cdot 10^{-16} \text{ m}^4 \text{ N}^{-1} \text{ s}^{-1}$. So, $\tau \approx 10$ s. Thus, the equilibrium assumption is reasonable.

The permeability was determined by fitting the curve of the sample height of the swelling and the consolidation stages. We fitted the permeability in such way that

the absolute difference between the measured and the computed curve for the sample height was minimised.

The values for the diffusion coefficients could not be estimated directly. Therefore we used the values determined by Maroudas [59]:

$$D^\beta = 0.63 (n^f)^2 D_w^\beta, \quad \beta = +, -, \quad (5.6)$$

where $D_w^+ = 13.34 \cdot 10^{-10} \text{ m}^2\text{s}^{-1}$ and $D_w^- = 20.32 \cdot 10^{-10} \text{ m}^2\text{s}^{-1}$ are the diffusion coefficients in an aqueous solution [54].

5.4 Results

Representative results of 4 successful experiments are shown in figure 5.4. Using the criteria 23 experiments out of 79 were successful [40].

In the figures, the four stages can be recognised. In the first stage, from an unknown starting condition a well defined equilibrium was reached.

In the second stage, the external salt concentration was reduced, causing the sample to swell in the range of 4.9% – 10.0%.

In the third stage, the sample shrank due to an increase of the mechanical load from 0.078 MPa to 0.195 MPa. The tissue shrinking was in the range of 8.1% – 17.8%.

In the final stage, the same equilibrium should be reached as at the end of the first stage.

The results of the fitting procedure are shown in figure 5.5 and table 5.2.

The values of the material properties were estimated by parameter fitting. The aggregate modulus H was 0.87 ± 0.22 MPa (mean \pm standard deviation), the osmotic coefficient ϕ inside the sample was 0.896 ± 0.008 , and the permeability was $2.6 \cdot 10^{-16} \pm 0.8 \cdot 10^{-16} \text{ m}^4\text{N}^{-1}\text{s}^{-1}$.

The measured values for the porosity n^f at the end of the first stage is 0.767 ± 0.043 and the fixed charged density c^{fc} is $0.115 \pm 0.016 \text{ mol l}^{-1}$.

parameter	value	
aggregate modulus H	$0.87 \cdot 10^6 \pm 0.22 \cdot 10^6$	N m^{-2}
hydraulic permeability K	$2.6 \cdot 10^{-16} \pm 0.8 \cdot 10^{-16}$	$\text{m}^4\text{N}^{-1}\text{s}^{-1}$
diffusion coefficient for the cations D^+	$5.0 \cdot 10^{-10} \pm 0.6 \cdot 10^{-10}$	$\text{m}^2 \text{ s}^{-1}$
diffusion coefficient for the anions D^-	$7.6 \cdot 10^{-10} \pm 0.9 \cdot 10^{-10}$	$\text{m}^2 \text{ s}^{-1}$
osmotic coefficient ϕ inside the sample	0.896 ± 0.008	

Table 5.2 The values of the parameters estimated by the fitting procedure.

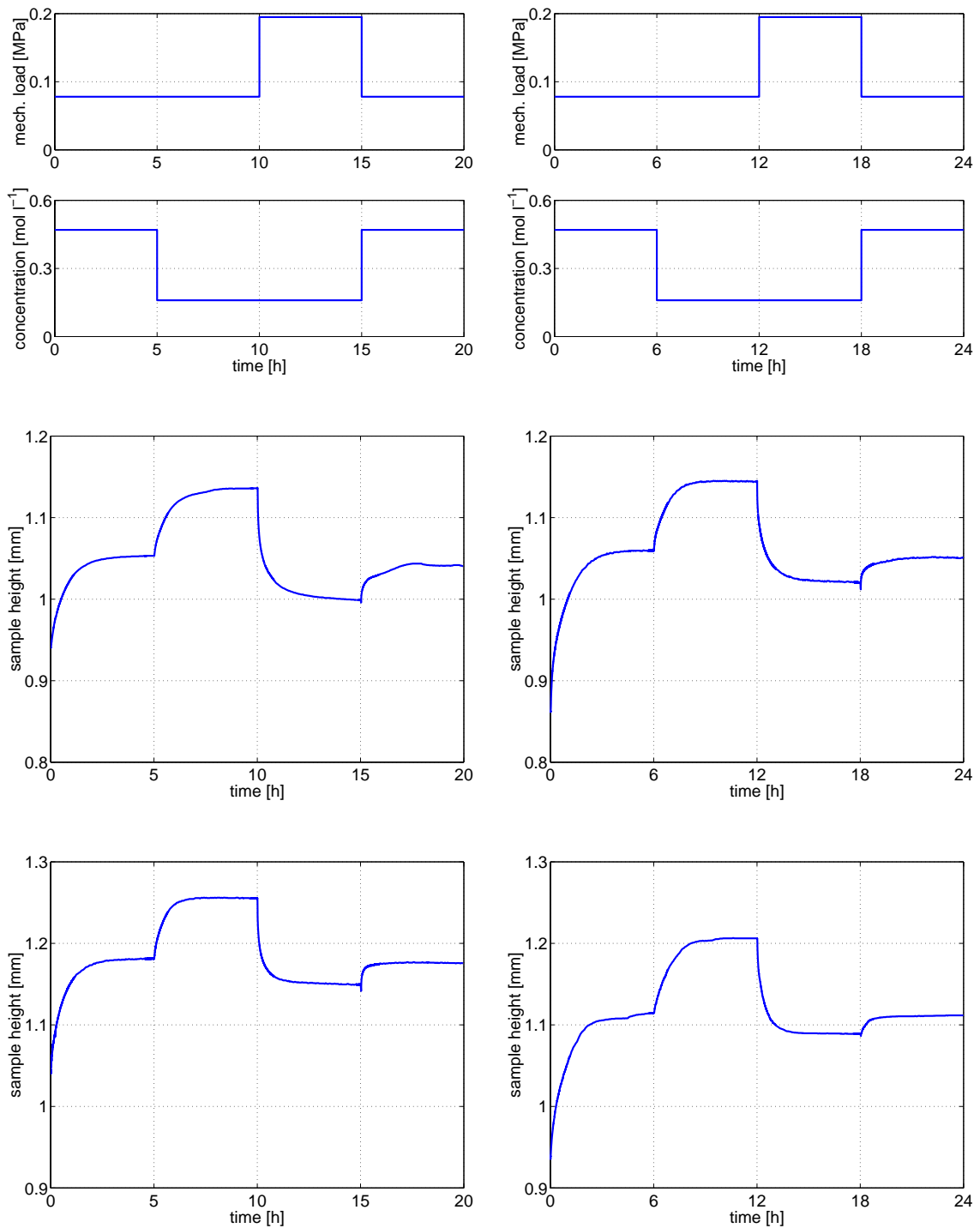


Figure 5.4 Experimental results for 4 confined swelling and compression experiments performed on intervertebral disc tissue. The boundary conditions are given in the corresponding top figures.

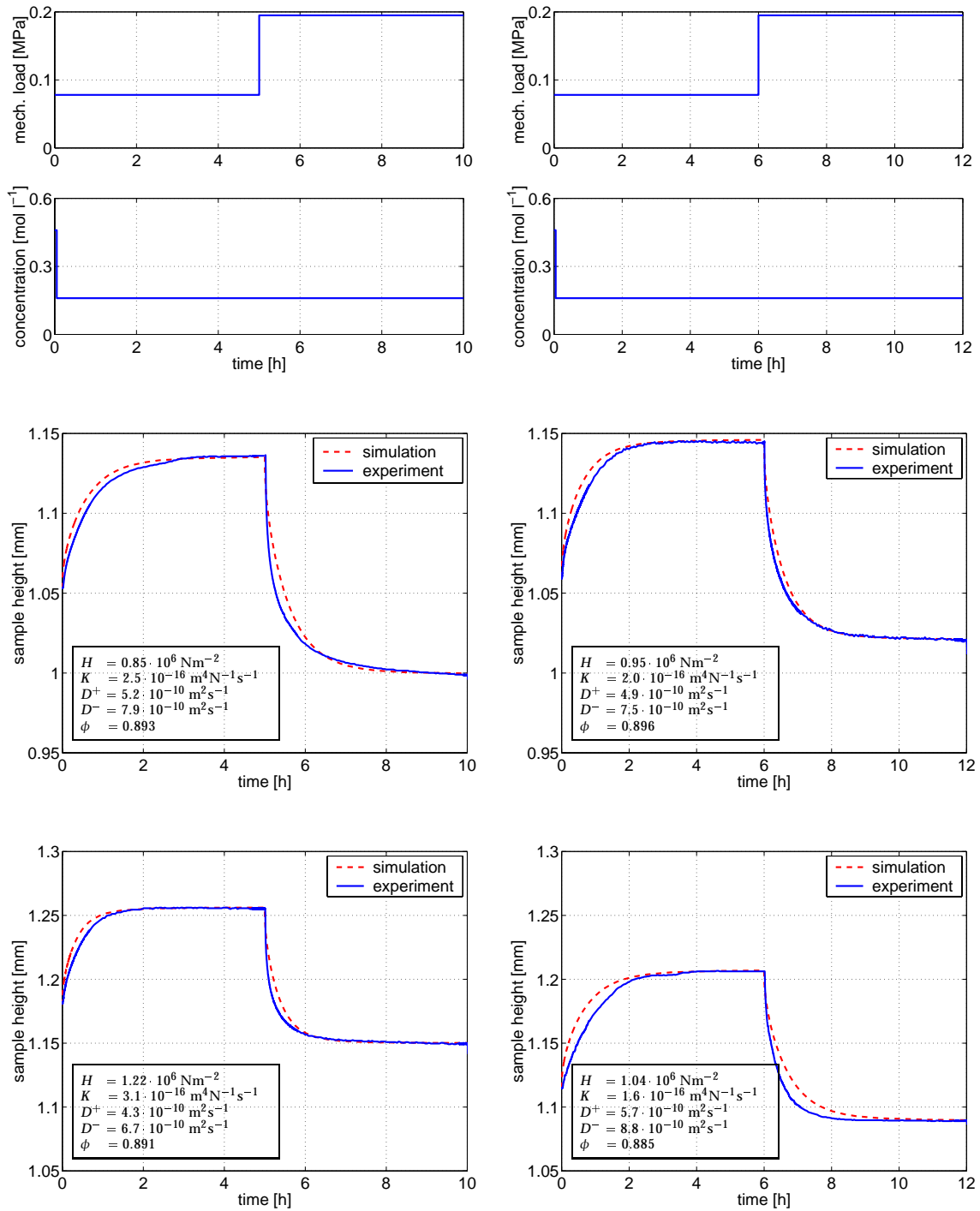


Figure 5.5 Experimental and numerical results for confined swelling and compression experiments performed on intervertebral disc tissue. The boundary conditions are given in the top figures.

5.5 Discussion

One-dimensional confined swelling and compression of annulus fibrosus samples were fitted reasonably well by the four-component model (absolute error in the sample height is maximal 3 %), although we assume that the material parameters are constant. The values for the aggregate modulus 0.87 ± 0.22 MPa (mean value \pm standard deviation) were in the same range as found in other studies, for example by Drost et al. [23]: 1.01 ± 0.31 MPa for specimens taken in axial direction and 0.66 ± 0.30 MPa for specimens taken in radial direction. The values for the permeability, $2.6 \cdot 10^{-16} \pm 0.8 \cdot 10^{-16} \text{ m}^4\text{N}^{-1}\text{s}^{-1}$, were also in the same range as found in other studies, for example by Best et al. [6] and Guilak et al. [36]: $2.2 \cdot 10^{-16} - 4.0 \cdot 10^{-16} \text{ m}^4\text{N}^{-1}\text{s}^{-1}$. However, the rate of swelling appeared to be overestimated, since the computed data for the sample height are above the measured data, whereas the rate of consolidation is underestimated. It appeared that the fluid inflow was slowed down by the ion outflow. The swelling in the second stage was caused by an osmotic pressure. In this stage, a new equilibrium had to be reached. This could be reached by an inflow of the fluid and an outflow of cations and anions. So, there were two flows in opposite direction. Both flows were slowed down due to the friction between the fluid particles and the ions. This process can be modelled by an 'effective' permeability that is smaller than the permeability that is needed when the swelling is caused by a decrease of the mechanical load. It can also be modelled by increasing the difference between the liquid and the ion osmotic coefficient: $\phi^l - \phi^\beta$, $\beta = +, -$. For example by taking $\phi^l = 1$. From equation (2.32) it follows that the fluid flux is slowed down. In the consolidation stage, another mechanism plays a role: the fluid flow and the flow of the ions are in the same direction, since the salt concentrations should stay the same. Since the flows are in the same direction, the friction between the molecules and the ions is less important and the resulting 'effective' permeability is larger. This follows also from equation (2.32), since the gradient in the ion concentrations is very small.

In contrast to the triphasic models used by de Heus [19], Snijders [70, 71] and Houben [40], physically realistic values for the diffusion coefficients were used to fit the experiments, because the electrical phenomena were not neglected in the four-component mixture theory.

For the set of experiments selected, the equilibrium height after the first (conditioning) and fourth (control) stage are the same within 5%. If this was not the case, the material had deteriorated during the experiment or some experimental problems had occurred, like air in the experimental set-up or a leakage between the piston and the cylinder wall.

As a rule the equilibrium height at the end of the fourth stage was lower than the equilibrium height at the end of the first stage. It means that some mechanical or osmotic stiffness is lost during the experiments. This loss is not included in the model simulations.

5.6 Conclusions

We were able to simulate the evolution in time of the confined swelling and compression experiments by the four-component mixture theory. We verified the theory by comparing the estimated material properties for the stiffness, the permeability and the diffusion coefficients by values reported by other studies [6, 23, 36, 59]. These values were in the same range.

6 Experiments on Hydrogel

6.1 Introduction

When a biological tissue is subjected to a mechanical load, an *electrical potential* gradient is generated [5, 15, 32, 31]. Bassett and Pawluk [5] showed this effect for cartilage, whereas Gross and Williams [32] showed the same effect for bone. Such potential gradient is associated with the flow of charged particles through a matrix with fixed charges [15, 26, 31]. A deformation of the matrix causes a fluid flow relatively to the solid matrix. This fluid flow tends to separate the freely moving ions in the fluid from the oppositely charged particles, that are attached to the matrix (figure 6.1). In this way, an electrical field is created collinear to the fluid flow. This results in an electrical potential, the *streaming potential*.

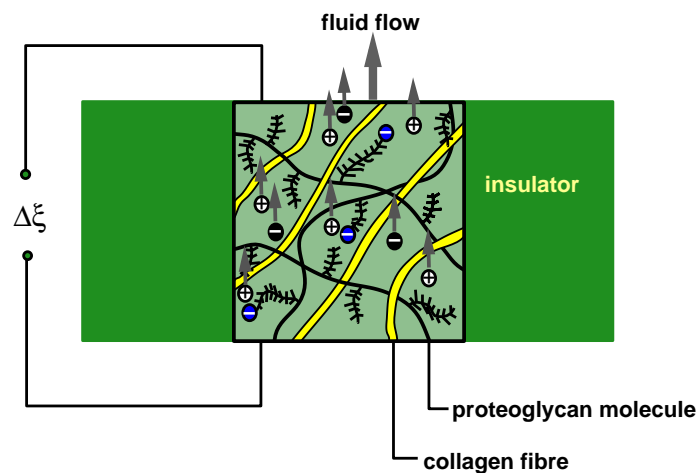


Figure 6.1 Schematic representation of the mechanism that creates a streaming potential $\Delta\xi$ in cartilaginous tissues.

In articular cartilage, streaming potentials have been demonstrated by permeation experiments and confined compression experiments [15, 27, 31, 33, 53, 58]. In the permeation experiments, a hydrostatic pressure gradient is applied across the sample. The pressure generates a fluid flow and a streaming potential that can be measured [33, 58].

Streaming potentials are also generated by deformation of the tissue. Lee et al. [53] and Frank et al. [27] measured streaming potentials generated by oscillatory compression experiments. Chen et al. [15] measured streaming potentials in confined compression experiments. In these experiments, bovine cartilage discs were subjected to step changes of the compressive stress.

The experiments by Lee et al., Frank et al. and Chen et al. can be described reasonably well by a combination of the biphasic theory [61] and linear, macroscopic laws for *electrokinetics* [15, 26, 27] for isotropic media. These laws relate the relative fluid velocity $n^f(\mathbf{v}^f - \mathbf{v}^s)$ and the current density \mathbf{J} to the gradients of the fluid pressure p and the electrical potential ξ [27]:

$$\begin{bmatrix} n^f(\mathbf{v}^f - \mathbf{v}^s) \\ \mathbf{J} \end{bmatrix} = \begin{bmatrix} -k_{11} & k_{12} \\ k_{21} & -k_{22} \end{bmatrix} \begin{bmatrix} \nabla p \\ \nabla \xi \end{bmatrix}, \quad (6.1)$$

where k_{11} is the hydraulic permeability, k_{12} and k_{21} are electrical coupling coefficients and k_{22} is the electrical conductivity. Note that when the electrical coupling coefficients are equal to zero, i.e. $k_{12} = k_{21} = 0$, this set of equations results in Darcy's law and Ohm's law. For the open circuit condition, i.e. $\mathbf{J} = \mathbf{0}$, and without an imposed fluid flow, the electromechanical coupling is characterised by an *electrokinetic coefficient* k_e that relates the change of the mechanical load $\Delta\sigma$ to the change in the electrical potential $\Delta\xi$ for a uniaxial confined compression experiment [15]

$$\Delta\xi = k_e \Delta\sigma. \quad (6.2)$$

Although this theory describes the change in the electrical potential caused by mechanical loads reasonably well, it can not describe the changes in the electrical potential caused by chemical loads. This can be done by the four-component mixture theory [43].

The first goal of this study is the measurement of the electrical potential field caused by mechanical and chemical loads in a confined swelling and compression experiment. The second goal is the verification of the four component mixture theory with respect to the tissue deformation and the electrical potential. Therefore, the material parameters are determined by fitting the measurements to the four-component mixture theory. The mixture theory is verified by comparing the values estimated by parameter fitting to the values reported in other studies

To our knowledge, it is the first time that a streaming potential is measured that is caused by mechanical and chemical loads in a confined swelling and compression experiment. We choose to do the experiments with a tissue that mimics the behaviour of biological tissues: a *hydrogel*. A hydrogel is a synthetic material that consists of large charged polymers that are linked to each other. They form a three-dimensional network. A hydrogel attracts water from its surroundings similar to cartilaginous tissues [19, 63]. Important advantages of the hydrogel compared to biological tissues [63] is that

1. the material degenerates less during the experiments,
2. the samples can be made repeatedly with the same material properties,

3. the material is homogeneous.

In this way the differences between the experimental and the numerical results can be caused by problems in the experimental set-up or by imperfections in the theory. They are not caused primarily by differences in material parameters between the samples or by the degeneration of the tissue.

6.2 Material and Methods

6.2.1 Sample preparation

The samples were made out of a hydrogel. The hydrogel consisted of 11 g acrylic acid monomer (AA), 11 g acrylamide monomer (AAm), 100 g water (H_2O), 0.5 g cross linker MBAAm (N,N'-methylenebisacrylamide) and 0.1 g of the initialisators $(NH_4)_2S_2O_8$ and $K_2S_2O_5$. The solution was neutralised by 6.2 g NaOH. These constituents were put in a test tube where they react with each other as described by de Heus [19]. After the reactions between the components stopped, the material was submerged in a 0.15 molar NaCl-solution for one or two days.

Then, the hydrogel was put in a cup filled with a 0.15 molar NaCl solution and was stored at room temperature.

After taking the hydrogel out of the test tube, it was cut by a scalpel in slices with a thickness of about 1 mm. The diameter of these samples was 4.0 mm.

6.2.2 Experimental set-up

The samples were put in a testing device that was similar to the testing device for the intervertebral disc tissue. In this set-up, we measured the deformation of the sample and the electrical potential difference over the sample (figure 6.2). The following changes were made:

- The confining ring was not made of stainless steel, but it was made of Athlon[®] (Trespa International B.V., The Netherlands). This was done in order to have an electrical insulating ring around the sample. Athlon[®] was used because it was an insulator and it did not swell due to water absorption (water absorption < 1 weight%, according to the manufacturer).
- The piston material was an insulator, glass, instead of stainless steel. Inside the piston was a chamber filled with a 0.15 M NaCl solution (figure 6.3). This chamber was closed at the bottom with a dense glass filter. Inside the chamber, a Ag/AgCl electrode was placed (MI-402 Micro-Reference Electrode, Microelectrodes Inc., USA).
- A similar electrode as in the piston was mounted in the fluid channel.

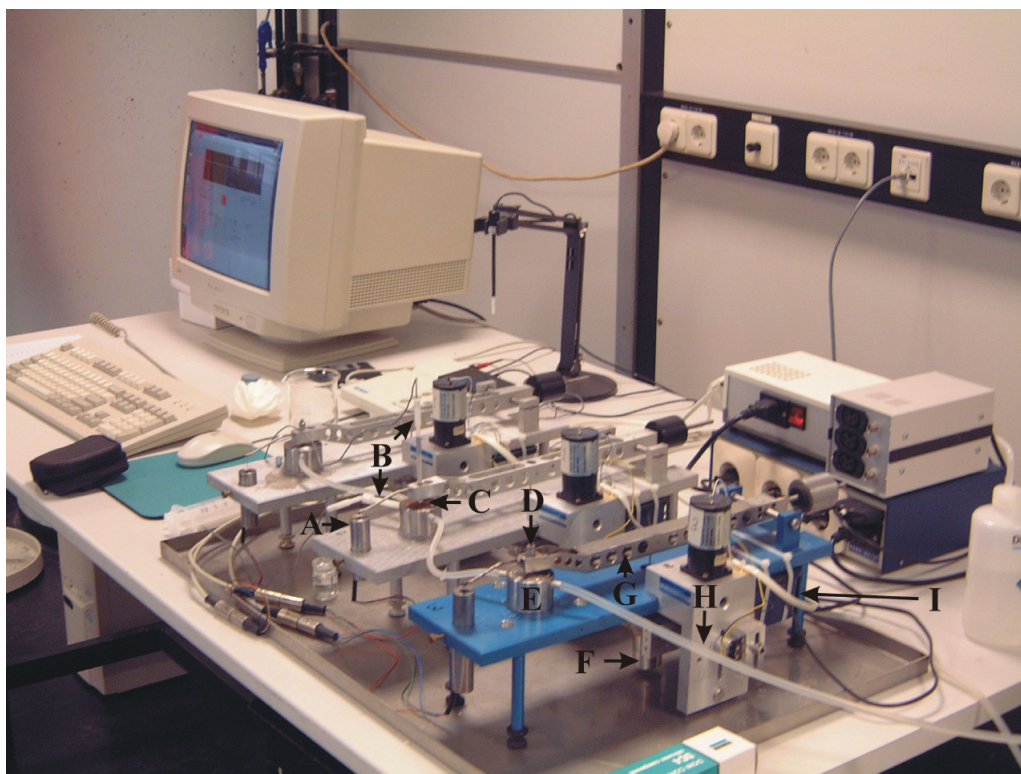


Figure 6.2 Experimental set-up. A: linear variable displacement transducer, B: electrode, C: confining ring, D: piston, E: measuring chamber, F: weights, G: loading arm, H: fluid inlet, I: vibrator.

The deformation of the sample and the electrical potential difference over the sample were measured. The electrical potential difference between both electrodes were amplified by an amplifier (Unicam 9460, Unicam, USA). During the experiments, the displacement of the piston was recorded via a linear variable displacement transducer (LVDT, Schaevitz, USA). The data acquisition sampling was 0.5 Hz. A vibrator was attached to the set-up in order to overcome the sticking of the piston to the wall. This device vibrated intermittently at 50 Hz during 1 second. The vibration started 0.5 second after the data-acquisition. Lateral forces on the piston were minimised by allowing free lateral motion of the measuring chamber floating on a silicon oil film. Furthermore, the piston was greased with vaseline to prevent leakage between the wall and the piston.

Before the experiment started, the electrodes were filled with an electrolyte solution from Microelectrodes Inc., USA (3.0 M KCl solution saturated with AgCl).

6.2.3 Experimental protocol

The experimental protocol (table 6.1) was similar to that of the intervertebral disc tissue. The first three stages were the same. Thereafter, a faster change in the external salt con-

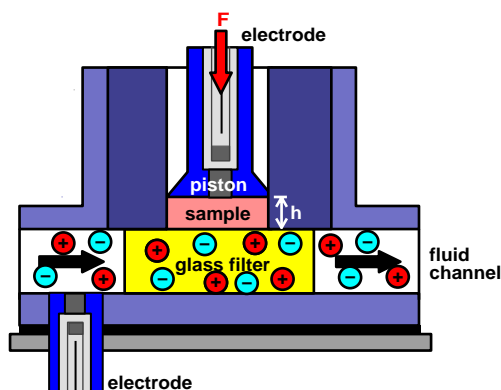


Figure 6.3 Schematic representation of the experimental set-up.

centration was applied. In these stages no equilibrium was reached for both the sample height and the electrical potential difference. The values for the ion concentration were chosen such that the shrinking of the sample due to the mechanical load was about the same as the swelling due to the chemical load.

stage	mechanical load [MPa]	concentration [mol l ⁻¹]
1	0.078	0.45
2	0.078	0.15
3	0.195	0.15
4	0.195	0.45
5	0.195	0.15
6	0.195	0.45
7	0.195	0.15
8	0.195	0.45
9	0.195	0.15
10	0.195	0.45
11	0.195	0.15

Table 6.1 The protocol for the hydrogel experiment.

6.2.4 Data analysis

The material parameters were obtained by fitting curves for the sample height and the electrical potential difference. We assumed that the values of the material parameters did not depend on the deformation. We fitted the experiments in the following way. In first approximation, the osmotic pressure was the same at the end of both stages, since there was no change in the concentration of the bathing solution, only a change in the fixed charged density. So, the value for the aggregate modulus $H := 2\mu_s + \lambda_s$ was

determined from the increase of the mechanical load $\Delta\sigma$ and the strain ϵ of the sample:

$$H := \frac{\Delta\sigma}{\epsilon}, \quad (6.3)$$

with

$$\epsilon := \frac{h_2 - h_3}{h_3}, \quad (6.4)$$

where h_2 and h_3 were respectively the sample heights at the end of the second and the third stage.

From the reactions that took place during the polymerisation, see e.g. [19], the amount of solid and the number of fixed charges were computed. When knowing the mass of the sample immediately after the reaction and the mass of the same sample in equilibrium with the 0.15 M bathing solution, the porosity of the gel is calculated by

$$n_0^f := \frac{V^f}{V^{tot}} = \frac{m^f / \rho^f}{m^{tot} / \rho^{tot}}. \quad (6.5)$$

We assumed that density of the sample ρ^{tot} is equal to the density of the fluid, since more than 90% of the sample consists of water: $\rho^{tot} \approx \rho^f \approx 1.0 \cdot 10^6 \text{ g m}^{-3}$. This porosity was valid for the unloaded case. Since there was a preload, the value had to be corrected according to equation (4.11). The deformation due to the preload was computed according to equation (6.3).

Since we knew the fluid volume V^f and the number of fixed charges, the fixed charged density was computed by

$$c^{fc} := \frac{\text{number of fixed charges}}{V^f}. \quad (6.6)$$

Next, the osmotic coefficients were fitted. According to the momentum balance (4.1) and Hooke's law (4.6), the equilibrium height depends on the aggregate modulus H and the fluid pressure p . In equilibrium, the fluid and ion flows are equal to zero. According to the extended Darcy's law (4.7) and the extended Fick's law (4.8), the fluid pressure p is coupled to the osmotic coefficients ϕ^l , ϕ^+ and ϕ^- , the ion concentrations c^+ and c^- , and the electrical potential field ξ . The aggregate modulus H was determined already. We assumed that the osmotic coefficients for the fluid, the cations, and the anions were the same:

$$\phi^l = \phi^+ = \phi^- = \phi. \quad (6.7)$$

The value for the osmotic coefficient in an aqueous NaCl solution depends on the concentration. However, in the range from 0.15 M to 0.50 M it is almost constant [40, 63]. So, we assumed a constant osmotic coefficient ϕ in the bathing solution: $\phi = 0.924$. The value inside the sample was estimated by a fitting procedure such that the absolute error between the measured and computed equilibrium height of the second stage was

minimised. Therefore, the experiments were simulated by a finite element code of the four-component mixture theory (chapter 4). We assumed that there was no leakage over the electrode filter. The material parameters did not depend on the tissue deformation. The mechanical loads at the top of the sample were prescribed (figure 6.4). There were no ion and fluid flows at the top. At the bottom, the ion concentrations, the fluid pres-

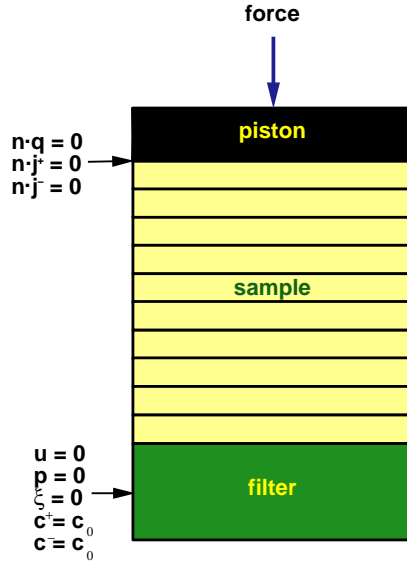


Figure 6.4 Boundary conditions for the uniaxial confined swelling and compression experiment.

sure ($p = 0$: free outflow) and the electrical potential ($\xi = 0$) were prescribed. Since these values had to be described in the middle of an element, we assumed that the element closest to the filter was immediately in equilibrium with the bathing solution. We checked this assumption by estimating the time constant τ . Since the convection is slower than the diffusion, the biphasic time constant is used [15]:

$$\tau := \frac{h^2}{HK}, \quad (6.8)$$

where h is the distance to the boundary and K is the hydraulic permeability. The total sample height is about 1 mm. We divided the sample in 10 uniform elements. Thus, $h \approx 0.05$ mm. The aggregate modulus H is about 0.2 MPa and the permeability K is about $5 \cdot 10^{-16} \text{ m}^4 \text{N}^{-1} \text{s}^{-1}$. So, $\tau \approx 25$ s. Thus, the equilibrium assumption is reasonable.

The permeability was determined by fitting the curve of the sample height of the second and the third stages. We fitted the permeability such that the absolute difference between the measured and the computed curve for the sample height was minimised.

The diffusion coefficients influence the slope of the streaming potential curve. The faster an ion diffuses, the faster the electrical potential difference over the sample decreases, since the potential difference depends on the concentration gradient, see (4.17). So, the values for the diffusion coefficients were estimated by fitting the curve for the

electrical potential, while keeping the relation between the diffusion coefficients for the cations and the anions in the sample (D^+ and D^-) the same as in an aqueous solution (D_w^+ and D_w^-) [54]:

$$\frac{D^+}{D^-} = \frac{D_w^+}{D_w^-} = \frac{13.34 \cdot 10^{-10}}{20.32 \cdot 10^{-10}} = 0.6565. \quad (6.9)$$

6.3 Results

The results of 2 representative experiments out of 11 are shown in figure 6.5.

After 4.5 hours, the sample started swelling due to a change in the chemical load: the concentration of the bathing solution was decreased from 0.45 M to 0.15 M. The tissue swelling was in the range of 30% – 36%.

After 12.5 hours, the sample shrank due to an extra mechanical load. The load was increased from 0.078 MPa to 0.195 MPa. The tissue shrinking was in the range of 33% – 36%. An equilibrium was reached after about 1 to 3 hours, depending on the sample thickness.

In the last part ($t > 20$ hours), the sample started swelling and shrinking because of changes of the chemical loads. These changes were prescribed before a new equilibrium was reached. The change of the salt concentration in the bathing solution was also responsible for the forming of an electrical potential difference over the sample. This is shown in the lower graphs of figure 6.5.

The experiments were fitted. The computed data for the porosity and the fixed charges density were used: $n^f = 0.945$ and $c^{fc} = 0.301 \text{ mol l}^{-1}$ at $t = 4\text{h}$. Two fitted experiments are shown in figure 6.6. The other 9 experiments were fitted too. The values are shown in table 6.2.

parameter	value	
aggregate modulus H	$0.20 \cdot 10^6 \pm 0.04 \cdot 10^6$	N m^{-2}
hydraulic permeability K	$5.5 \cdot 10^{-16} \pm 2.4 \cdot 10^{-16}$	$\text{m}^4 \text{N}^{-1} \text{s}^{-1}$
diffusion coefficient for the cations D^+	$4.4 \cdot 10^{-10} \pm 2.0 \cdot 10^{-10}$	$\text{m}^2 \text{s}^{-1}$
diffusion coefficient for the anions D^-	$6.7 \cdot 10^{-10} \pm 2.9 \cdot 10^{-10}$	$\text{m}^2 \text{s}^{-1}$
osmotic coefficient ϕ inside the sample	0.971 ± 0.005	

Table 6.2 The values of the parameters estimated by the fitting procedure.

6.4 Discussion

Although we assumed the material parameters to be constant, we were able to fit the experiments reasonably well. The deformation in the first part of the experiment (un-

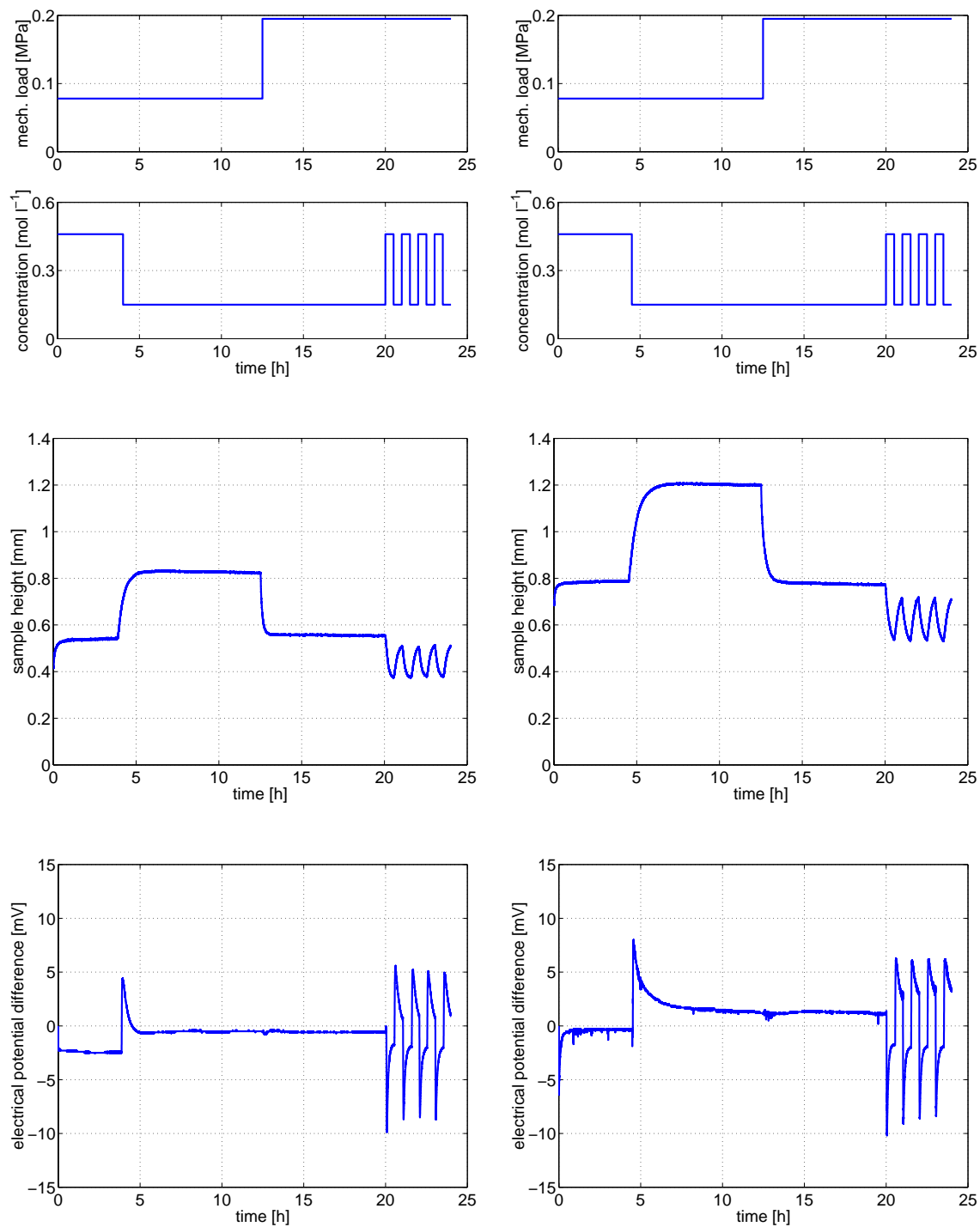


Figure 6.5 Experimental results for 2 confined swelling and compression experiments performed on hydrogel. The boundary conditions are given in the corresponding top figures.

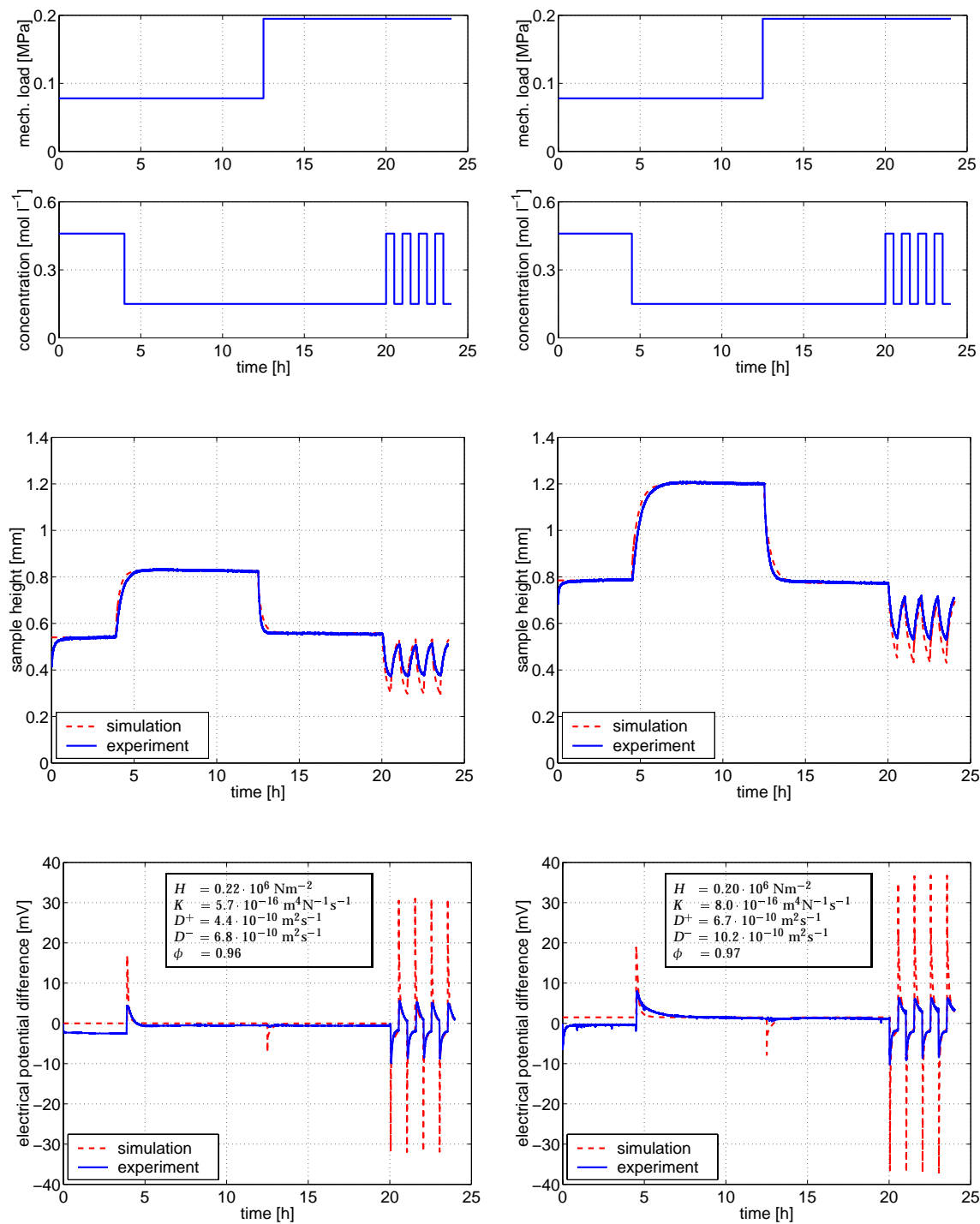


Figure 6.6 Experimental and numerical results for 2 confined swelling and compression experiments performed on hydrogel. The boundary conditions are given in the corresponding top figures.

til 20 h) is fitted reasonably by the four-component mixture theory. Then, the sample deformation is overestimated. This is because the permeability is too large. This is caused by neglecting the deformation dependency of the permeability. When the tissue is compressed, the permeability should decrease because the pores are squeezed.

It seems that the permeability is lower in the case of swelling that was caused by an osmotic pressure change, than in the case of shrinking caused by a mechanical load. This effect was probably caused by friction between the ions and the fluid. The flows of the ions and the fluid have opposite directions, when the swelling is caused by an osmotic pressure. When the fluid flow is hindered by the ion flow, the 'effective' permeability will be lowered. This can be modelled by increasing the difference between the liquid and the ion osmotic coefficient: $\phi^l - \phi^\beta$, $\beta = +, -$. For example by taking $\phi^l = 1$. From equation (2.32) it follows that the fluid flux is slowed down. In the third stage, the ions flow and the fluid flow were in the same direction. Hence, the fluid flow was not slowed down by the ion flow: the 'effective' permeability is larger. This follows also from equation (2.32), since the gradient in the ion concentrations is very small.

The diffusion coefficients for the cations and the anions were respectively $4.4 \cdot 10^{-10} \pm 2.0 \cdot 10^{-10} \text{ m}^2\text{s}^{-1}$ and $6.7 \cdot 10^{-10} \pm 2.9 \cdot 10^{-10} \text{ m}^2\text{s}^{-1}$. These values were in the same range as reported by Lanir et al. [52]: $D^+ \approx 6.0 \cdot 10^{-10} \text{ m}^2\text{s}^{-1}$ and $D^- \approx 10.4 \cdot 10^{-10} \text{ m}^2\text{s}^{-1}$.

The values for the diffusion coefficients hardly influenced the evolution in time of the deformation. This evolution was mainly influenced by the permeability of the sample. The diffusion coefficients influenced the width of the peaks of the electrical potential difference: when the value of the diffusion coefficient decreases, the width of the peak increases. Then, the electrical potential difference decreases slower. So, the values for the diffusion coefficients were fitted by looking at the last part of the curve for the electrical potential difference ($t > 20$ h). The measured electrical potential difference was smaller than the computed one, because the concentration of the bathing solution changed slower in the experiment than in the simulation. In the simulation we assumed that at a certain moment the external salt concentration changes from one concentration immediately to another. In the experiment, this concentration went gradually from one value to another. This effect decreased the peaks in the electrical potential signal, because the electrical potential difference was lowered rapidly in the first couple of seconds. Qualitatively, the signals were predicted reasonably well.

In other confined compression experiments, a streaming potential was measured when a mechanical load was applied [15]. This streaming potential is characterised by an electrokinetic coefficient k_e :

$$k_e := \frac{\Delta\xi}{\Delta\sigma}. \quad (6.10)$$

Here, ξ is the electrical potential and σ is the mechanical load. The value for the electrokinetic coefficient k_e for bovine cartilage was found to be in the range from -2 to -12 mV MPa⁻¹ [15].

In our confined swelling and compression experiment, we also applied a mechanical load to the sample ($t = 12.5$ h). We measured a streaming potential $\Delta\xi = 0.85 \pm 0.65$ mV. The change in the mechanical load $\Delta\sigma$ equals -0.117 MPa. Thus, the value for

the electrokinetic coefficient is -7.3 ± 5.6 mV MPa⁻¹. This was in the same range as measured for bovine cartilage.

In the experiments, it is seen that the equilibrium values for the electrical potential difference were different for different concentrations of the bathing solution. The difference between the equilibrium values of the first and the second stage is -0.93 ± 2.96 mV. This may indicate that there was a small leakage over the electrode filters.

6.5 Conclusions

We were able to measure the electrical potential differences over the samples that were caused by a change in the mechanical loads or by a change in the chemical load. The evolution in time of the tissue deformation as well as the evolution in time of the electrical potential differences were simulated by the four-components mixture theory. Furthermore, the estimated values for the stiffness, permeability, the diffusion coefficients and the electrokinetic coefficients were in the same range as reported by other studies.

7 Conclusions and Recommendations

7.1 Conclusions

7.1.1 Numerical aspects

We have considered the four-component mixture theory and a reduction to a two-component mixture theory. Two finite element formulations for the two-component mixture theory were derived: a conforming finite element method and a mixed-hybrid finite element method. One finite element formulation for the four-component mixture theory was used: a mixed finite element method. We conclude that

- The finite element implementations of the two-component mixture theory show that the error is linear with respect to the size of the time-steps and quadratic with respect to element size.
- For a time-step size $\Delta t < \Delta t_{crit}$, oscillations may appear in the solution for the displacement-pressure formulation of the two-component mixture theory in the one-dimensional case.
- For a time-step size $\Delta t < \Delta t_{crit}$, oscillations in the solution may appear for the mixed-hybrid finite element formulation of the two-component mixture theory in the one-dimensional case. This critical time-step size Δt_{crit} is 1.5 times smaller than in the displacement-pressure formulation.
- The critical bounds for the time-steps appear to hold for the two-dimensional case too.
- The extension to the four-component mixture theory, does not result in a symmetric matrix-vector system. The size reduction of the matrix-vector system, that is used in the two-component mixture theory, does not hold anymore.
- In a special case, the discontinuous fluid pressure, cation and anion concentrations, and electrical potential can be replaced by continuous electrochemical potentials. The related equations are however highly non-linear.

7.1.2 Experimental aspects

We performed confined swelling and compression experiments on intervertebral disc tissue and on a hydrogel. These experiments were used to verify the four-component mixture model by comparing the estimated values for the material parameters to values reported by other studies. We conclude that

- The confined swelling and compression experiments yield reproducible results with respect to the evolution in time of the deformations for the intervertebral disc tissue.
- In the confined swelling and compression experiments, the evolution in time of the deformations as well as the evolution in time of the electrical potential difference for the hydrogel are found to be to be reproducible.
- We are able to fit the experimental data by the four-component mixture model. The values for the stiffness, the permeability, the diffusion coefficients and for the osmotic coefficients are in the same range as reported in other studies [6, 23, 36, 52, 59].
- The measured values for the streaming potentials lie in the same range as reported for bovine cartilage [15, 26, 27].
- Using the four-component mixture theory, the behaviour of cartilaginous tissues is simulated while using physically realistic values for the material parameters.

7.2 Recommendations

7.2.1 Numerical aspects

The following aspects with respect to the finite element methods may be investigated further:

- We used a direct solver for one-dimensional finite element code. The performance of the code can be improved by an iterative method without loss of accuracy.
- We assumed that the material parameters, like the stiffness, the permeability and the diffusion coefficients do not depend on the deformations and/or salt concentrations. Although, the experiments were fitted reasonably well with these constant values, it is better to implement these dependencies, since the deformations and the changes in the salt concentrations are relatively large.
- We assumed that the solid matrix behaves linearly elastic. Since the solid matrix consists of fibres that can be stretched or folded, it should be possible to replace the constitutive equation for the stress by, for example, a visco-elastic relation.

- We assumed that all components are incompressible. This is a reasonable assumption in biomechanics. However, in geomechanics the fluid pressures are much larger. Then, this assumption is not valid anymore. So, the compressibility of the components has to be taken into account.

7.2.2 Experimental aspects

- We verified the four-component mixture theory for one-dimensional experiments. The model has to be verified for two-dimensional experiments, for example by unconfined swelling and compression experiments.
- By connecting a voltage source to the electrodes in the set-up of figure 6.3, an electrical potential field is generated. By this electrical potential field, the particles will start to flow and the tissue will deform. In this way an extra verification of the four-component mixture theory is achieved.

Bibliography

- [1] S. Achanta, J. H. Cushman, and M. R. Okos. On multicomponent, multiphase thermodynamics with interfaces. *International Journal of Engineering Science*, 32:1717–1738, 1994.
- [2] S. I. Barry and G. N. Mercer. Flow and deformation in poroelasticity - I unusual exact solutions. *Mathematical and Computer Modelling*, 30:23–29, 1999.
- [3] J. M. G. Barthel, H. Krienke, and W. Kunz. *Physical Chemistry of Electrolyte Solutions: Modern Aspects*, volume 5 of *Topics in Physical Chemistry*. Steinkopff, Darmstadt, 1998.
- [4] P. J. Basser and A. J. Grodzinsky. The Donnan model derived from microstructure. *Biophysical Chemistry*, 46:57–68, 1993.
- [5] C. A. L. Bassett and R. J. Pawluk. Electrical behavior of cartilage during loading. *Science*, 178:982–983, 1972.
- [6] B. A. Best, F. Guilak, M. Weidenbaum, and V. C. Mow. Compressive stiffness and permeability of intervertebral disc tissues: Variation with radial position, region and level. In *Proceedings Winter Annual Meeting ASME*, pages 73–74, San Fransisco, 1989.
- [7] M. A. Biot. General theory of three-dimensional consolidation. *Journal of Applied Physics*, 12:155–164, 1941.
- [8] M. A. Biot. Theory of finite deformation of porous solids. *Indiana University Mathematical Journal*, 21:597–620, 1972.
- [9] N. Bogduk and L. T. Twomey. *Clinical Anatomy of the Lumbar Spine*. Churchill Livingstone, 1985.
- [10] R. M. Bowen. Incompressible porous media models by the use of the theory of mixtures. *International Journal of Engineering Science*, 18:1129–1148, 1980.

- [11] R. M. Bowen. Compressible porous media models by the use of the theory of mixtures. *International Journal of Engineering Science*, 20:697–735, 1982.
- [12] D. Braess. *Finite Elements: Theory, Fast Solvers, and Applications in Solid Mechanics*. Cambridge University Press, Cambridge, 1997.
- [13] F. Brezzi and M. Fortin. *Mixed and Hybrid Finite Element Methods*. Springer-Verlag, New York, 1991.
- [14] M. D. Buschmann and A. J. Grodzinsky. A molecular model of proteoglycan-associated electrostatic forces in cartilage mechanics. *Journal of Biomechanical Engineering*, 117:179–192, 1995.
- [15] A. C. Chen, T. T. Nguyen, and R. L. Sah. Streaming potentials during the confined compression creep test of normal and proteoglycan-depleted cartilage. *Annals of Biomechanical Engineering*, 25:269–277, 1999.
- [16] S. C. Cowin. Strain or deformation rate dependent finite growth in soft tissues. *Journal of Biomechanics*, 29:647–649, 1996.
- [17] S. C. Cowin, L. Moss-Salentijn, and M. L. Moss. Candidates for the mechanosensory system in bone. *Journal of Biomechanical Engineering*, 113:191–197, 1991.
- [18] H. Darcy. *Les Fontaines Publique de la Ville Dijon*. Dalmont, Paris, 1856.
- [19] H. J. de Heus. *Verification of Mathematical Models Describing Soft Charged Hydrated Tissue Behaviour*. PhD thesis, Eindhoven University of Technology, Eindhoven, 1994.
- [20] A. de Loof. The electrical dimension of cells: the cell as a miniature electrophoresis chamber. *International Review of Cytology*, 104:251–361, 1986.
- [21] B. V. Derjaguin and N. V. Churaev. Properties of water layers adjacent to interfaces. In C. A. Croxton, editor, *Fluid Interfacial Phenomena*, pages 663–738, Chichester, 1986.
- [22] B. V. Derjaguin and L. Landau. The theory of stability of highly charged lyophobic sols and adhesion of highly charged particles in solutions of electrolytes. *Acta Physicochimica URSS*, 14:633–662, 1941.
- [23] M. R. Drost, P. Willems, H. Snijders, J. M. Huyghe, and J. D. Janssen. Confined compression of canine annulus fibrosus under chemical and mechanical loading. *ASME Journal of Biomechanical Engineering*, 117:390–396, 1995.
- [24] S. R. Eisenberg and A. J. Grodzinsky. Swelling of articular cartilage and other connective tissues: electromechanochemical forces. *Journal of Orthopaedic Research*, 3:148–159, 1985.

- [25] A. Fick. Über Diffusion. *Annalen der Physik und Chemie*, 94:59–86, 1855.
- [26] E. H. Frank and A. J. Grodzinsky. Cartilage electromechanics–I. Electrokinetic transduction and the effects of electrolyte pH and ionic strength. *Journal of Biomechanics*, 20:615–627, 1987.
- [27] E. H. Frank and A. J. Grodzinsky. Cartilage electromechanics–II. A continuum model of cartilage electrokinetics and correlation with experiments. *Journal of Biomechanics*, 20:629–639, 1987.
- [28] A. J. H. Frijns, J. M. Huyghe, and J. D. Janssen. A validation of the quadriphasic mixture theory for intervertebral disc tissue. *International Journal of Engineering Science*, 35:1419–1429, 1997.
- [29] A. J. H. Frijns, J. M. Huyghe, and J. D. Janssen. Four components mixture theory applied to soft biological tissue. In J. Middleton, M. L. Jones, and G. N. Pande, editors, *Computer Methods in Biomechanics and Biomedical Engineering*, volume 2, pages 519–526, 1998.
- [30] A. J. H. Frijns, E. F. Kaasschieter, and J. M. Huyghe. Numerical modelling of cartilage as a deformable porous medium. In W. Ehlers, editor, *IUTAM Symposium on Theoretical and Numerical Methods in Continuum Mechanics of Porous Materials*, to appear.
- [31] A. J. Grodzinsky, H. Lipshitz, and M. J. Glimcher. Electromechanical properties of articular cartilage during compression and stress-relaxation. *Nature*, 275:448–450, 1978.
- [32] D. Gross and W. S. Williams. Streaming potential and the electromechanical response of physiologically-moist bone. *Journal of Biomechanics*, 15:277–295, 1982.
- [33] W. Y. Gu, W. M. Lai, and V. C. Mow. Transport of fluid and ions through a porous-permeable charged-hydrated tissue, and streaming potential data on normal bovine articular cartilage. *Journal of Biomechanics*, 26:709–723, 1993.
- [34] W. Y. Gu, W. M. Lai, and V. C. Mow. Transport of multi-electrolytes in charged hydrated biological soft tissues. *Transport in Porous Media*, 34:143–157, 1999.
- [35] W. Y. Gu, X. G. Mao, B. A. Rawlins, J. C. Iatridis, R. J. Foster, D. N. Sun, M. Weidenbaum, and V. C. Mow. Streaming potential of human lumbar annulus fibrosus is anisotropic and affected by disc degeneration. *Journal of Biomechanics*, 32:1179–1182, 1999.
- [36] F. Guilak, W. B. Zhu, M. Weidenbaum, B. A. Best, and V. C. Mow. Compressive material properties of human annulus fibrosus. In *Abstracts First World Congress Biomechanics, Vol. II*, page 41, San Diego, 1990.

- [37] W. Hackbusch. *Elliptic Differential Equations, Theory and Numerical Treatment*. Springer-Verlag, Berlin, 1992.
- [38] F. Helfferich. *Ion Exchange*. McGraw-Hill Book Company, New York, 1962.
- [39] R. Helmig. *Multiphase Flow and Transport Processes in the Subsurface: a Contribution to the Modeling of Hydrosystems*. Springer, Berlin, 1997.
- [40] G. B. Houben. *Swelling and Compression of Intervertebral Disc Tissue: Model and Experiment*. PhD thesis, University of Maastricht, Maastricht, 1996.
- [41] G. B. Houben, M. R. Drost, J. M. Huyghe, J. D. Janssen, and A. Huson. Nonhomogeneous permeability of canine annulus fibrosus. *Spine*, 22:7–16, 1997.
- [42] J. M. Huyghe, T. Arts, D. H. van Campen, and R. S. Reneman. Porous medium finite element model of the beating left ventricle. *American Journal of Physiology*, 262:1256–1267, 1992.
- [43] J. M. Huyghe and J. D. Janssen. Quadriphasic mechanics of swelling incompressible porous media. *International Journal of Engineering Science*, 35:793–802, 1997.
- [44] J. M. Huyghe and J. D. Janssen. Thermo-chemo-electro-mechanical formulation of saturated charged porous solids. *Transport in Porous Media*, 34:129–141, 1999.
- [45] J. M. Huyghe, D. H. van Campen, and T. Arts. A two-phase finite element model of the diastolic left ventricle. *Journal of Biomechanics*, 24:527–538, 1990.
- [46] J. M. R. J. Huyghe. *Non-linear Finite Element Models of the Beating Left Ventricle and the Intramyocardial Coronary Circulation*. PhD thesis, Eindhoven University of Technology, Eindhoven, 1986.
- [47] J. Israelachvili and H. Wennerström. Role of hydration and water structure in biological and colloidal interactions. *Nature*, 379:219–225, 1996.
- [48] J. N. Israelachvili. *Intermolecular and Surface Forces, 2nd edn*. Academic, New York, 1991.
- [49] E. F. Kaasschieter and A. J. H. Frijns. Squeezing a sponge: a three-dimensional analytic solution in poroelasticity. submitted.
- [50] E. F. Kaasschieter and A. J. M. Huijben. Mixed-hybrid elements and streamline computation for the potential flow problem. *Numerical Methods for Partial Differential Equations*, 8:221–266, 1992.
- [51] W. M. Lai, J. S. Hou, and V. C. Mow. A triphasic theory for the swelling and deformation behaviors of articular cartilage. *ASME Journal of Biomechanical Engineering*, 113:245–258, 1991.

- [52] Y. Lanir, J. Seybold, R. Schneiderman, and J. M. Huyghe. Partition and diffusion of sodium and chloride ions in soft charged foam: the effect of external salt concentration and mechanical deformation. *Tissue Engineering*, 4:365–378, 1998.
- [53] R. C. Lee, E. H. Frank, A. J. Grodzinsky, and D. K. Roylance. Oscillatory compressional behavior of articular cartilage and its associated electromechanical properties. *ASME Journal of Biomechanical Engineering*, 103:280–292, 1981.
- [54] D. R. Lide, editor. *CRC Handbook of chemistry and physics : a ready-reference book of chemical and physical data*, volume 78. CRC Press, 1997.
- [55] J. R. Mabee, T. L. Bostwick, and M. K. Burke. Iatrogenic compartment syndrome from hypertonic saline injection in bier block. *The Journal of Emergency Medicine*, 12:473–476, 1994.
- [56] A. F. T. Mak. Streaming potential in bone. In V. C. Mow, A. Ratcliffe, and S. L.-Y. Woo, editors, *Biomechanics of Diarthrodial Joints*, pages 175–194, New York, 1990.
- [57] R. A. Marcus. Calculation of thermodynamic properties of polyelectrolytes. *The Journal of Chemical Physics*, 23:1057–1068, 1955.
- [58] A. Maroudas. Physicochemical properties of cartilage in the light of ion exchange theory. *Biophysical Journal*, 8:575–595, 1968.
- [59] A. Maroudas. Nutrition and metabolism of the intervertebral disc. In P. Gosh, editor, *The Biology of the Intervertebral Disc*, pages 1–38, Florida, 1988.
- [60] V. C. Mow, M. H. Holmes, and W. M. Lai. Fluid transport and mechanical properties of articular cartilage: a review. *Journal Biomechanics*, 17:377–394, 1984.
- [61] V. C. Mow, S. C. Kuei, W. M. Lai, and C. G. Armstrong. Biphasic creep and stress relaxation of articular cartilage in compression: theory and experiments. *ASME Journal of Biomechanical Engineering*, 102:73–84, 1980.
- [62] C. W. J. Oomens. *A Mixture Approach to the Mechanics of Skin and Subcutis*. PhD thesis, Twente University, Enschede, 1985.
- [63] C. W. J. Oomens, H. J. de Heus, J. M. Huyghe, L. Nelissen, and J. D. Janssen. Validation of triphasic mixture theory for a mimic of intervertebral disk tissue. *Biomimetics*, 3:171–185, 1995.
- [64] C. W. J. Oomens, D. H. van Campen, and H. J. Grootenboer. A mixture approach to the mechanics of skin. *Journal of Biomechanics*, 20:877–885, 1987.
- [65] E. G. Richards. *An Introduction to the Physical Properties of Large Molecules in Solution*. Cambridge University Press, Cambridge, 1980.

- [66] Y. Saad. *Iterative Methods for Sparse Linear Systems*. PWS Publishing Company, Boston, 1996.
- [67] R. L. Sah, Y. L. Kim, J. Y. H. Doong, A. J. Grodzinsky, A. K. Plaas, and J. D. Sandy. Biosynthetic response of cartilage explants to dynamic compression. *J. Orthop. Res.*, 7:619–639, 1989.
- [68] B. R. Simon, J. P. Liable, D. Pflaster, Y. Yuan, and M. H. Krag. A poroelastic finite element formulation including transport and swelling in soft tissue structures. *ASME Journal of Biomechanical Engineering*, 118:1–9, 1996.
- [69] B. R. Simon, O. C. Zienkiewicz, and D. K. Paul. An analytical solution for the transient response of saturated porous elastic solids. *International Journal for Numerical and Analytical Methods in Geomechanics*, 8:381–398, 1984.
- [70] H. Snijders, J. M. Huyghe, and J. D. Janssen. Triphasic finite element model for swelling porous media. *International Journal for Numerical Methods in Fluids*, 20:1039–1046, 1995.
- [71] J. M. A. Snijders. *The Triphasic Mechanics of the Intervertebral Disc: a Theoretical, Numerical and Experimental Analysis*. PhD thesis, University of Limburg, Maastricht, 1994.
- [72] J. Stefan. Über das Gleichgewicht und die Bewegung, insbesondere die Diffusion von Gasgemengen. *Sitzungsbericht Akademie der Wissenschaften, Mathematische Naturwissenschaftliche Klasse Abteilung II a*, 63:63–124, 1871.
- [73] K. Terzaghi. Die Berechnung der Durchlässigkeitsziffer des Tones aus dem Verlauf der hydrodynamischen Spannungserscheinungen. *Sitzungsbericht Akademie der Wissenschaften, Mathematische Naturwissenschaftliche Klasse Abteilung II a*, 132:123–138, 1923.
- [74] K. Terzaghi. *Erdbaumechanik auf bodenphysikalischer Grundlage*. Deuticke, Wien, 1925.
- [75] J. P. G. Urban and S. Roberts. Intervertebral disc. In W. D. Comper, editor, *Extracellular matrix*, volume 1: Tissue function, pages 203–233, Amsterdam, 1996.
- [76] E. J. W. Verwey and J. T. G. Overbeek. *Theory of the Stability of Lyophobic Colloids*. Elsevier, Amsterdam, 1948.
- [77] A. A. White III and M. M. Panjabi. *Clinical Biomechanics of the Spine*. J. B. Lippincott Company, Philadelphia, 1990.
- [78] R. Woltman. *Beyträge zur Hydraulischen Architectur*. Johann Christian Dietrich, Göttingen, 1797. Dritter Band.

Index

- activity coefficient, 24, 25
- annulus fibrosus, 12
- biphasic model, 18
- chemical force, 11
- collagen fibre, 12
- component, 22
- concentration, 23
- confined swelling and compression experiment, 75
- Darcy's law, 27, 86
 - extended, 27
- data analysis
 - hydrogel, 89
 - intervertebral disc tissue, 77
- displacement-pressure formulation, 34
- displacement-pressure-velocity formulation, 35
- DLVO-model, 14
- Donnan equilibrium, 63
- Donnan model, 15
- effective stress-tensors, 23
- electrical force, 11
- electrical potential, 85
- electro-neutrality, 23
- electrochemical potentials, 24, 69
- electrokinetic coefficient, 86
- electrokinetics, 86
- elliptic, 38
- energy equation, 25
- existence of the solution of a two-component problem, 38
- experimental protocol
 - hydrogel, 88
 - intervertebral disc tissue, 76
- experimental set-up
 - hydrogel, 87
 - intervertebral disc tissue, 75
- Fick's first law, 28
- Fick's law
 - extended, 27
- Fick's second law, 17
- fixed charge, 23
- fixed charge density, 13
- fluid flux, 62
- four-component mixture theory, 19, 21, 61
- friction tensor, 27
- GAG, *see* glycosaminoglycan
- glycosaminoglycan, 13
- Hilbert space, 33
- Hooke's law, 24
- hybrid mixture theory, 19
- hydrogel, 86
- inf-sup condition, 38
- intrinsic density, 23
- ionflux, 62
- kernel, 37, 43

- Korn's second inequality, 38
- LBB condition, 42
- M-matrix, 51
- macromodel, 14
- mass balance, 23
- mechanical force, 11
- microfibrils, 12
- micromodel, 14
- mixture theory, 15
- molar mass, 23
- momentum equation, 22
- motion segment, 12
- multiplier space, 42
- Nernst potential, 64
- nucleus pulposus, 12
- Ohm's law, 86
- osmotic coefficient, 25
- osmotic pressure, 25
- parameter fitting, 79
- PB-model, 14, 15
- phase, 22
- Poincaré-Friedrichs inequality, 39
- Poisson-Boltzmann unit-cell model, *see*
PB-model
- polynomial space, 40
- polysaccharide, 13
- projection, 43
- proteoglycan, 12
- Raviart-Thomas space, 42
- relative volume change, 32
- representative elementary volume, 15, 21
- saddle point problem, 37
- sample preparation
 - hydrogel, 87
 - intervertebral disc tissue, 75
- space
 - $H_0(\text{div}, \Omega)$, 33
 - $H_1(\Omega)$, 33
 - $H_{1,0}(\Omega)$, 33
 - $H_1(\Omega)^d$, 33
 - $H_{1,0}(\Omega)^d$, 33
 - $H(\text{div}, \Omega)$, 33
 - $L_2(\Omega)$, 33
 - $\mathbf{L}_2(\Omega)$, 33
 - $M^0(\Omega_h)$, 42
 - $M_{-1,0}^0(E_h)$, 45
 - $M_{-1}^0(E_h)$, 45
 - $M_{-1}^0(\Omega_h)$, 42
 - $P^n(\Omega_h)$, 40
 - $RT_0^0(\Omega_h)$, 42
 - $RT_{-1}^0(\Omega_h)$, 42
 - $RT_{0,0}^0(\Omega_h)$, 42
- specific discharge, 32
- streaming potential, 85
- stress-tensor, 22
- triphasic theory, 18
- tropocollagen, 12
- two-component mixture theory, 31
- u-p formulation, *see* displacement-pres-
sure formulation
- u-p-v formulation, *see* displacement-pres-
sure-velocity formulation
- uniqueness of the solution of a two-com-
ponent problem, 38
- unit-cell, 15
- volume fraction, 22
- volume fractions, 16

Summary

Cartilaginous tissues, like intervertebral disc tissue, and hydrogels exhibit swelling and shrinking behaviour. This behaviour is caused by water bound by the charged solid skeleton of the tissue through an interplay of mechanical, chemical and electrical mechanisms. In order to develop more insight into the mechanism, this swelling and compression behaviour is modelled by the four-component mixture theory. In this theory, the tissue is represented as a charged, deformable porous medium which is saturated with a fluid in which ions are dissolved. By distinguishing between cations and anions, the electrical phenomena can be modelled.

The objectives of this study are:

- The development of a finite element description for the four-component mixture theory. With this finite element model, we are able to compute the deformations, the fluid and ion flows, the fluid pressure, the cation and anion concentrations and the electrical potential field.
- The verification of the four-component mixture theory with respect to the evolution in time of the deformations and the electrical potential field by confined swelling and compression experiments.

In this thesis, the four-component mixture theory is derived from the balance equations and the constitutive equations for the solid matrix, the fluid flow and the ion flows: Hooke's law for the solid matrix and an extended Darcy's law and an extended Fick's law for the fluid flux and the ion fluxes, respectively. This theory reduces to the biphasic theory when assuming that there are no particles dissolved in the fluid phase.

First, we consider the two-component mixture theory. The problem definition has a unique solution when making adequate assumptions on the behaviour of the displacements, fluid velocity and the fluid pressure. These assumptions are not in conflict with the physical problem we are interested in.

The two-component problem is described in two ways: the displacement-pressure formulation and the displacement-pressure-velocity formulation. An advantage of the second one is that the fluid flux is computed more accurately than with the displacement-pressure formulation. From the displacement-pressure formulation, a conforming finite element method is derived. From the displacement-pressure-velocity formulation,

a mixed-hybrid finite element method is derived. In the mixed-hybrid finite element model, a Lagrange multiplier is introduced, that enforces the continuity of the normal component of the fluid fluxes across the inter element boundaries. Using the properties of the matrix, the matrix-vector system is reduced to a system with only the displacements and the Lagrange multipliers as unknowns. The fluid pressure and the fluid flux are computed a posteriori without loss of accuracy. For both methods, the errors are considered that are caused by size of the elements and by the size of the time-steps. From the numerical analysis, it follows that the global error is linear with respect to the size of the time-steps and quadratic with respect to element size for both methods. It is shown that oscillations in the solution may appear in the one-dimensional case, when the time-step size is smaller than a critical value. This critical size is 1.5 times smaller in the the mixed-hybrid finite element formulation than in conforming finite element formulation. This critical size of the time-steps appears to hold for the two-dimensional case too.

Then, the two-component mixture model is extended to the four-component mixture model. From this model, a mixed finite element method is derived. It results in a non-symmetric matrix-vector system. In a special case, the discontinuous fluid pressure, cation and anion concentrations, and electrical potential can be replaced by continuous electrochemical potentials. The related equations are however highly non-linear.

The four-component mixture theory was verified by uniaxial confined swelling and compression experiments on intervertebral disc tissue. These experiments were performed on cylindrical samples made out of the annulus fibrosus part of intervertebral discs from the lumbar spine of dogs. The values of the material parameters were estimated by fitting the experiments with the mixed finite element model. The theory was verified by comparing the estimated values to values reported by other studies. The estimated values were in the same range. So, the four-component mixture theory is able to describe the evolution in time of the displacements.

The four-component mixture theory was also verified by uniaxial confined swelling and compression experiments on a hydrogel. A hydrogel is an artificial material that has similar properties as cartilaginous tissues. The evolution in time of the deformation as well as the evolution in time of the electrical potential difference over the sample were measured. The electrical phenomena gives an extra possibility to check the theory. The values of the material parameters were estimated by fitting the experiments with the mixed finite element model. The values for the stiffness, the permeability and the osmotic coefficients were fitted by the evolution in time of the deformation; the diffusion coefficients were fitted by the evolution in time of the electrical potential difference. The theory was verified by comparing the estimated values to the values reported in other studies. The estimated values were in the same range. So, the four-component mixture theory is able to describe the evolution in time of the displacements as well as the evolution in time of the electrical potential field.

Samenvatting

Kraakbeenachtige materialen, zoals tussenwervelschijven, maar ook hydrogelen vertonen zwel- en krimpgedrag. Dit gedrag wordt veroorzaakt doordat er water aan de elektrisch geladen vaste-stofmatrix wordt gebonden door een samenspel van mechanische, chemische en elektrische mechanismen. Om het inzicht in deze mechanismen te vergroten, wordt het zwellen en krimpen van het weefsel gemodelleerd door een vier-componentenmengseltheorie. In deze theorie wordt het weefsel beschouwd als een elektrisch geladen vaste-stofmatrix, die verzadigd is met een vloeistof waarin ionen zijn opgelost. Door onderscheid te maken tussen de positief geladen ionen en negatief geladen ionen kunnen de elektrische verschijnselen gemodelleerd worden.

De doelstellingen van dit onderzoek zijn:

- Het ontwikkelen van een eindige-elementenbeschrijving van het vier-componentenmengselmodel. Met behulp van dit eindige-elementenmodel berekenen we de vervormingen, de vloeistof- en de ionenstromingen, de vloeistofdruk, de ionenconcentraties en het elektrisch potentiaalveld.
- De verificatie van het vier-componentenmengselmodel met betrekking tot het tijdsverloop van de vervormingen en van het elektrisch potentiaalveld door één-dimensionale zwel- en consolidatie-experimenten.

In dit proefschrift wordt het vier-componentenmengselmodel afgeleid uit de balanswetten en constitutieve relaties voor de vaste-stofvervormingen en de vloeistof- en ionenstromingen: de wet van Hooke voor de vaste stof en uitgebreide wetten van Darcy en Fick voor respectievelijk de vloeistof- en de ionenstromingen. Als men aanneemt dat er geen deeltjes in de vloeistof zijn opgelost, is deze theorie gelijk aan de twee-componentenmengseltheorie.

Als eerste wordt het twee-componentenmengselmodel bekeken. Het probleem heeft een unieke oplossing, wanneer er adequate aannamen worden gemaakt met betrekking tot de (wiskundige) eigenschappen van de verplaatsingen, de vloeistofstroming en de vloeistofdruk. Deze aannamen zijn in niet strijd met het onderzochte fysische probleem.

Het twee-componenten probleem wordt op twee manieren onderzocht: met behulp van de 'verplaatsing-druk'-formulering en met behulp van de 'verplaatsing-druk-snelheid'-formulering. De laatste formulering heeft als voordeel dat de vloeistofstroming

nauwkeuriger wordt berekend dan in de 'verplaatsing-druk'-formulering. Uit de 'verplaatsing-druk'-formulering wordt een conforme eindige-elementenmethode afgeleid. Uit de 'verplaatsing-druk-snelheid'-formulering wordt een gemengd-hybride eindige-elementenmethode afgeleid. In dit model wordt een extra Lagrange multiplicator ingevoerd, die de continuïteit van de normale componenten van de vloeistoffluxen afdwingt over de inwendige randen van de elementen. Door gebruik te maken van de speciale eigenschappen van de matrix, wordt het matrix-vectorstelsel verkleind tot een stelsel waarin alleen de vaste-stofverplaatsingen en de Lagrange multiplicatoren nog onbekend zijn. De vloeistofdrukken en de vloeistofstroming kan a posteriori worden berekend zonder verlies in nauwkeurigheid.

Voor beide methoden wordt de fout onderzocht, die samenhangt met de grootte van de elementen en de grootte van de tijdstappen in een één-dimensionaal experiment. Uit numerieke analyse volgt dat voor beide methoden de fout lineair afhangt van de grootte van de tijdstappen en kwadratisch afhangt van de grootte van de elementen. Bovendien is aangetoond, dat er oscillaties in de oplossing kunnen optreden wanneer de tijdstappen kleiner worden dan een kritische waarde. Deze kritische waarde is in de gemengd-hybride formulering 1,5 keer zo klein als in de conforme formulering. De berekende kritische tijdstapgrootte blijkt ook voor een twee-dimensionaal probleem te gelden.

Vervolgens wordt het twee-componentenmengselmodel uitgebreid tot het vier-componentenmengselmodel. Uit dit model wordt een gemengd eindige-elementenmodel afgeleid. Dit resulteert echter in een niet-lineair, niet-symmetrisch matrix-vectorstelsel. In een speciaal geval kunnen de discontinue vloeistofdruk, ionenconcentraties en het elektrisch potentiaalveld vervangen worden door continue electrochemische potentialen. Het matrix-vectorstelsel wordt dan echter sterk niet-lineair.

Het vier-componentenmengselmodel wordt geverifieerd aan de hand van één-dimensionale zwel- en consolidatie-experimenten aan tussenwervelschijfmateriaal. Deze experimenten zijn gedaan aan cilindrische proefstukjes, die afkomstig waren uit het annulus fibrosus gedeelte van tussenwervelschijven uit de lumbale wervelkolom van honden. De vervorming van het proefstuk is gemeten. De waarden voor de materiaalparameters zijn bepaald door het 'fitten' van de experimentele data met het eindige-elementenmodel. De mengseltheorie wordt geverifieerd door de geschatte materiaalparameters te vergelijken met waarden, die in andere studies bepaald zijn. De geschatte waarden liggen in hetzelfde bereik. Het vier-componentenmengselmodel is dus in staat om het verloop van de vervorming goed te beschrijven.

Het vier-componentenmengselmodel wordt ook geverifieerd aan de hand van één-dimensionale zwel- en consolidatie-experimenten aan hydrogelen. Een hydrogel is een kunststofmateriaal dat vergelijkbare eigenschappen heeft als kraakbeenachtige weefsels. De vervormingen van het proefstuk en het elektrisch potentiaalverschil over het proefstuk zijn gemeten. De waarden van de materiaalparameters zijn bepaald door het 'fitten' van de experimentele resultaten met het eindige-elementenmodel. De stijfheid, de permeabiliteit en de osmotische coëfficiënten zijn gefit aan de vervormingsmeting; de diffusiecoëfficiënten van de ionen zijn gefit aan de metingen van het elektrisch po-

tentiaalverschil. De mengseltheorie wordt geverifieerd door de geschatte materiaalparameters te vergelijken met waarden, die in andere studies bepaald zijn. De geschatte waarden liggen in hetzelfde bereik. Het vier-componentenmengselmodel is dus in staat om het tijdsverloop van de vervorming en het tijdsverloop van het elektrisch potentiaalverschil goed te beschrijven.

Acknowledgements

This research was financed by the cooperative research fund between the Eindhoven University of Technology and the University of Maastricht.

Many people have contributed to the realisation of the research presented in this thesis. I wish to thank them. First of all, I wish to thank Jacques Huyghe, Rik Kaasschieter, Bob Mattheij and Theo Arts for their support and guidance throughout the years and for reading my manuscripts carefully. Furthermore, I wish to thank the people who helped me with the experiments: Gerard Houben with whom I performed the experiments on the intervertebral disc tissue, Paul Willems for his assistance with the experiments at the University of Maastricht, and Marcel Wijlaars, who made the hydrogels and assisted me with the experiments at the faculty of Mechanical Engineering.

I thank my colleagues in the Scientific Computing Group and the department of Movement Science (University of Maastricht) for the pleasant atmosphere.

I thank Martijn Anthonissen, Ramon Clout and Roy Willemen for the pleasant time we spent together in the 'Kookclub' and in the theatre.

Finally, I thank my family and friends for their support throughout the years.

Curriculum Vitae

Arjan Frijns was born on November 26, 1972, in Cadier en Keer, the Netherlands. After his pre-university education (VWO) at the Sint-Maartenscollege in Maastricht, he started in 1991 to study Biomechanical Engineering at the Eindhoven University of Technology. He graduated in May 1996 on the subject of the swelling and shrinking behaviour of intervertebral disc tissue. He performed confined swelling and compression experiments on this tissue and compared the results to numerical simulations. This project was carried out in cooperation with the department of Movement Science of the University of Maastricht. His Master's thesis was written under supervision of dr.ir. J.M. Huyghe and prof.dr.ir. J.D. Janssen.

From June 1996, he worked as a trainee research assistant (AIO) in the Scientific Computing Group of prof.dr. R.M.M. Mattheij at the faculty of Mathematics and Computing Science of the Eindhoven University of Technology in cooperation with the faculty of Mechanical Engineering and the department of Movement Science of the University of Maastricht. The research, in which he combined his interests in applied mathematics, biomechanics and physics, resulted in this thesis.

Stellingen

behorende bij het proefschrift

A Four-Component Mixture Theory Applied to Cartilaginous Tissues Numerical Modelling and Experiments

door

A.J.H. Frijns

1. Het bewijs voor de existentie en uniciteit voor het twee-componentenmengselmodel kan worden uitgebreid tot het algemenere geval waarin Neumann, Dirichlet en Robin randvoorwaarden voorgeschreven zijn. Daartoe moeten wel extra Hilbert-ruimtes $\mathcal{H}(\text{div}, \Omega) = \{\mathbf{v} \in \mathbf{L}_2(\Omega) \mid \nabla \cdot \mathbf{v} \in L_2(\Omega), \mathbf{n} \cdot \mathbf{v} \in L_2(\Gamma^R)\}$, en $\mathcal{H}_0(\text{div}, \Omega) = \{\mathbf{v} \in \mathcal{H}(\text{div}, \Omega) \mid \mathbf{n} \cdot \mathbf{v} = 0 \text{ on } \Gamma^N\}$ geïntroduceerd worden.
2. Het bewijs voor de LBB-conditie in hoofdstuk 3 kan ook worden gehouden met betrekking tot $b(\mathbf{w}_h, q_h)$ in plaats van $d(\mathbf{s}_h, q_h)$. In dat geval is er een extra vrijheid met betrekking tot het kiezen van de eindige-elementenruimte voor \mathbf{s}_h , omdat $d(\mathbf{s}_h, q_h)$ niet meer aan de LBB-conditie hoeft te voldoen.
3. De theorie voor het vier-componentenmengselmodel uit hoofdstuk 4, kan eenvoudig worden uitgebreid tot een n-componentenmengselmodel.
4. Men kan beter de mengselmodellen rangschikken aan de hand van het aantal componenten dan aan de hand van het aantal fasen: afhankelijk van de definitie is het vier-componentenmengselmodel een één-fasenmodel [1], een twee-fasenmodel [2], een drie-fasenmodel [3] of zelfs een vier-fasenmodel [4].
[1] R. Helmig, *Multiphase Flow and Transport Processes in the Subsurface*, 1997.
[2] J. Schweers & P. van Vianen, *Natuurkunde op Corpusculaire Grondslag, deel 1*, 1980.
[3] W.M. Lai, J.S. Hou & V.C. Mow, *J. Biomech. Eng.*, **113**, 245, 1991.
[4] J.M. Huyghe & J.D. Janssen, *Int. J. Engng. Sci.*, **35**, 793, 1997.
5. De experimentele en numerieke resultaten geven geen aanleiding om een chemische expansiespanning in te voeren zoals Lai et al. [1] voorstellen.
[1] W.M. Lai, J.S. Hou & V.C. Mow, *J. Biomech. Eng.*, **113**, 245, 1991.

6. Die Mathematiker sind eine Art Franzosen. Redet man zu ihnen, so übersetzen sie es in ihre Sprache und dann ist es alsobald ganz etwas anderes.
J.W. Goethe, Maximen und Reflexionen.
7. Een praktische werktuigbouwkundige zoekt een oplossing bij zijn probleem, terwijl een theoretische wiskundige een probleem bij zijn oplossing zoekt.
8. In verband met het groeiend aantal interdisciplinaire en interuniversitaire onderzoeken, moet het mogelijk zijn om naast twee promotoren ook twee copromotoren te benoemen.
9. Het is in psychologisch opzicht beter om in het journaal te spreken over een stijging van de dollar ten opzichte van de euro dan van een daling van de euro ten opzichte van de dollar.
10. Vele ouderen leven als het ware in de sciencefiction van hun jeugd.
Troonrede, 19 september 2000.
11. Door telewerken zal het file-probleem zich verplaatsen van de autosnelweg naar de digitale snelweg.
12. Door bezuinigingen in de gezondheidszorg is het beddentekort veranderd in een personeelstekort.
13. Door de eigen bijdragen in de gezondheidszorg veroorzaakt pijn in het lichaam ook pijn in de portemonnee.
14. Het vier-componentenmengselmodel vormt de ruggengraat van mijn proefschrift.